

Bulk Material Handling by Conveyor Belt

Edited by
Mark Alspaugh

Published by



Society for Mining,
Metallurgy, and Exploration, Inc.

Society for Mining, Metallurgy, and Exploration, Inc. (SME)

8307 Shaffer Parkway

Littleton, Colorado, USA 80127

(303) 973-9550 / (800) 763-3132

www.smenet.org

SME advances the worldwide mining and minerals community through information exchange and professional development. SME is the world's largest association of mining and minerals professionals.

Copyright © 2008 Society for Mining, Metallurgy, and Exploration, Inc.

All Rights Reserved. Printed in the United States of America.

Information contained in this work has been obtained by SME, Inc. from sources believed to be reliable. However, neither SME nor its authors guarantee the accuracy or completeness of any information published herein, and neither SME nor its authors shall be responsible for any errors, omissions, or damages arising out of use of this information. This work is published with the understanding that SME and its authors are supplying information but are not attempting to render engineering or other professional services. If such services are required, the assistance of an appropriate professional should be sought.

No part of this publication may be reproduced, stored in a retrieval system, or transmitted in any form or by any means, electronic, mechanical, photocopying, recording, or otherwise, without the prior written permission of the publisher. Any statement or views presented here are those of the authors and are not necessarily those of SME. The mention of trade names for commercial products does not imply the approval or endorsement of SME.

ISBN-13: 978-0-87335-260-4

Library of Congress Cataloging-in-Publication Data

Bulk material handling by conveyor belt 7 / edited by Mark Alspaugh.

p. cm.

Includes bibliographical references and index.

ISBN 978-0-87335-260-4

1. Mine haulage--Equipment and supplies. 2. Conveyor belts. I. Alspaugh, M. A.

TN335.B852 2008

622'.6--dc22

2007051825

Preface

The Mineral Information Institute of Golden, Colorado, states that every person currently born in the United States will use 3.6 million pounds of minerals, metals, and fuels during their lifetime. In 2004, 293.7 million people required almost 7 billion tons of minerals and solid fuels. That's over 23 tons per man, woman, and child per year. These materials are not just used for luxury items but are required to provide the basic needs of food, clothing, and shelter. Additionally, these bulk materials are needed to build transportation systems, and manufacture the items we use to pursue everyday activities. A 1999 study stated that the simple process of ordering a book from Amazon.com required 0.5 pounds of coal to energize the transaction. We take these daily transactions for granted as our book arrives on our doorstep within a few days. Yet in the background, those 7 billion tons per year of bulk materials must be transported to make these things happen.

Although I cannot cite a specific number, I would venture a guess that almost 100 percent of raw materials find themselves on a belt conveyor at least once and often many times during their journey from raw to finished product.

Formal belt conveyor design and engineering for mining applications can be traced back to Thomas Edison's developments prior to 1900 at the Ogden iron ore mine near Ogdensburg, New Jersey. Mr. Edison understood the benefits of automation and the need to

move large volumes of iron ore reliably. He turned to belt conveyors. In the last 100 years, all mining has come to depend on belt conveyors, which have developed into huge, complex machines carrying up to 40,000 tons per hour over many miles.

In the last 20 years, the evolution of belt conveyor technology has increased its pace as impressive numerical analysis and simulation techniques have led to changes in system and component designs. Applied during the design cycle when changes and improvements are easy and cheap, use of time-based, numerical modeling tools that consider belt elasticity, as well as discrete particle-based bulk material flow methods, are giving engineers unprecedented insight into expected performance. In the last 5 years, these advanced tools—once the domain of a few specialists—have become more readily available to all engineers, and the technology is becoming more widely used on applications large and small.

In this symposium, we have heard from many leading researchers and engineers who are pushing the envelope to understand, design, and build larger, more reliable, more efficient equipment and components. We must listen, as the demand for raw materials is exploding at a rate not seen since the Industrial Revolution. Each of the authors was invited to present their specific experiences and expertise, and we thank them for taking the time (and in some cases considerable expense) to share with us.

.....

Contents

PREFACE v

PART 1 DESIGN CONSIDERATIONS FOR LONG OVERLAND CONVEYORS 1

Evolutionary Belt Conveyor Design—Optimizing Costs
C.A. Wheeler 3

Dynamics of Long Belt Conveyors with Distributed Drives
G. Lodewijks and A.J.G. Nuttall 13

Applied Rubber Belt Cover Loss Prediction from Indentation
Thomas J. Rudolphi 25

Belt Conveyor Idler Roll Behaviors
Allen V. Reicks 35

PART 2 SOLVING REAL PROBLEMS USING NUMERICAL ANALYSIS AND SIMULATION 41

Simulation for Equipment Sizing, Longwall to Stockpile
Edmond O'Donovan 43

Simulation as a Tool to Determine Stockyard Handling Capacity
Eric Monrad and Harry King 47

Interfacing Belt Feeders and Hoppers to Achieve Reliable Operation
John Carson, Francisco Cabrejos, and Michael Rulff 53

Discrete Element Modeling of Sag Energy Losses in a Conveyor Belt System
Graham G.W. Mustoe and Ren Bin 65

PART 3 CASE STUDIES OF LARGE BELT CONVEYANCE PROJECTS 69

Increasing Kaltim Prima Coal Overland Conveyor Speed to 8.5 mps
Poltak Sinaga 71

Limestone Transportation by 17-km Cross-Border Long Belt Conveyor for Lafarge
Surma Cement Limited
Kumar Vikram and Pabak Mukhopadhyay 77

Cadman Downhill Overland Conveyor, Blending into the Washington State

Forest Area

Bill Sayer, Manuel Mendez, and Peter Sehl **83**

Thirty-Year-Old Transfer Point Challenge

Robert McEwen **89**

Large-Scale Stacking System at the Freeport-McMoRan Safford Mine

Michael Schmalzel, Andrew Osterloh, and Grant Graber **93**

INDEX 101

.....
PART 1

Design Considerations for Long Overland Conveyors

- Evolutionary Belt Conveyor Design—Optimizing Costs **3**
- Dynamics of Long Belt Conveyors with Distributed Drives **13**
- Applied Rubber Belt Cover Loss Prediction from Indentation **25**
- Belt Conveyor Idler Roll Behaviors **35**

Evolutionary Belt Conveyor Design—Optimizing Costs

C.A. Wheeler*

This paper presents the initial findings of a research program to reduce the annual equivalent costs of belt conveying systems. The work utilizes models to predict the motion resistance of belt conveyors that take into consideration the influence of key conveyor variables, such as idler roll diameter, spacing, troughing configuration and belt width. Given a specified conveyor configuration, the capital and ongoing costs of the system can then be approximated based on the required belt, idler rolls, structure, drives, etc. The research provides a computational means to rapidly analyze a large number of potential conveyor configurations and to compare each on an annual equivalent cost basis.

INTRODUCTION

Work discussed in this paper has resulted from an ongoing research program in belt conveying technology undertaken at The University of Newcastle, Australia. Initial work to develop numerical models to calculate the motion resistance of belt conveyors was undertaken by the author during doctoral studies (Wheeler [1]). These models have more recently been coupled with numerical optimization techniques to design optimized conveyor systems. The optimization strategies can be focused on minimizing motion resistance, energy consumption or life cycle cost. The latter involves the integration of economic models originally developed by Roberts et al. [2]. These original economic models have been updated to reflect recent costing data, with the optimization process now being undertaken using state of the art numerical evolutionary optimization algorithms.

Recent work by Wheeler and Ausling [3,4] has demonstrated the successful use of evolutionary numerical optimization techniques to belt conveyor design. The optimization program aims to minimize particular conveyor characteristics, such as motion resistance, energy consumption or annual equivalent cost. The optimization process selects conveyor variables, such as belt width, idler roll diameter, spacing and troughing configuration to minimize the required characteristic. For example, if a conveyor system is to be optimized for annual equivalent cost, then the program will explore and compare many thousands of potential solutions to determine the system with the lowest annual equivalent cost. For specific performance requirements and bulk material characteristics, both the capital and operating costs of the system are calculated from the required belt

strength and width, idler diameter and spacing, drive and structure costs, as well as the energy consumption. The numerical optimization process provides a computational means to analyze a wide variety of potential conveyor configurations and to evaluate each in terms of the annual equivalent cost per metre length of belt. The evolutionary approach mimics biological evolution in order to fully explore a wide variety of potential solutions, eventually arriving at the most suitable configuration for optimal performance.

The optimization process relies on the accurate determination of the motion resistance of the belt conveyor and the calculation of the life cycle cost of components. The motion resistances that occur along the length of the conveyor are known as the main resistances and include the effects of the belt and bulk solid flexure, the rotation of the idler rolls and the indentation of the idler rolls into the rubber belt. Work by Wheeler [1] provides the computational methods for calculating each of the main resistances using measured conveyor belt and bulk solid properties. The economic model considers both capital and operating costs, and involves the use of annual equivalent cost functions for major conveyor components over the design life of the system, in addition to annual energy cost.

This paper will provide an overview of the optimization process used to minimize the life cycle cost of belt conveyor systems. The paper will firstly discuss the background of the selected optimization technique, followed by the approach used to calculate the motion resistances, an outline of the optimization computer program, and finally demonstrate by way of examples typical program outputs and findings.

* Centre for Bulk Solids and Particulate Technologies, The University of Newcastle, Australia.

EVOLUTIONARY OPTIMIZATION

Just as biological evolution provides highly optimized species, similarly the application of numerical evolutionary strategies can be used to solve complex engineering optimization problems, often involving hundreds of variables with a single objective to be optimized. Designing optimized belt conveyor systems is undoubtedly a complex engineering problem, with many interrelations between conveyor variables compounding the complexity. For example, increasing idler spacing has non-linear effects on the belt and material flexure resistance, the idler rotating resistance per unit length, and the indentation rolling resistance per idler roll due to the change in load. Therefore, while an increase in idler spacing will reduce the number of idler rolls and frames required and therefore the capital and maintenance costs, motion resistance and resulting energy costs may increase to levels that outweigh these benefits. To further increase the difficulty, the problem clearly involves the interrelation, and therefore optimization, of both discrete and continuous variables. Discrete variables include belt widths, idler diameters and troughing configurations, while continuous variables include belt speed and idler spacing, which can take on any values within practical limits.

An evolutionary computational technique was selected for the current problem due to widespread use in many similar applications requiring a large number of variables are to be optimized, such as air traffic control, structural optimization and timetabling. Furthermore, recent work by Wensrich [5], and Wensrich and Wheeler [6] has proven the potential of such optimization methods to the design of conveyor transfer chutes. This work involved single-objective evolutionary methods applied to conveyor loading chute design. The work provided a means to achieve optimum performance with minimum chute wear as well as minimum belt wear at the loading point. This work formed the platform for the current optimization technique.

Evolutionary computational methods imitate biological evolution in order to find optimum solutions to complex problems involving many variables. When applied to belt conveyor design, the initial population of potential conveyor configurations (idler roll diameter, spacing, belt speed, etc.) is randomly generated within upper and lower boundaries set by the designer. The designs are then evaluated using a fitness function to evaluate the annual equivalent cost of the system. Systems that perform well (those with low annual equivalent costs) are used to generate (or breed) a new population, passing on their selected variables (or genes) to the next generation with small induced modifications or "mutations." The process of evaluating and breeding is repeated until a range of optimal solutions is obtained.

LIFE CYCLE COST MODELS

To compare the life cycle cost of each potential conveyor configuration, an objective function that sums the annual equivalent cost of both operating and capital costs over the design life of the system was derived from the work of Roberts et al. [2]. The objective function takes into consideration the annual energy cost and annual equivalent costs of major conveyor components over the design life of the system, taking into account component life, inflation, taxation rate and rate of return on investment.

Operating Costs

Operating costs for a belt conveyor system include energy consumption, repairs and maintenance, and labor costs. Like the work of Roberts et al. [2], the operating costs considered in the current analysis only consider the life of the conveyor idler rolls and the annual energy cost. While it is acknowledged that repairs and maintenance, and labor costs of other components can be significant, to the authors knowledge limited research has been published on the influence of factors such as belt speed and width, idler roll diameter and spacing, and troughing configuration on these costs.

The life of conveyor idler rolls is considered in the current analysis, with design life assumed to be governed by the fatigue life of the ball or roller bearings. The fatigue life is based on the type and size of the bearing, operating load and belt speed. While it is recognized that idler roll failure is often the result of contaminant ingress through seals, once again limited research is available to quantitatively predict this failure mechanism. Based on the expected life, the total number of idler rolls requiring replacement each year is added as an extra cost component to the annual equivalent cost of the idler rolls.

The other operating cost considered in the analysis is the energy cost per annum, and is calculated from the actual power consumption of the belt conveyor. The annual energy consumption, A_{energy} is given by:

$$A_{energy} = k_1 t_a e_c P_A \quad \text{EQ. 1}$$

Where k_1 is the annual equivalent energy cost coefficient that takes into consideration inflation and annual escalation rate of energy, t_a is the operating hours per annum, e_c is the unit cost of energy, and P_A is the actual power consumption. The actual motor power is calculated from the motion resistance models.

Capital Costs

The capital cost functions were also derived from the work of Roberts et al. [2]. The cost functions used have been modified to allow for additional variables such as, idler roll diameter and load, and the influence of belt width on structural costs. Furthermore, rather than linear relationships between variables, current costing data showed power relationships modeled the cost functions more accurately. The annual equivalent cost functions for a number of major capital items are given below.

$$\text{Belt} \quad A_{belt} = k_2 B(c_1 + c_2 T_1^{c_3})/L \quad \text{EQ. 2}$$

$$\text{Drive} \quad A_{drive} = k_3(c_4 + c_5 P_M^{c_6})/L \quad \text{EQ. 3}$$

$$\text{Gearbox} \quad A_{gearbox} = k_4(c_7 + c_8 T_R^{c_9})/L \quad \text{EQ. 4}$$

Idler rolls

$$\text{Carry side} \quad A_{carry \text{ idlers}} = k_5[c_{10} + c_{11} D^{c_{12}} + c_{13}(q_m + q_b)^{c_{14}} + c_{15} B^{c_{16}}]/L \quad \text{EQ. 5}$$

$$\text{Return side} \quad A_{return \text{ idlers}} = k_6[c_{17} + c_{18} D^{c_{19}} + c_{20} q_b^{c_{21}} + c_{22} B^{c_{23}}]/L \quad \text{EQ. 6}$$

Where: B is the belt width, T_1 is the maximum belt tension, L is the belt length, P_M is the rated motor power, T_R is the rated gearbox torque, D is idler roll diameter, q_m and q_b are the mass per unit length of the bulk material and conveyor belt respectively, $c_1 \dots c_{23}$ are the initial cost coefficients, and $k_2 \dots k_6$ are the annual equivalent cost coefficients. The initial cost coefficients are derived from present day values of the capital items as a function of the nominated conveyor variables. The annual equivalent cost coefficients are a function of the component life, inflation, taxation rate and rate of return on investment.

Costs of other items such as, the drive, snub and tail pulleys, take-up stations, structure, etc, are also included in the analysis. However, several assumptions have been made to simplify the analysis. For example, transfer chutes, transfer stations, walkways, covers and civil works have not been included in the current analysis, but may be added if required.

MOTION RESISTANCE MODELS

In order to calculate the power consumption of the belt conveyor, an accurate prediction of the motion resistance as a function of each conveyor variable is necessary. When considering the motion resistance of a horizontal belt conveyor, it is well recognized that this resistance comprises of the belt and bulk solid flexure resistance, the rotating resistance of the idler rolls and the indentation rolling resistance of the conveyor belt. This section discusses each component of the main resistance and provides details of methods developed by the author to calculate the contribution of each component. A finite difference solution that applies orthotropic plate mechanics is described to calculate the deflection of the conveyor belt due to the loading induced from the weight of the belt and bulk solid, and the loading induced from the relative movement of the bulk solid. Given the displacement of the belt and bulk solid the flexure resistance of the belt and bulk material is calculated. The rotating resistance of the idler rolls is briefly discussed and, a finite element model is presented which calculates the indentation rolling resistance occurring at each idler set from the viscoelastic properties of the bottom cover of the conveyor belt.

Bulk Solid and Belt Flexure Resistance

As the conveyor belt moves from one idler set to the next, the belt and bulk solid being conveyed undergo deflections due to the sag of the belt. Flexure resistance of the conveyor belt and bulk solid occurs due to the cyclic transverse and longitudinal movement as the belt progresses from one idler set to the next. The losses attributable to the belt flexure resistance occur due to the hysteretic losses associated with the induced bending of the conveyor belt, while the flexure resistance of the bulk solid occurs due to internal friction and friction at the belt interface.

In order to calculate the flexure resistance of the belt and bulk solid an accurate prediction of the deflection of the troughed belt between idler sets is required. Orthotropic plate mechanics is used to model the belt, which in addition to longitudinal tensile loading is also subjected to a pressure distribution resulting from the weight of the belt and bulk solid and loading induced from the relative movement of the bulk solid.

Calculating the pressure distribution due to the self-weight and relative movement of the bulk solid is essen-

tial in order to calculate the belt deflection and therefore the flexure resistance. Work by Krause and Hettler [7] is utilized to analyze the induced stress states resulting from the cyclic transverse and longitudinal deformation of the bulk solid. Krause and Hettler [7] applied a modified version of Coulomb's earth pressure theory to calculate the normal forces acting on the idler rolls of a belt conveyor due to the transverse opening and closing of the belt. Based on this theory, for the active stress state, the slip plane angle θ_a to the horizontal as a function of the idler toughing angle β , bulk solid internal friction angle ϕ_i , belt and bulk solid friction angle ϕ_w and conveyor surcharge angle δ , can be given by

$$\theta_a = \tan^{-1} \left[\frac{\left(\sqrt{\lambda_a} \sin(\beta - \phi_w) \right) \sin \delta - \sin \phi_i}{\left(\sqrt{\lambda_a} \sin(\beta - \phi_w) \right) \cos \delta - \cos \phi_i} \right] \quad \text{EQ. 7}$$

Where the active pressure factor λ_a , is given by:

$$\lambda_a = \left[\frac{\sin(\beta + \phi_i)}{\sqrt{\sin(\beta - \phi_w)} + \sqrt{\frac{\sin(\phi_w + \phi_i) \sin(\phi_i - \delta)}{\sin(\beta + \delta)}}} \right]^2 \quad \text{EQ. 8}$$

Figure 1 illustrates the active and passive stress states due to the opening and closing of the conveyor belt. Recent work by Ilic et al. [8] has shown that in most cases the passive failure planes propagating from each side roll will intersect within the material cross-section. Under these circumstances an approximation of the passive failure plane is best given by θ_p , drawn from the idler junction to the centre of the top of bulk solid material pile, also shown in Figure 1.

Similarly, for the passive stress state, the slip plane angle θ_p to the horizontal can be given by:

$$\theta_p = \tan^{-1} \left[\frac{\left(\sqrt{\lambda_p} \sin(\beta + \phi_w) \right) \sin \delta + \sin \phi_i}{\left(\sqrt{\lambda_p} \sin(\beta + \phi_w) \right) \cos \delta - \cos \phi_i} \right] \quad \text{EQ. 9}$$

Where the passive pressure factor λ_p , is given by

$$\lambda_p = \left[\frac{\sin(\beta - \phi_i)}{\sqrt{\sin(\beta + \phi_w)} + \sqrt{\frac{\sin(\phi_w + \phi_i) \sin(\phi_i + \delta)}{\sin(\beta + \delta)}}} \right]^2 \quad \text{EQ. 10}$$

Ilic et al. [8] experimentally investigated the active and passive failure planes for both non-cohesive and cohesive bulk solids. Experimental tests were undertaken on the oscillating test rig illustrated in Figure 2. High speed video footage of the failure planes was recorded and compared to the theoretical approximation, an example of which is shown in Figure 3.

Accurately calculating the formation of the active and passive stress states enables the load induced by the bulk solid on the conveyor belt to be determined. This therefore allows the belt deflection to be calculated, and thus the relative movement of the belt and bulk solid. The flexure resistance of the bulk solid and the conveyor belt

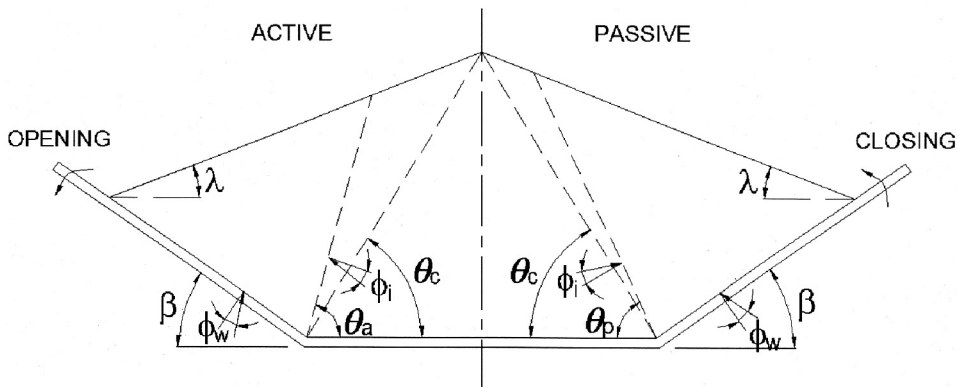


FIGURE 1 Active and passive stress states (Ilic et al. [8])

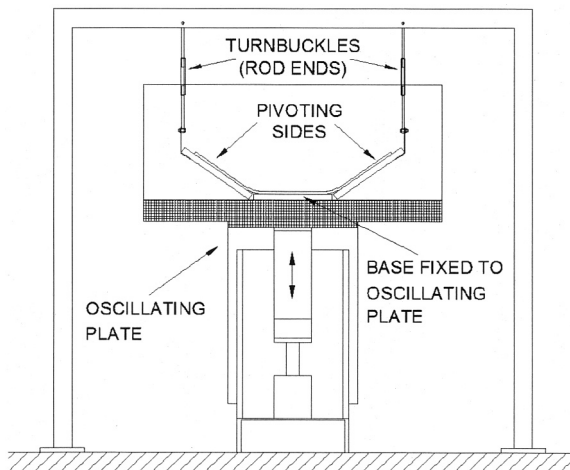


FIGURE 2 Bulk material flexure test facility (Ilic et al. [8])

is then calculated by the difference between the work done between the opening and closing of the conveyor belt.

Indentation Rolling Resistance

As the conveyor belt travels over the idler rolls, the bottom cover of the belt is indented due to the weight of the belt and bulk solid. Indentation rolling resistance occurs due to the viscoelastic nature of the bottom cover of the belt. A finite element analysis provides a means to calculate the indentation rolling resistance using experimentally measured viscoelastic properties. The finite element method developed incorporates the asymmetric loading profile with the added advantage of not having to specify an indentation depth or contact length. The roll diameter prescribes the lower boundary conditions, while an iterative procedure is used to increase the depth of indentation until a specified vertical load is reached. The finite element representation of the indentation region is shown diagrammatically in Figure 4.

The results from the finite element method were found to compare favorably to experimentally measured values obtained from a recirculating belt test facility for a range of idler roll diameters, belt speeds and applied loads. The experimental test facility comprises of a recirculating

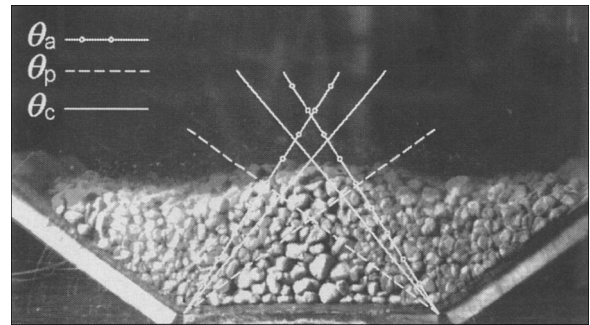


FIGURE 3 Overlad still images used to experimentally verify development of active and passive slip planes (Ilic et al. [8])

conveyor belt. The indentation rolling resistance is measured using an instrumented idler roll, shown in Figure 5. The horizontal force, F_H is a sum of the indentation rolling resistance and the idler roll rotating resistance. The idler roll rotating resistance is measured as a separate component using an auxiliary load beam and is subtracted from the total horizontal force measured, leaving the indentation rolling resistance.

In the analysis the indentation rolling resistance is calculated for each idler roll set and is summed along the length of the conveyor for both the carry side and return side. The load distribution across the idler sets on the carry side is calculated from the bulk solid flexure resistance program, while the return side is calculated due to the weight of the belt. Given the normal load, the indentation rolling resistance is calculated by integrating across the width of the belt.

Rotating Resistance of Idler Rolls

The rotating resistance of belt conveyor idler rolls occurs due to the friction of the rolling elements in the bearings, the viscous drag of the lubricant and the friction of the contact lip seals. Furthermore, any misalignment of the idler rolls to the direction of the belt also adds to the rotating resistance. Theoretical methods to individually calculate each component of the rotating resistance of the idler rolls are used in the current analysis. The components considered include, the viscous drag due to the shearing of the grease within the labyrinth seal, the friction torque of the rolling bearings generated from the

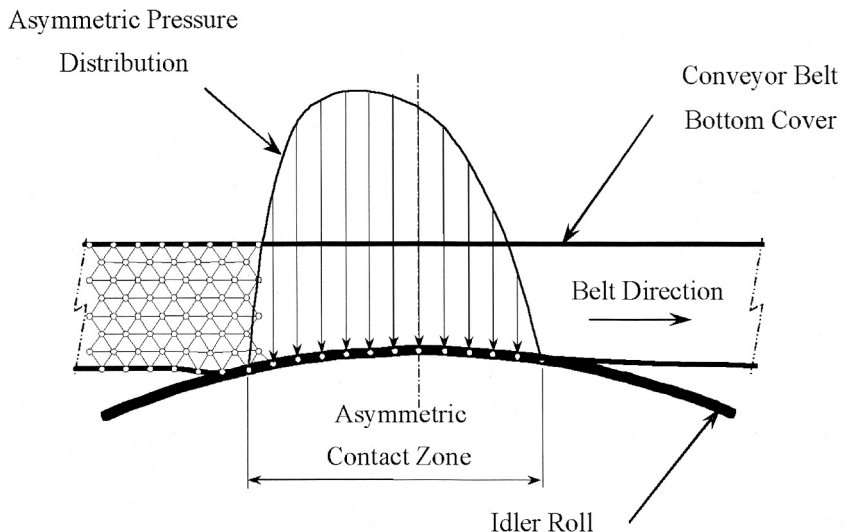


FIGURE 4 Viscoelastic finite element method to calculate conveyor belt Indentation rolling resistance (Wheeler [1])

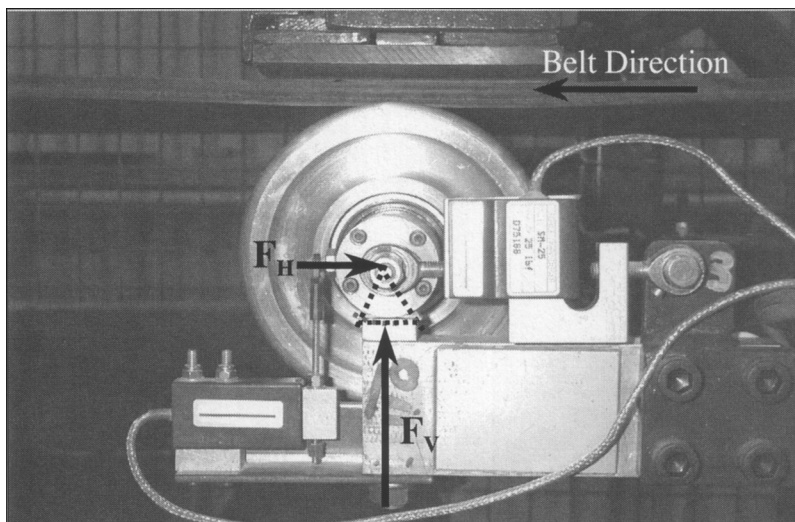


FIGURE 5 Conveyor belt Indentation rolling resistance measurement (Wheeler [1])

no-load and load dependent moments, and the rotating resistance of the contact lip seals.

Total Motion Resistance Measurement

The total motion resistance of the belt conveyor is a summation of the contribution of each of the motion resistance components discussed. In order to verify the theoretical approximations, field tests have been conducted using an instrumented idler frame, shown in Figure 6. The normal and horizontal force as well as the rotating resistance is measured on each idler roll. Belt speed, idler roll spacing and idler roll diameter can each be varied and the influence on the motion resistance measured.

OPTIMIZATION COMPUTER PROGRAM

Figure 7 shows the structure of the optimization program developed to minimize annual equivalent cost. Inputs include the system performance requirements, and bulk



FIGURE 6 Motion resistance measurement test rig

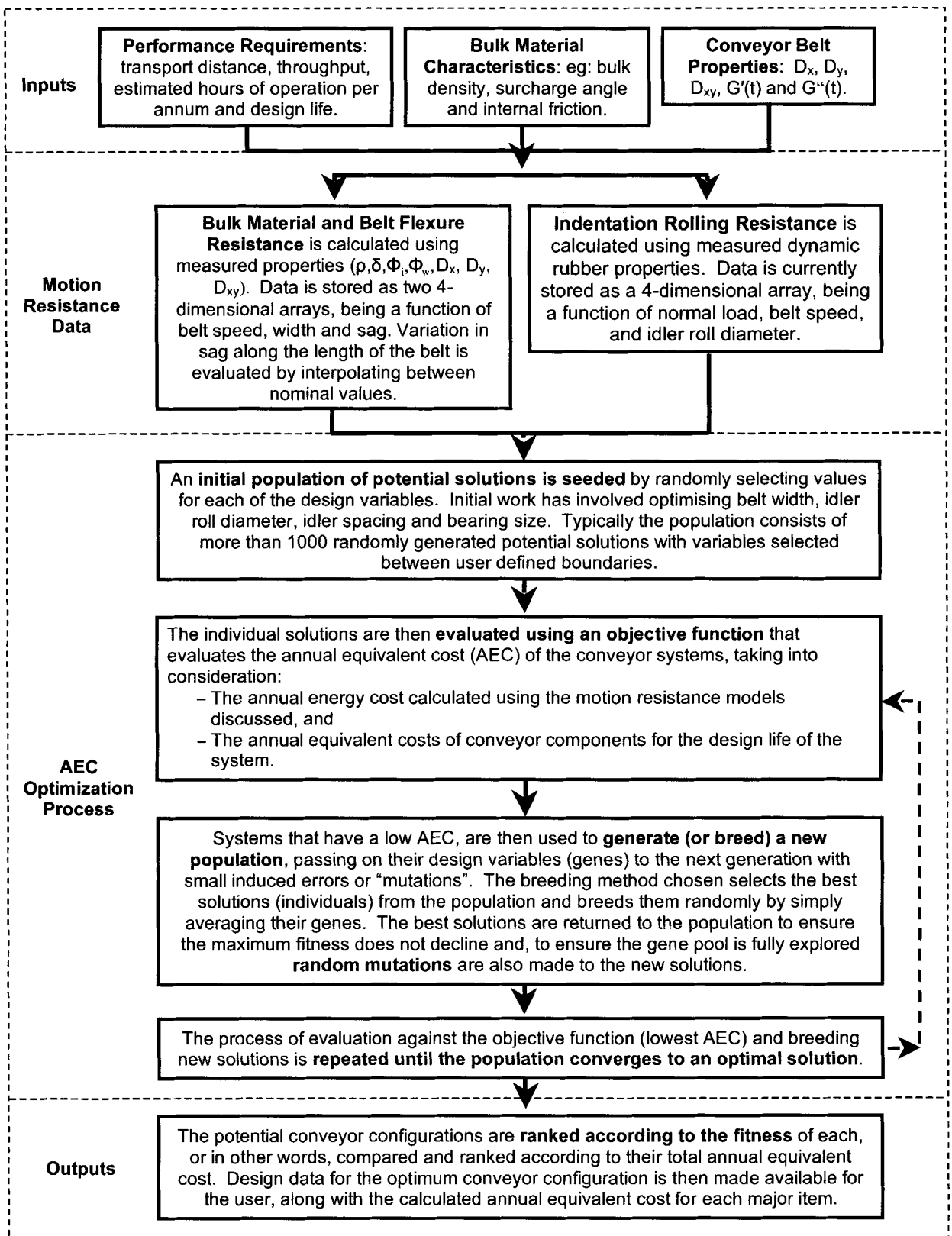


FIGURE 7 Evolutionary optimization program—AEC mode (Wheeler and Ausling [4])

solid and conveyor belt properties. Performance requirements of the system include transport distance, throughput, estimated hours of operation per annum and design life. Bulk solid properties include the bulk density, conveyor surcharge angle, internal friction and friction between the conveyor belt and the bulk solid. The bulk material properties are used to calculate the bulk solid loading on the conveyor belt and the resulting bulk material flexure resistance. Required conveyor belt properties include the flexural and torsional rigidities of the conveyor belt and the rubber dynamic properties of the bottom cover. The flexural and torsional rigidities are used to determine the deflection of the conveyor belt, while the dynamic properties of the bottom cover are used to calculate the indentation rolling resistance.

The optimization program begins by calculating the motion resistance data for the belt and bulk solid flexure resistance and the indentation rolling resistance. The program generates data files of the motion resistance data using the models discussed earlier for a range of potential solutions. This task is necessary to reduce the computational time of the optimization process, since the numerical methods that calculate the motion resistance components are computationally intensive, involving iterative finite element and finite difference methods where the computational times are typically measured in hours. Consequently, rather than having to run these programs for each individual in the population when evaluating their fitness against the objective function, the pre-calculated data provides much quicker data access, greatly reducing total computational time. Conversely, the rotating resistance of the idler rolls is calculated for each conveyor configuration due to the relatively small computational time required.

The optimization process begins with an initial population of potential solutions. Each solution is generated by randomly selecting values for each of the design variables. Initial work has involved optimizing belt width, idler roll diameter, idler roll spacing, idler roll bearing size and troughing configuration. Typically the population consists of more than 1,000 randomly generated potential solutions with variables selected between user defined boundaries. For example, idler rolls diameters are restricted to discrete sizes ranging from 4" to 7" in $\frac{1}{2}$ " size increments, while belt speed may be limited depending on particle size of the bulk material to be conveyed.

The individual solutions are then evaluated by summing the annual equivalent costs of the operating and capital items. Systems that have a low annual equivalent cost are then used to generate (or breed) a new population, passing on their design variables (genes) to the next generation with small induced errors or "mutations." The breeding method chosen selects the best solutions (individuals) from the population and breeds them randomly by simply averaging their genes. For example, if two potential solutions have different idler spacings, then the new individual generated will have an idler spacing equal to the average of both. Furthermore, the best solutions are also returned to the population to ensure the maximum fitness does not decline and, to ensure the gene pool is fully explored random mutations are also made to the new solutions.

The process of evaluation against the objective function (lowest AEC) and breeding new solutions is repeated

until the population converges to an optimal solution. The potential conveyor configurations are compared and ranked according to their total annual equivalent cost. Design data for the optimum conveyor configuration is then made available for the user, along with the calculated annual equivalent cost for each major item.

RESULTS AND DISCUSSION

The results presented aim to provide an overview of the current capabilities of the optimization program. Results to date have provided valuable insight into the mechanisms by which particular conveyor variables influence both the life cycle cost and the motion resistance of belt conveyors.

As previously mentioned, in order to reduce computational time the program makes use of pre-calculated data for both the belt and bulk solid flexure resistance and the indentation rolling resistance. Calculating the belt and bulk solid flexure resistance data for a specific bulk material involves analyzing a variety of belt widths and speeds, idler roll spacings and sag ratios. These values are then stored in a 4-dimensional array which the optimization program accesses. When individuals in the population have variables which lay between calculated values the optimization program interpolates between these values to estimate the flexure resistance. For example, as the belt sag varies along the length of the belt with belt tension, the program interpolates between calculated sag ratios to determine the corresponding change in belt and bulk material flexure resistance.

Figure 8 shows data for a bulk material with an internal friction angle $\phi_i = 35^\circ$, bulk density $\rho = 1,000 \text{ kg/m}^3$ and conveyor surcharge angle $\delta = 20^\circ$. The centre and outside idler rolls are set to be equal length and the troughing angle $\beta = 35^\circ$. The data presented in Figure 1 shows typical trends for the bulk material flexure resistance component. For example, increasing sag ratio results in bulk material undergoing greater relative movement, therefore resulting in increasing bulk material flexure resistance. Similarly, increasing belt width also results in greater flexure resistance due to more material being displaced. While increasing belt speed results in greater flexure resistance due to the transition between the active and passive stress states occurring closer to the next idler set resulting in more work being done.

A similar approach is used to access the indentation rolling resistance data. However, rather than accessing data arrays, functions for the indentation rolling resistance versus normal load are derived directly from the linear viscoelastic finite element analysis. The functions are derived for each idler roll diameter to be considered in the analysis over a range of belt speeds. Since the roll diameter can only take on discrete sizes, interpolation is only required for variations in belt speed. Like the bulk solid flexure resistance analysis, the use of pre-calculated data greatly reduces computational time by not having to run the computationally intensive viscoelastic finite element analysis for each individual in the population.

The final component of the motion resistance is the rotating resistance of the idler rolls. The calculation of this component is not computationally intensive and is incorporated directly into the optimization program. The total motion resistance is then calculated by summing each of the individual motion resistance components along the length of the conveyor. The annual equivalent

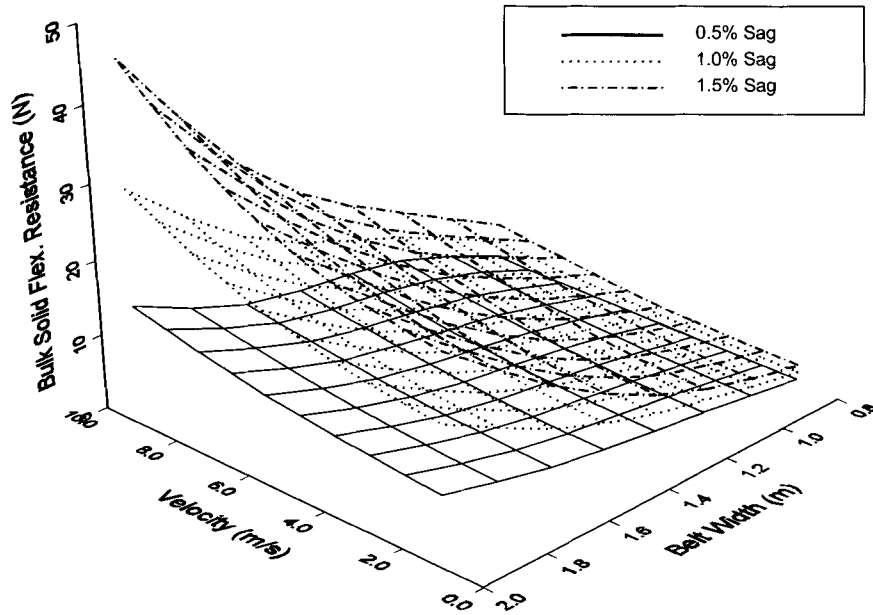


FIGURE 8 Bulk material flexure resistance versus belt width and velocity for a range sag ratios. Internal friction $\phi_i = 35^\circ$; Bulk density $\rho = 1,000 \text{ kg/m}^3$; Surcharge angle $\delta = 20^\circ$; Troughing angle $\beta = 35^\circ$. (Wheeler and Ausling [3])

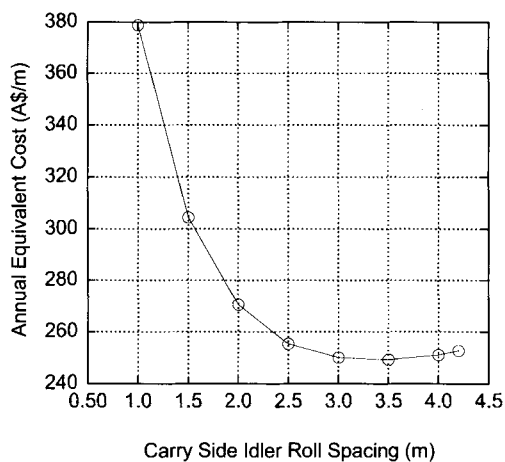


FIGURE 9 Carry side idler roll spacing versus annual equivalent cost

energy cost is calculated and added to the annual equivalent costs of major components, including the structure, belt, drives, gearboxes, idler rolls and frames, etc.

To demonstrate the capabilities of the optimization program the influence of a variety of conveyor variables will be discussed. Firstly, consider a 2 km long horizontal overland conveyor with a throughput of 2,000 t/hr transporting bulk material with a bulk density of $1,250 \text{ kg/m}^3$. The bulk material has an internal friction angle $\phi_i = 35^\circ$, conveyor surcharge angle $\delta = 20^\circ$ and a troughing angle $\beta = 35^\circ$. Figure 9 shows the variation in annual equivalent cost with carry side idler spacing, with a minimum

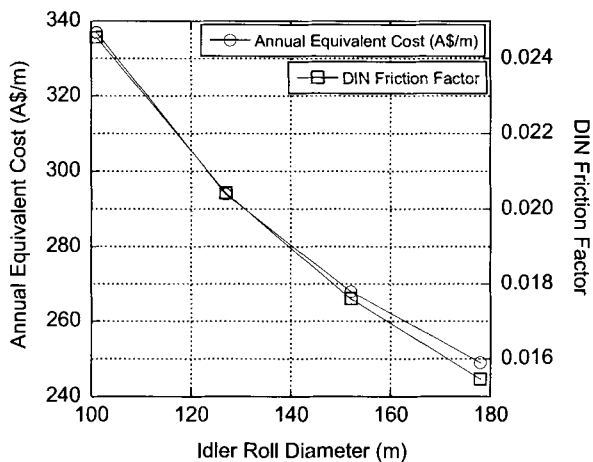


FIGURE 10 Carry side idler roll diameter versus annual equivalent cost and equivalent DIN friction factor

cost occurring at 3.4 m. The optimized solution is a conveyor with a belt width of 800 mm, operating at 6.2 m/s with idler roll diameters of 178 mm at a carry side spacing of 3.4 m. Trends indicate that closely spaced idler rolls result in a higher annual equivalent cost due to the larger number of idler rolls and frames, while increasing idler spacing requires higher strength belts to limit sag, resulting in increased belting costs dominating. For each solution there is a clear minimum annual equivalent cost which the optimization program determines.

Figure 10 shows a plot of carry side idler roll diameter versus annual equivalent cost and equivalent DIN friction

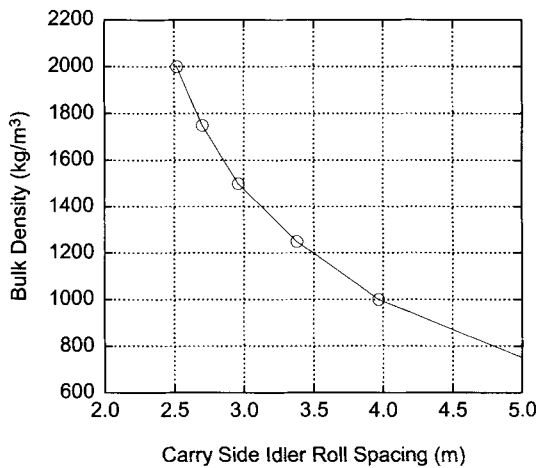


FIGURE 11. Carry side idler roll spacing versus bulk density of material

factor. The data clearly shows both the cost and motion resistance benefits of increased idler roll diameters. The two graphs show similar trends due to the reduced energy costs, with only a small divergence occurring with larger idler roll diameters due to increased capital cost.

Figure 11 shows a plot of the optimized carry side idler roll spacing versus bulk density for a 2 km long horizontal overland conveyor with a throughput of 2,000 t/hr and a belt width of 800 mm. The results show that as the bulk density increases the optimum carry side idler roll diameter decreases. As bulk density increases, an alternative solution would be to maintain large idler roll spacings and increase belt tensions to retain acceptable sag ratios. However in this case, the cost of higher strength belting dominated the additional cost of idler rolls and frames and as such the program optimized the solutions by reducing belt strength.

When considering the results presented, it should be noted that the costs are included for relative, rather than absolute comparison only, since they do not consider full

system costs. Similarly, costs will vary from one installation to another due to variations in labor costs, location, civil works, etc.

CONCLUSION

This paper has provided an overview of a numerical evolutionary optimization method applied to the design of belt conveyor systems. The optimization process presented focuses on reducing the life cycle cost of belt conveyors by selecting variables to minimize the total operating and capital costs expressed as annual equivalent costs over the life of the installation.

REFERENCES

- [1] Wheeler, C.A., Analysis of the Main Resistances of Belt Conveyors, PhD Thesis, The University of Newcastle, Australia, 2003.
- [2] Roberts, A.W., Harrison, H., and Hayes J.W., Economic Factors Relating to the Design of Belt Conveyors for Long Distance Transportation of Bulk Solids, *Bulk Solids Handling*, Vol. 5, pp. 1143–1149, 1985.
- [3] Wheeler, C.A., and Ausling, D., *Evolutionary Belt Conveyor Design*, Beltcon 14, Johannesburg, South Africa, August 1–2, 2007.
- [4] Wheeler, C.A., and Ausling, D., Reducing Life Cycle Costs of Belt Conveyors, *Proc. 9th International Conference on Bulk Materials Handling*, Newcastle, Australia, Oct. 9–11, 2007.
- [5] Wensrich, C.M., Evolutionary Optimisation in Chute Design. *Powder Technology*, Vol. 138, pp. 118–123. 2003.
- [6] Wensrich, C.M., and Wheeler, C.A., Evolutionary Optimisation in Loading Chute Design. *Proc. 8th International Conference on Bulk Materials Storage, Handling and Transportation*, University of Wollongong, Australia, July 5–8, 2004.
- [7] Krause, F., and Hettler, W., Die Belastung der Tragrollen von Gurtförderern mit dreiteiligen Tragrollenstationen infolge Fördergut unter Beachtung des Fördervorganges und der Schüttguteigenschaften, *Wissenschaftliche Zeitschrift der Technischen Hochschule Otto von Guericke*, Magdeburg, Germany, Heft 6/7, 18, pp. 667–674, 1974.
- [8] Ilic, D.D., Wheeler, C.A., and Roberts, A.W., Experimental Investigation of Bulk Solid and Conveyor Belt Interactions, *Australian Bulk Handling Review*, Vol. 12, No. 6, 2007.

.....

Dynamics of Long Belt Conveyors with Distributed Drives

G. Lodewijks* and **A.J.G. Nuttal***

Today most belt conveyors used for the transportation of bulk solid materials are driven in a centralized way with all drives in one location. The dynamics of these systems has been studied since the early seventies of the previous century and are well understood. Compared to the more conventional belt conveyor system with a centralized drive station positioned at the head and/or tail of the system, a decentralized driven layout with drive stations distributed along the whole length of the belt offers a number of advantages. However, to make a decentralized driven configuration a good alternative to a centralized driven, the system designer will have to balance these benefits with the increased complexity. The full potential of a decentralized driven system can only be realized if the right balance is found between the locally applied drive force and the motion resistances occurring along the system. From previous research it was found that in a multiple driven belt conveyor system the most dominant belt behavior occurs in the belt section between the tensioning device and the first drive station. In this paper different possibilities are analyzed to improve this dominant belt response and optimize the starting behavior. This can be accomplished by changing the predescribed start up profile, starting the drive stations in sequence rather than all at the same time and altering the locations of the drive stations.

INTRODUCTION

Worldwide belt conveyors are the most favorable transport system when it comes to moving bulk solid materials overland, especially in areas where infrastructure, such as road, is underdeveloped or non-existent. Although the basic belt conveyor configuration, with an endless belt spanned between a head and a tail pulley and supported by idlers, plates or air, is a well proven concept, the ever increasing bulk transport requirements continually press belt conveyor technology to its very limits. The desire to carry higher tonnages over longer distances and more diverse routes, while keeping exploitation costs as low as possible, has not only fuelled technological advances in the field of technical design, but in the field of monitoring system health, and dynamic analysis and simulations for optimal design as well. An interesting development in the recent past is the distribution of drive power along the path of the belt conveyor.

Initially, the idea of distributing drive power along the length of the belt conveyor found its way into the mining industry. Due to a growing trend in mining efficiency production capacity and transport distances, the required drive power and belt strength surpassed that of what had ever been used underground before. This development combined with the fact that the mining equipment is

continually moved with the progressing mining face gave rise to a number of conveyance concerns. Problems included the large size of high power drives and the inability to move them around. Although belting technology could have handled the increased strength requirements, it also meant moving from fabric to steel reinforced belting that was much harder to handle and required time consuming vulcanized splicing to connect new sections of belt to the system [1]. With the introduction of intermediate drives the required belt strength and drive unit size was reduced and by combining this with a belt take-up device with integrated belt storage, belt conveyor equipment had become flexible enough to solve the before mentioned problems. Figure 1 shows examples of drive configurations that turn the conventionally centralized driven flat or troughed conveyor into a decentralized driven system.

The first configuration in Figure 1A is the tripper. In this configuration the belt is wrapped around two additional drive pulleys in the carrying strand of the conveyor. To create a sufficiently large wrap angle (required to apply the desired drive force) while keeping the belt traveling in the same direction, the belt has to discharge the bulk solid material onto itself. This additional transfer is

* Delft University of Technology, the Netherlands.

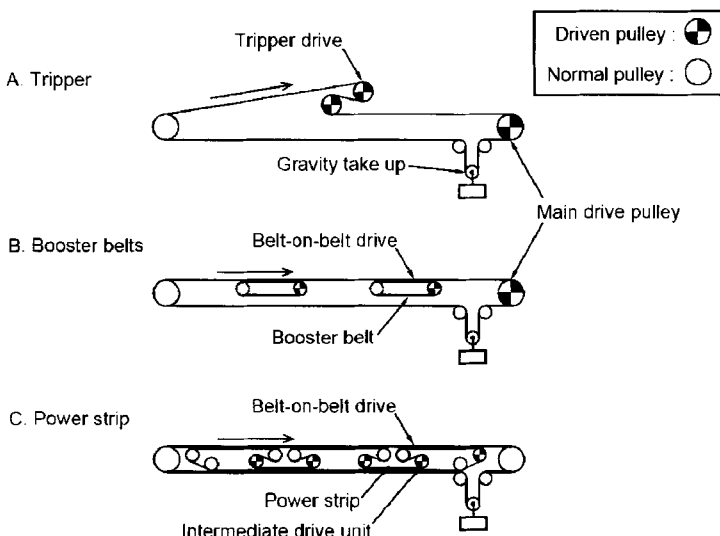


FIGURE 1 Different concepts of decentralized driven belt conveyors

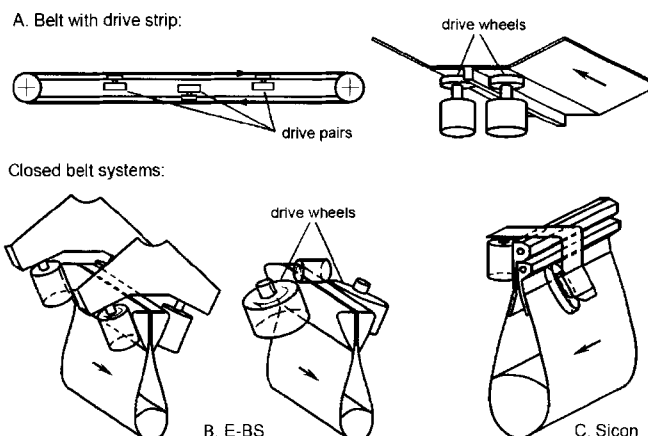


FIGURE 2 Special belt conveyors featuring decentralized drives

also the downside of the tripper drive configuration as it is a source for dust, spillage, belt surface wear, and it costs energy. The belt-on-belt drive configuration, where the main carrying belt rests on a smaller dedicated drive belt, does not interfere with the flow of material on the belt because it requires no transfer. In this case the weight of the bulk solid material and carry belt pressing down on the drive belt generates a friction based drive force. Figure 1B and 1C present two different variants of the belt-on-belt principle. The first variant is the booster belt configuration that has a number of small belt conveyors built inside the larger conveyor. In the second variant the double function a conveyor belt normally has to fulfill, both carrying the bulk solid material and transmitting the drive force, is effectively separated. This is achieved by placing a centralized drive belt or power strip within the main conveyor. With the power strip spanning a large part of the system length, the main carry belt is subjected to very low drive forces and can have much lighter construction. In this configuration decentralized drive

stations can be introduced without interfering with the material flow on the carry belt, as shown in Figure 1C.

A more recent development is the design and construction of special belt conveyors with highly flexible layout capabilities that inherently feature intermediate drive stations. Due to the special characteristics involved in such systems, they have been developed with the utilization of decentralized drives in mind, making it possible to offer systems with relatively light standardized belts, compact drive units and a light support structure. Figure 2 shows examples of these special belt conveyor systems.

The first system, proposed by Bekel [1] and shown in Figure 2A, consists of a more conventional trough shaped belt conveyor that has a special drive strip vulcanized to its bottom cover, acting as a drive rail. To apply traction, two motors with drive wheels press onto each side of the strip. The main idea behind this configuration is to have a trough shaped belt with a relatively low strength, so it can flex easily in horizontal curves, making it possible to

negotiate sharp radii. The second and third systems are two different types of pouch shape belt conveyors that completely enclose the conveyed material. In the Enerka-Becker System (or E-BS), shown in Figure 2B, triangular profiles have been vulcanized to the edges of a flat belt. When the belt is folded and closed at the top, the profiles form the running surface for the supporting rolls or idlers as well as the drive wheels. With this configuration the drive units can be placed at virtually any location along the belt. The drive units in the Sicon pouch belt conveyor system, shown in Figure 2C, cannot be placed as freely. The edges of this belt overlap at the top when the belt is folded and form a double v-shaped profile on one side of the pouch. This double v-shaped profile is used to wrap the belt around a drive or horizontal cornering pulley. Due to the fact that the Sicon belt has to be wrapped around such a drive pulley, the placement of drive units directly affects the layout of the system and has to be taken into account when designing the system.

The dynamics of belt conveyors with distributed drives was discussed extensively in [2]. From this paper it was clear that in a multiple driven belt conveyor system the most dominant belt behavior occurs in the belt section between the tensioning device and the first drive station. In this paper different possibilities are analyzed to improve this dominant belt response and optimize the starting behavior. This can be accomplished by changing the predescribed start up profile, starting the drive stations in sequence rather than all at the same time and altering the locations of the drive stations.

START-UP PROFILE

In [2] only one type of single start up of curve was implemented based on Harrison's [3] start up profile. When using the Harrison's start up profile the belt speed v_b is ramped up during starting time T_a as follows:

$$v_b(t) = \frac{v_{b,t}}{2} \left(1 - \cos\left(\frac{\pi t}{T_a}\right) \right), \quad 0 \leq t \leq T_a \quad \text{EQ. 1}$$

where $v_{b,t}$ represents the target speed. For the simulations the belt speed profile is converted to a ramp up curve for the AC drive motor's supply frequency. This is required because the simulated belt conveyor system is controlled in an open loop manner. In this simple control strategy, often applied to belt conveyor systems, the synchronous speed of the drive motor increases linearly with the applied supply frequency. Due to the stiff torque-slip characteristic of the AC drive motor and the gradual speed increase the drive motor will closely follow the synchronous speed. With Harrison's start up profile the acceleration changes continually, creating a smooth transition to the belt conveyor's operational speed and at the halfway point of the start up procedure the acceleration reaches its highest peak. This peak in acceleration also causes a peak in drive force and belt tension at about the same time. To analyze if it is possible to reduce these peak values, Harrison's profile is altered and split into three parts. In the first part speed is ramped up smoothly with a cosine function. This followed by the second part where the acceleration remains constant. In the last part the acceleration is smoothly ramped down again. In Harrison's case the first part is directly followed by the last part at the halfway point of the start procedure. In the altered case the formulas for each part of the

speed profile are setup in such a manner that the duration of the acceleration smooth in and out can be altered. This leads to the following equations for the ramp up of the stator supply frequency f_s .

$$f_s(t) = \begin{cases} c_1 \left(1 - \cos\left(\frac{t}{2t_1}\pi\right) \right) & 0 \leq t \leq t_1 \\ c_2 t + c_3 & t_1 \leq t \leq t_2 \\ c_4 - c_5 \cos\left(\frac{T_a - t}{2(T_a - t_2)}\right) & t_2 \leq t \leq T_a \end{cases}, \quad \text{EQ. 2}$$

where t_1 represents the smooth in time and t_2 indicates at which point in time the smooth out starts. The values of constants c_1 to c_5 depend on both t_1 and t_2 and they are calculated based on the fact that the acceleration and speed profile at t_1 and t_2 has to be a continuous function and that at T_a the speed profile has to reach the target speed. This leads to a set of 5 equations that can be solved linearly. To investigate the effect of the start curve's shape, a similar approach is applied to Nordell's [3] start up profile. This second order polynomial used to describe this start up curve in this case is also split into three parts, which results in the following set of equations:

$$f_s(t) = \begin{cases} c_1 t^2 & 0 \leq t \leq t_1 \\ c_2 t + c_3 & t_1 \leq t \leq t_2 \\ c_4 t^2 + c_5 t + c_6 & t_2 \leq t \leq T_a \end{cases}, \quad \text{EQ. 3}$$

This set of equations requires an additional condition to find the appropriate values for the constants c_1 to c_6 . This condition states that the acceleration should be zero at the end of the start up procedure. Note that when t_1 and t_2 are both set to $\frac{1}{2}T_a$ the original Nordell curve is revealed and when t_1 is set to zero and t_2 to T_a a linear curve results. Figure 3 illustrates a number of examples that are produced when different values are chosen for t_1 and t_2 in equation set (2) and (3). The solid line in the right diagram represents Nordell's original profile, while the one in the left diagram represents Harrison's profile. Also note that both original profiles have a steeper maximum gradient than the derived curves of which the linear curve has the smallest gradient. This indicates that the original curves have the highest peak acceleration. In both diagrams a start up time of 60 seconds is employed because the multiple driven configuration with a belt length of 4 km and a drive spacing of 1 km is used to simulate the effect of the different start up profiles.

The start up of the 4 km belt was simulated with t_1 and t_2 ranging from 0 to 60 seconds where t_2 is always larger than t_1 . For each simulated result the minimum and maximum belt stress values were picked out and stored together with the peak belt acceleration and the applied drive force. Figure 4 presents the result for the Harrison based cosine start up profiles. In this figure the horizontal axis of each diagram indicates the magnitude of the smooth in time t_1 , while the vertical axis indicates the smooth out time, which is equal to the time interval between t_2 and T_a .

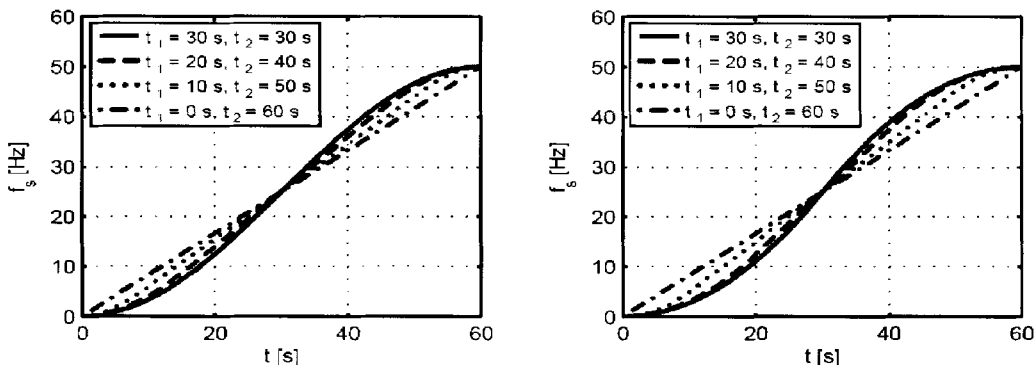


FIGURE 3 Start curve shapes with cosine (left) and polynomial (right)

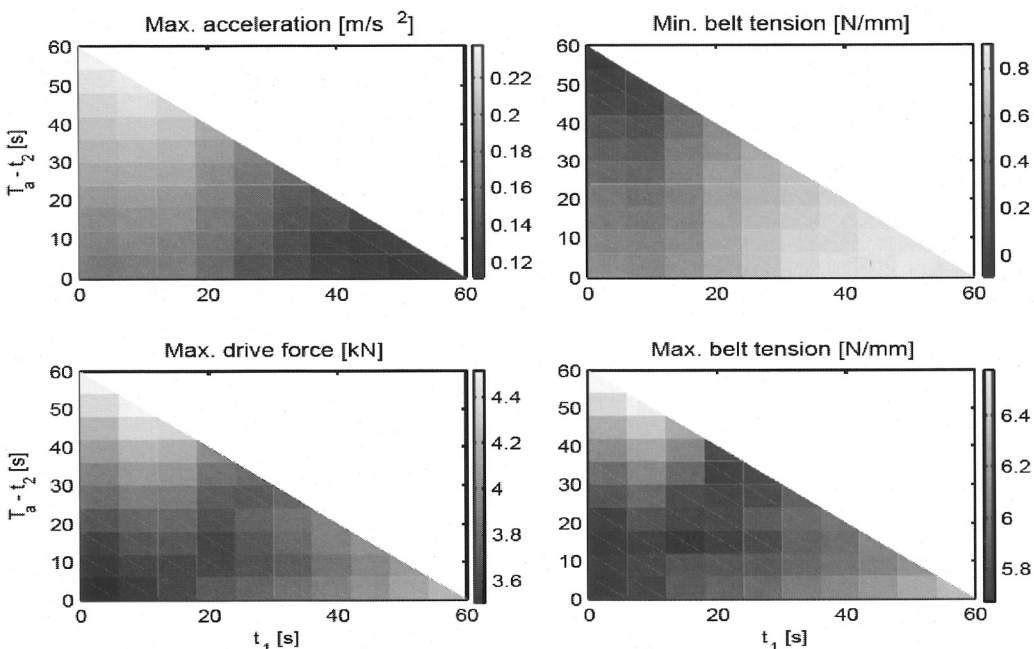


FIGURE 4 Effect of varying smooth in and out time for cosine based start profile

The lowest peak acceleration occurs when the smooth in time is maximized, indicated by the dark area on the right side of the maximum acceleration diagram. This is a result of the fact that a more gradual ramp up at the beginning of the start up reduces the initial overshoot, which occurs when the stator frequency reaches the value where the drive motors overcome the static friction. This effect is also favored when the minimum belt tension is considered because it drops the least when the smooth in time is large. However, this is not the case when the maximum drive force and belt stress are considered. The bottom diagrams in Figure 4 show that the lowest peaks for these quantities occur when the length of the smooth in and out time are balanced. This is indicated by the dark areas that occur near the line where the smooth in and out time are equal. Consequently, Harrison's original start up profile, where both t_1 and t_2 are equal to 30 seconds, generates one of the most desirable system responses.

Figure 5 presents similar results for the polynomial start up profiles. However in this case the diagrams show a slightly higher maximum acceleration, drive force and belt stress. This is a result of the fact that the polynomial based profile curve has a higher peak acceleration compared to a curves derived from Harrison's start up profile. Further, Figure 5 also shows that the most optimal situation with regard to the belt acceleration and minimum belt tension does not occur at the maximum smooth in time. In this case the optimal point lies somewhere in between a smooth in time of 35 and 40 seconds. Looking at the maximum drive force and belt tension the lowest values are also found for a balanced smooth in and out time, but now the darker area has shifted more towards the point where both times are shorter. As a result, the polynomial defined by Nordell, where t_1 and t_2 are both set to 30 seconds, does not produce the most optimal system response in this case. The system response improves when a smooth-in time of approximately

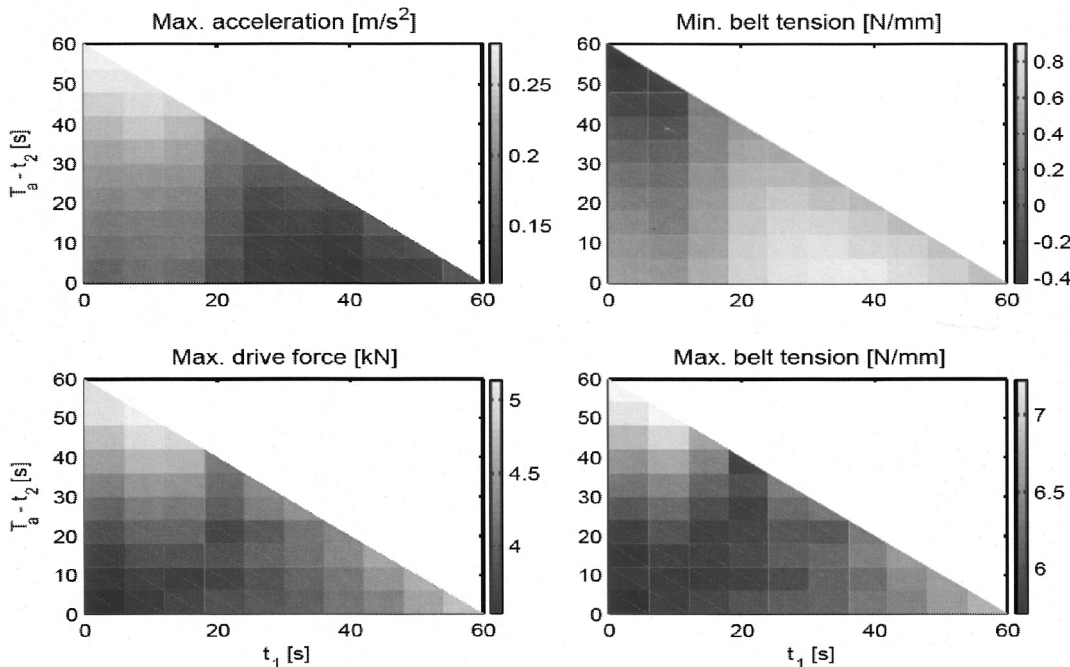


FIGURE 5 Effect of varying smooth in and out time for polynomial start profile

20 seconds is chosen together with a smooth-out time of 10 seconds. Note that these settings depend on the characteristics of the system and the chosen start up time. A different selection of the smooth in and out time may produce better results for other cases.

From the presented results it can be concluded that alterations made to the shape of the start up profile can improve a belt conveyor system's response. Slight improvements can be made with profiles like those defined by Harrison and Nordell by altering the smooth in and out time. Although Harrison's original profile already produces a satisfactory result, different values are recommended for Nordell's profile when it is used to start up the 4 km belt conveyor system with a drive-spacing of 1 km. The simulation result also show that Nordell's profile causes a slightly higher peak drive force and belt tension compared to Harrison's profile. Lodewijks [3] also observed this phenomenon and he attributed it to the higher peak acceleration present in Nordell's speed profile.

SEQUENCED STARTING

The simulations presented up until this point show that it is possible to successfully start up a multiple driven belt conveyor system in an open loop manner by applying a speed profile to each drive station. During the acceleration phase each drive station receives exactly the same power input signal. With this simple control strategy the maximum applied drive force and belt stress does not change significantly when the system length is increased, while keeping the same drive spacing. However, the simulations in [2] also showed that the minimum belt tension decreases when the system scale increases increase. This is especially true for multiple driven systems with large motor stations. To prevent the belt tension from falling below the minimum required opera-

tional tension, it is possible to increase the pretension in the belt. Opting for this solution does have a downside because the maximum belt stress will also increase when the pretension is increased. Another option is to implement a sequenced start up procedure. The idea behind the sequenced start up procedure is that a drive station is not started until the acceleration wave generated by the previous drive station has reached it. As the initial acceleration wave passes a drive station that is not started, the local belt tension tends to increase. Consequently, if this drive station is started exactly at the time when the belt tension would start to increase, it is possible to compensate the fall in slack side belt tension. The drive station located directly next to the gravity take up device has to initiate the acceleration because the tensioning device will guarantee a near constant minimum belt tension. In the case of the multiple driven configuration with 4 km and 4 drive stations this would mean that drive station D_4 , which is the drive station nearest to the head in the carry strand, is started first. As it is started, an acceleration wave begins traveling towards drive station D_3 . When this acceleration wave reaches D_3 , this drive station is also started. Similarly, drive station D_2 and D_1 are started sequentially as the wave also passes them in turn.

Initially, each drive station has to follow the same speed up ramp when they are started. Due to the fact that the previous drive station has already been running for a while before the following drive station is started, a speed difference will occur between the different stations, with D_4 running the fastest and D_1 the slowest. To get them all running at a synchronous speed at the end of the start up procedure a special sequencing strategy is adopted.

Figure 6 illustrated the principle behind this strategy. In this figure the left diagram shows how the initial acceleration wave travels through the system. The sequence

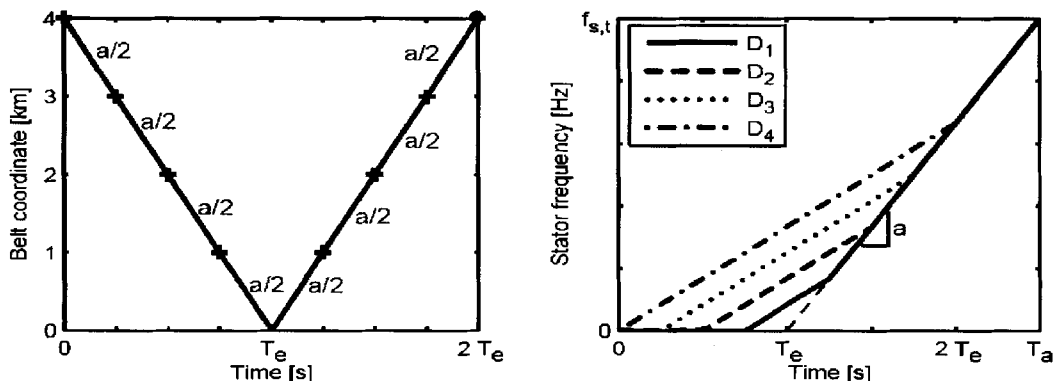


FIGURE 6 Start ramp for simple sequenced start

starts with the direct speed ramp up of drive station D₄. The initial acceleration is half of what will become the final acceleration. As a result, an acceleration wave with magnitude $\frac{1}{2}a$ starts to travel towards the other end of the system. When this wave reaches the other drive stations they also start accelerating at $\frac{1}{2}a$. After the wave passes the last drive station D₁ and it reaches the tensioning device at time T_e, it is reflected and it travels back through the system. To synchronize the drive station, the acceleration of each drive station is increased to its final value a when the reflected wave passes each drive in reverse order. The right diagram illustrates the resulting frequency profiles that will be applied to each drive station. This diagram clearly shows that the initial sequenced start with half the end acceleration causes an offset between the profiles. This difference disappears when the acceleration is further increased as the reflected wave passes each drive station. After the reflected wave reaches drive station D₄ again, all drive stations will be accelerating at the same rate until the end of the start up procedure, where the target speed is reached and the acceleration is removed.

With the aid of the diagram on the right of Figure 6 it is possible to determine the magnitude of the final acceleration, so the target frequency f_{s,t} is reached at the end of the start up procedure. For this sequenced strategy the acceleration is calculated as follows:

$$a = \frac{f_{s,t}}{(T_a - T_e)} \quad \text{EQ. 4}$$

Note that the start up time T_a has to be at least twice as long as T_e. This guarantees that all drive stations are synchronized before the end of the start up procedure is reached. To be able to use this sequenced start up, the acceleration wave has to occur the moment the supply frequency of drive station D₄ is increased. However, as observed in previous simulations, the drive stations do not directly apply the required drive force to initiate the acceleration of the belt. As a result, a delay occurs before the belt is set into motion. This delay is undesirable when adopting a sequenced strategy because such a strategy relies on a precise timing between passing of the initial acceleration wave and the start of each drive station. To compensate for this delay, the stator frequency of all drive stations is initially ramped up quickly to a low frequency, so the drive stations will already start

applying the minimum force required to set the belt in motion. After a short delay that allows the system to settle down from the step in drive force, the main sequence is started. Figure 7 presents the result of the sequenced starting procedure for the 4 km multiple driven configuration with a drive spacing of 1 km. The upper left diagram shows the stator frequency supplied to each drive station. It clearly illustrates the initial increase in frequency before the starting sequence is applied after 7 seconds. In the upper right diagram drive station D₄, which is started first, delivers the most work during the starting procedure. It produces an even higher peak tension than was found when the drive stations were started simultaneously, see [2].

Drive station D₄ clearly delivers the most work and the more a drive station is removed from D₄ the smaller the delivered effort. The last drive station D₁ only applies a larger drive force after its acceleration is increased to the final value. This contrary to the initial expectation that drive station D₁ would increases its effort directly after it is commanded to start acceleration at $\frac{1}{2}a$. However, as the initial acceleration wave, emanating from the previous drive stations, already forces the belt to accelerate at $\frac{1}{2}a$, drive station D₁ hardly has to apply any addition effort to guarantee its imposed start up profile. Up until drive station D₁ also increases its effort drive station D₄ and D₃ are mainly acceleration the belt. As the lower right diagram of Figure 7 shows, this imbalance in drive force causes a significantly higher belt tension than observed in previous simulations. The minimum belt tension now also increases rather than decreases when the sequence starts, so as expected low belt tensions should pose no problems in this case. A small dip in tension only occurs before the sequence due to the required initial frequency offset. The lower left diagram shows the belt acceleration along the belt as a function of time. In this diagram the initial acceleration wave is clearly visible. After the initial frequency offset it appears at drive station D₄ the moment the main starting sequence begins. At 20 seconds the wave arrives at the other end of the belt where it reflects and travels back through the system. After the reflected wave reaches drive station D₄ again, the belt accelerates at a constant rate until the end of the start up procedure. At the end the acceleration is removed suddenly, which causes residual oscillations. A smooth-out could be implemented

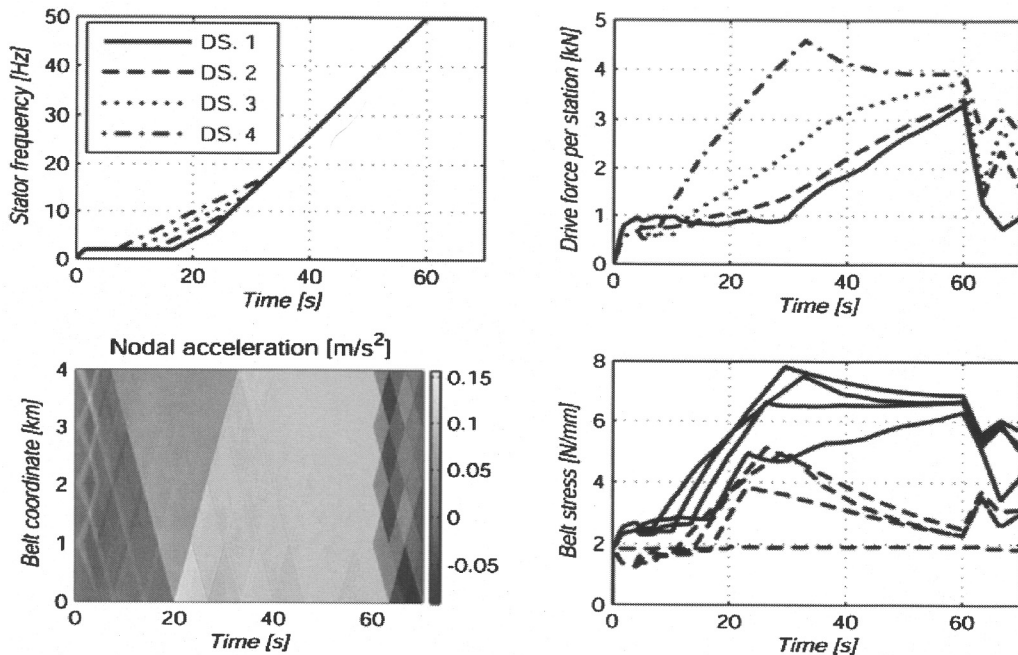


FIGURE 7 Simulation results of a simple sequenced start

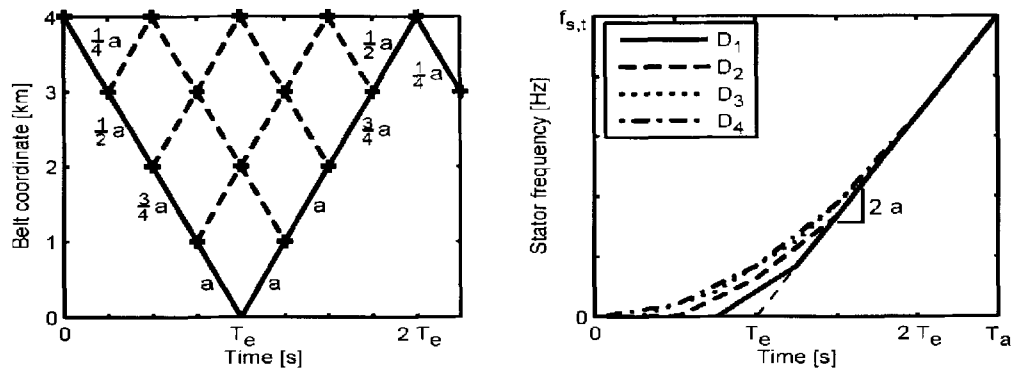


FIGURE 8 Start ramp for simple sequenced start

to prevent this from happening. From the presented results it can be concluded that a sequenced start up procedure will prevent the belt tension from falling below the minimum required belt tension. However, the adopted sequencing strategy also generates a significant imbalance of the work delivered by each drive station. The drive station that initiates the acceleration wave applies the most drive force because the other drive stations have to add little extra power when they are started with the same acceleration as the wave passing them. As a result of the imbalance in drive power the peak belt tension increases undesirably. To prevent the imbalance in power, while keeping the positive effect for the minimum belt tension an alternative sequenced start up is proposed.

Figure 8 presents the principle idea of this alternative strategy. Instead of having an initial acceleration wave that does not change in magnitude as it travels through the system, the acceleration is increased each time it

passes a drive station. As the left diagram in Figure 8 depicts, drive station D_4 initially starts accelerating at a rate of $\frac{1}{4}a$. Each time the generated acceleration wave reaches a drive station the acceleration is increased with $\frac{1}{4}a$. The idea behind this is that each drive station will be forced to apply at least the drive force to achieve the additional acceleration. However, the increase in acceleration also generates an acceleration wave in opposite direction of $\frac{1}{4}a$. These waves are indicated by the dashed lines. To account for these additional waves, the acceleration is further increased with $\frac{1}{2}a$ each time one of the dashed lines crosses the location of a drive station. After the initial acceleration wave has reflected at the tensioning device the magnitude of the wave is decreased in steps of $\frac{1}{4}a$ when it passes drive station D_3 again. This allows a gradual and controlled reduction of the wave's magnitude.

At the end of the start up procedure drive station D_4 will have increased its acceleration 5 times, first with $\frac{1}{4}a$

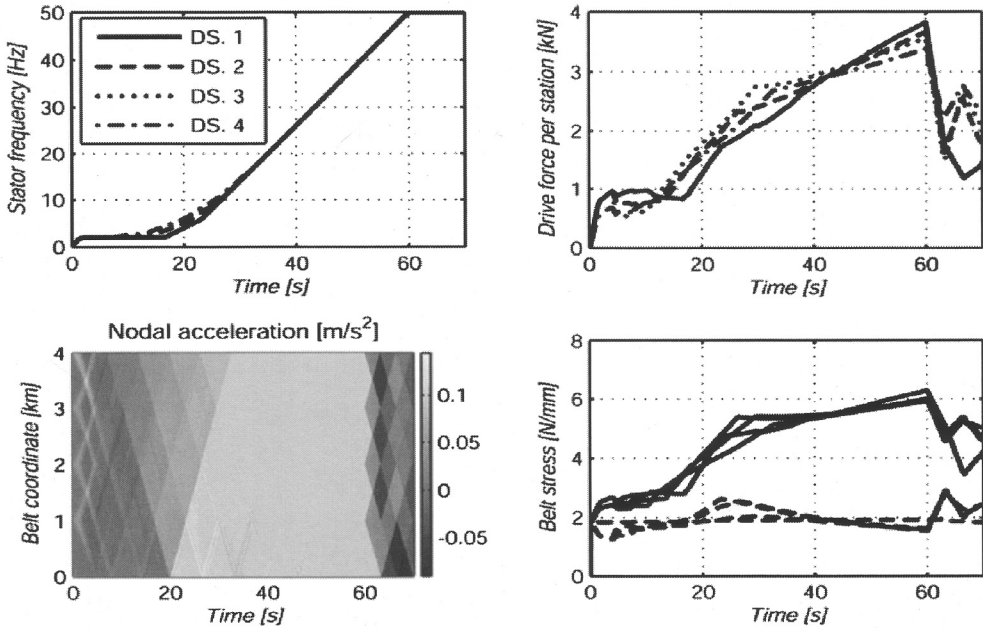


FIGURE 9 Simulation results of a complex sequenced start

than 3 times with $\frac{1}{2}a$ and finally with $\frac{1}{4}a$ again. Therefore, the final acceleration is equal to $2a$. Drive station D_1 also reaches the same final acceleration, but it accomplishes this with two equal steps. The right diagram in Figure 8 presents the resulting speed profiles for each drive station. Note that the speed differences in this case are significantly smaller than for the simple sequenced start in Figure 6 and that the required acceleration expressed in the stator frequency is now calculated as follows:

$$a = \frac{f_{s,t}}{2(T_a - T_e)} \quad \text{EQ. 5}$$

Figure 9 presents the results for the complex starting sequence. The upper left diagram shows the applied stator frequency profiles with the initial offset that was also used for the simple sequence to get a well defined start of the acceleration wave. The improvement that is obtained with these frequency profiles is observable in the upper right diagram because it shows that the drive stations apply about the same amount of work during the start up procedure. Therefore, the imbalance has become significantly smaller and the belt stress peaks much lower than with the simple starting sequence in the lower right diagram. The minimum tension does also not fall as much. However, in this case the belt tension does drop below the pretension force at the end of the start up procedure, but it does not fall below than the minimum tension caused by the initial frequency offset applied at the beginning of the procedure.

The results show that the more complex starting sequence can guarantee the minimum tension, while it only produces a slightly higher belt tension compared to the case where an s-curve is applied simultaneously, see [2]. It is even expected that the difference in peak tension between both cases can be decreased by also adding a smooth out period at the end of sequenced start

up profiles. To analyze the scalability of the sequenced start up strategy, different belt lengths, ranging from 2 to 8 km, were simulated with a motor spacing of 1 km. For each simulation the peak drive force and belt stress were analyzed and stored. Figure 10 present the results of this exercise for the simultaneously applied Harrison profile, the simple sequenced and complex more balanced sequenced starting strategy.

The result shows that the simple sequenced starting strategy already starts experiencing difficulty when the system becomes longer than 3 km because from this point on both the peak drive force and belt stress start to increase. At a belt length of 6 km it even causes the drive force to reach the friction limit. Note that the left diagram only shows the maximum occurring drive force. Not all drive station will reach the friction limit and it will only be reached during a certain time. For systems longer than 6 km the severity of the occurring friction limit will still increase as the system length increases. Therefore, the belt tension shown in the right diagram will still rise. The balanced sequenced starting procedure performs nearly as good as the simultaneously applied s-curve with respect to the peak drive force and belt tension. However, for belt lengths beyond 5 km both values start to increase, but at a lower rate compared to the simple sequenced start up. Although both sequenced starting strategies do cause an increase in the maximum belt stress, the minimum occurring belt stress remains constant contrary to the falling stress in the simultaneous controlled approach. In conclusion, the balanced sequenced start up could have an advantage up to a belt length of 5 km, beyond this length it will have to be considered if the increase in belt tension falls within an acceptable range. If the tension rise is too large, either the starting sequence will have to be improved or the simultaneous controlled strategy will have to be adopted, most probably with an increased pretension force to guarantee the minimum required belt tension.

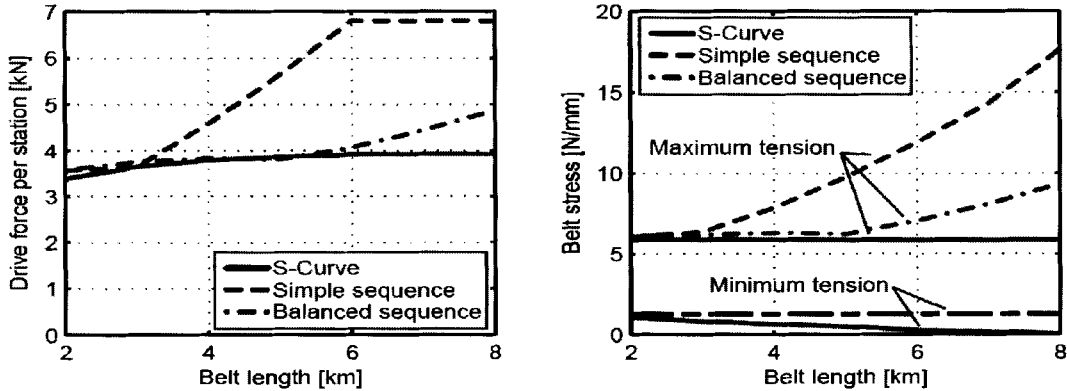


FIGURE 10 Performance of starting strategies for different belt lengths

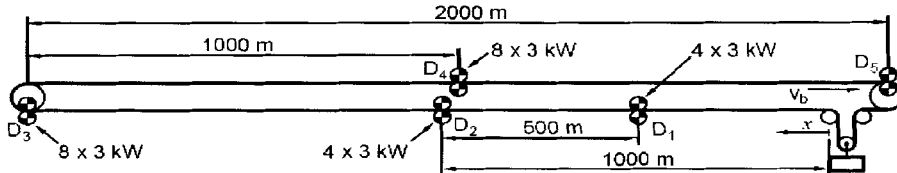


FIGURE 11 Layout with two smaller drive stations near gravity take up device

LAYOUT ALTERATIONS

Apart from changing the start up profiles to improve the belt's start up response, as discussed in the previous chapters, it is also possible to influence the dynamic belt behavior by altering the layout of the multiple driven belt conveyor configuration. [2] also revealed that during a simultaneous start up procedure the most dominant belt behavior occurs in belt section between the tensioning device and the first drive station, regardless of the belt length. This is due to the fact that the drive station at this location has to accelerate the longest section of belt. Therefore, an attempt is made to reduce the dominant behavior in this part by shortening the distance between the gravity take up device. Figure 11 illustrates a possible solution to shorten the belt section near the gravity take up device. The figure shows the 4 km multiple driven belt system with most drive stations spaced at 1 km, accept for the two located after the gravity take up device. For these drive stations the spacing is halved together with their installed drive power. Where the other stations have 8 times the nominal power of an E-BS drive motor, these drive stations only have 4 times the nominal power of a single motor. This is sufficient because these drive stations now only have to drive 500 m of belt during normal operation. As a result, the redistribution of the installed drive power has effectively halved the distance between the gravity take up device and the first drive station.

Figure 12 presents the simulation results of the altered configuration, when it is started in 60 seconds with Harrison's speed profile. If these results are compared with those of the unaltered configuration, see [2], it is clearly visible that there are no oscillations anymore. The peak drive force and belt stress that occurred at drive station D₁ have now also gone and have been replaced by the much lower values produced by the smaller drive

stations. The unaltered drive stations deliver about the same effort in both cases. Consequently, the removal of the dominant belt behavior causes a significant reduction in peak belt stress together with a smoother start up procedure. Instead of having a peak belt stress of approximately 6 N/mm the peak stress now only just passes 5 N/mm. Although the system becomes slightly more complex due to the higher motor count and the use of a large and small drive station type, the resulting reduction in required belt strength could compensate for the additional costs, making this modified configuration an interesting alternative.

Another alternative is to shift all drive stations towards the tensioning device, so the belt section between the first drive station D₁ and the tensioning device becomes equal to the distance between the last drive station D₄ and the head pulley. Figure 13 presents the resulting system configuration. In the system with a motor spacing of 1 km the length of the belt section before and after the tensioning device is now equal to 500 m. This effectively halves the length of the section with the dominant belt behavior and actually creates a symmetrical system. With no drive station located directly next to the tensioning device, special measures have to be taken to prevent the belt tension from falling to far during the start up procedure. When no sequenced start is adopted, a fall in tension is inevitable. Therefore, the pretension is increased to keep the minimum tension at a desired level. To see how much the pretension has to increase, the results from the simulations with a belt length of 8 km and a drive spacing of 1 km can be used, see [2]. These simulations showed that at the centre of the system the minimum belt stress drops about 2 N/mm. Consequently, the pretension is increased with this value.

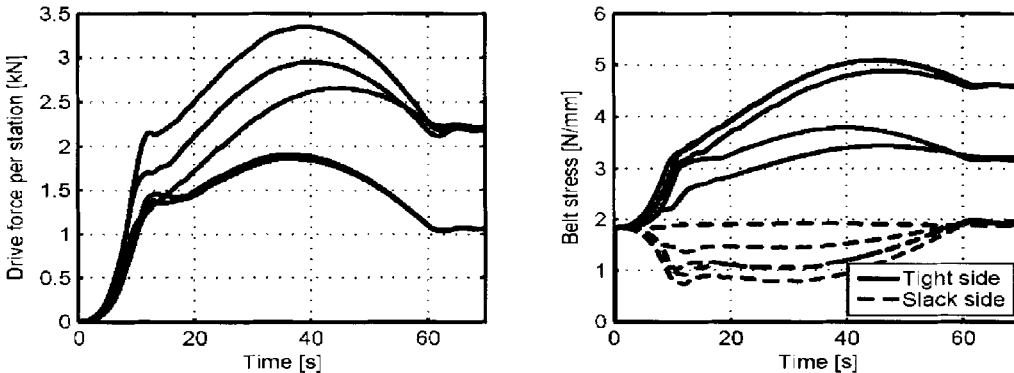


FIGURE 12 Simulation results for layout with helper drive

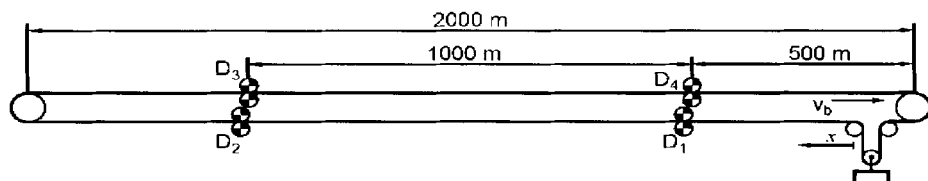


FIGURE 13 Layout with gravity take up device centered between drive stations

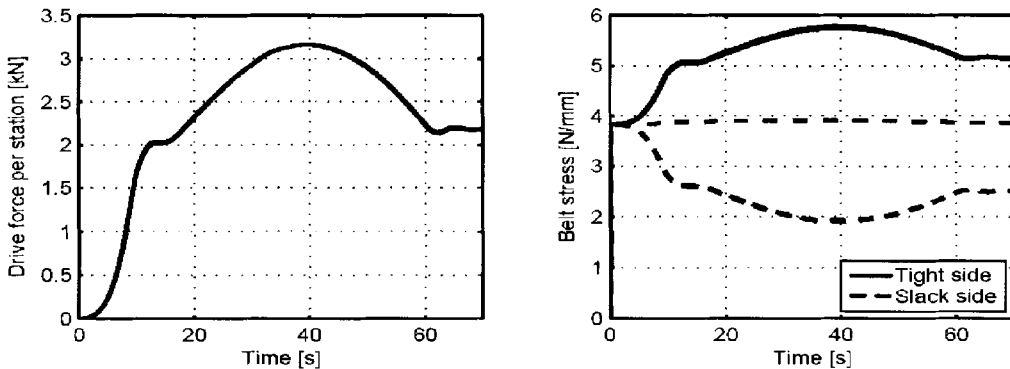


FIGURE 14 Simulation results with tension weight centered between drive stations

Figure 14 presents the results with the shifted drive station locations and the increased pretension. In this case each drive station virtually delivers the same amount of work during the whole start up procedure. This causes the overlap of the graphs for the applied drive force and belt stress. Although the pretension has been increased, the maximum belt stress is actually slightly lower than the value found during the start up simulation of the unaltered case, see [2]. The transition is also much smoother with no oscillations.

As expected the belt tension drops at the slack side of the drive stations. However, due to the increased pretension, it does not drop below the previously implemented pretension force. Even if the system length is increased, while keeping the drive spacing the same, the belt tension will not drop further because it is expected that all drive station will still generate the same drive force and belt stress graphs. Consequently, this type of

multiple driven configuration, where the first and last drive station are offset half a motor spacing away from the tensioning device and the head pulley respectively, is very appealing. Furthermore, due to symmetry of this configuration, it does not matter in which direction the belt conveyor is operated because in both directions the start up response will be exactly the same.

CONCLUSIONS

The dynamics of belt conveyors with distributed drives was discussed extensively in [2]. From this paper it was clear that in a multiple driven belt conveyor system the most dominant belt behavior occurs in the belt section between the tensioning device and the first drive station. Three ways of improving the belt dynamics during start-up were investigated: changing the pre-described start up profile, starting the drive stations in sequence rather than

all at the same time and altering the locations of the drive stations.

From the results presented in the Startup Profile section, it can be concluded that alterations made to the shape of the start up profile can improve a belt conveyor system's response. Slight improvements can be made with profiles like those defined by Harrison and Nordell by altering the smooth in and out time. Although Harrison's original profile already produces a satisfactory result, different values are recommended for Nordell's profile when it is used to start up the 4 km belt conveyor system with a drive-spacing of 1 km. The simulation result also show that Nordell's profile causes a slightly higher peak drive force and belt tension compared to Harrison's profile.

In the Sequenced Starting section, alternative starting sequences were discussed. The results show that the more complex starting sequence can guarantee the minimum tension, while it only produces a slightly higher belt tension compared to the case where an s-curve is applied simultaneously. The results show further that the simple sequenced starting strategy already starts experiencing difficulty when the system becomes longer than 3 km because from this point on both the peak drive force and belt stress start to increase. At a belt length of 6 km it even causes the drive force to reach the friction limit.

The Layout Alterations section discussed alternative drive configurations. One alternative was to use a multiple driven belt system with most drive stations spaced at 1 km, accept for the two located after the gravity take up device that are spaced at 500 m. Another alternative is to shift all drive stations towards the tensioning device, so the belt section between the first drive station D_1 and the tensioning device becomes equal to the distance between the last drive station D_4 and the head pulley. It turned out that the last configuration is the most appealing since it leads to a situation were all drives perform the same amount of work. Furthermore, due to symmetry of this configuration, it does not matter in which direction the belt conveyor is operated because in both directions the start up response will be exactly the same.

REFERENCES

- [1] Bekel, S., *Horizontalkurvengänger Gurtförderer met dezentralen Reibantrieben*, PhD Thesis, Hameln, 1998.
- [2] Lodewijks, G. and Nuttall, A.J.G., Dynamics of Decentralized Driven Belt Conveyors, *Proceedings of the 9th International Conference on Bulk Material Handling*, Newcastle, October 9–11, 2007 (to be published).
- [3] Lodewijks, G., *Dynamics of Belt Systems*, PhD Thesis, Delft University of Technology, 1996.

Applied Rubber Belt Cover Loss Prediction from Indentation

Thomas J. Rudolphi*

INTRODUCTION

Efficient transport of bulk materials by belt conveyor systems is an important engineering design issue, especially as conveyors become longer and power requirements increase. It is well known within the industry that the parasitic energy loss of a belt conveyor, due to the indentation of the idlers into the belt backing material can be upwards of half the total energy required to drive it on a horizontal flight. Other loss sources includes the rolling resistance of the idlers, belt/roller misalignments, material trampling, frictional and acceleration losses on loading, etc., but energy absorbed by indentation of the belt backing as it passes over each successive idler is the dominant power consuming factor.

INDENTATION LOSS MODELS

Models to predict the rolling resistance of a cylinder (idler) on a viscoelastic foundation (backing material) have been available for some time. As a contact problem, it is nonlinear (contact length or indentation depth is a dependent on the load and vice versa) in load/deformation response. Rubber backing material is generally assumed to behave as a linear viscoelastic solid, even though it is known that most rubber compounds retain linearity only at very low strains. Because completely general solutions are impossible, practical solutions require simplifying assumptions. Those assumptions relate naturally to two separate parts of any analytical model:

1. The **deformation** model—aspects of the problem relating to the geometry, boundary conditions and kinematics of how the material deforms.
2. The **material** model—aspects of the problem relating to the material properties, or constitutive relationships, i.e., the stress/strain relationships.

For example, a simple deformation model is to assume that the belt backing deforms like a Winkler foundation, where the backing material behaves as a set of one-dimensional elements through the thickness, each

behaving independently. By this assumption, there is no shear in the deformation model. For a simple material model it is often assumed that the backing behaves according to the simple 3-parameter Maxwell material, the so-called standard linear solid (SLS)—two springs and a dashpot in parallel.

To be specific, the early work of Jonkers [1] and Spaans [2] are both based on modeling the belt backing by a Winkler foundation. Four parameters— h , the backing thickness; D , the idler diameter; and W , the carry weigh or load per unit width of belt and the indentation depth—characterize this deformation. The material is characterized by the SLS model with storage and loss moduli E' and E'' , and hence loss tangent $\tan(\delta) = E''/E'$, that are assumed to be independent of the loading frequency. The effective rolling resistance is determined by calculation of the energy absorbed by the backing material in the loading/unloading process during one pass over the idler. The lost energy would presumably go into heating of the backing material. Slightly different assumptions about how the energy per cycle is determined leads to slightly different results, but Jonkers' is representative and gives an indentation resistance factor,

$$f = \left(\frac{Wh}{E'D^2} \right)^{\frac{1}{3}} \frac{\pi}{2} \tan(\delta) \left[\frac{(\pi + 2\delta) \cos(\delta)}{4\sqrt{1 + \sin(\delta)}} \right]^{\frac{4}{3}} \quad \text{EQ. 1}$$

It is observed that this Winkler foundation/energy absorbed per cycle approach produces an indentation resistance factor proportional to $\tan(\delta)$. Thus, as might be expected, the loss tangent $\tan(\delta)$ is the important parameter in the rolling resistance factor.

As a more exact deformation model, Hunter [3] and May, et al. [4], presume the belt backing to be a two-dimensional viscoelastic half-plane, which, unlike and more general than the Winkler model, allows for shear deformation. In distinction to the Jonkers' and Spaans' approach these models calculate the rolling resistance by direct determination of the backing/idler interface stress,

* Iowa State University, Ames, Iowa.

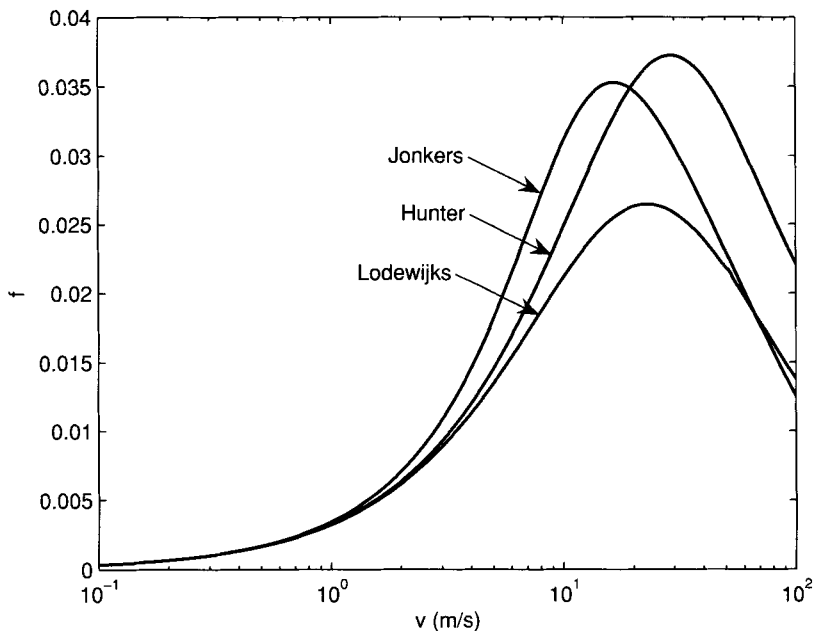


FIGURE 1 Indentation resistance by three methods with an SLS material model

assuming frictionless contact, and the moment of that normal stress about the idler axis. The rolling resistance is thus determined by the moment of the interface stress about the idler bearing. However, as based on a semi-infinite region, the backing thickness h is not inherently involved. The material model used by both Hunter and May is the simple three-parameter SLS.

This latter determination of the indentation resistance through the moment of the interface pressure is a more direct than the energy absorption approach of Jonkers and Spaans, since it circumvents the assumption of the lost energy per cycle absorbed by the backing by direct calculation of the moment of the interface stress. However, extension of this two-dimensional deformation model to more sophisticated materials beyond the relatively simple SLS, and finite backing thickness, is considerably more difficult. Full two-dimensional models with finite backing thickness require the solution of coupled integral equations as that of Margetson [6] or totally computational approaches such Wheeler [7] by finite elements or of Qiu [8] by boundary elements. The disadvantage of these numerical approaches is that solution dependence on critical parameters like roll radius, carry weight, backing thickness, etc., cannot be separated out explicitly as in equation (1).

Lodewijks [5] took an intermediate approach by using the Winkler foundation model for the backing, but determined the interface pressure between the roller and backing while using the SLS material model. This method is readily generalized to a more realistic material model and that has been done by Rudolphi and Reicks [9] for the generalized Maxwell, or Weichert model with $n + 1$ parameters. The form for that result may be written

$$f = \left(\frac{Wh}{E_0 R^2} \right)^{\frac{1}{3}} F(E_i, \tau_i) \quad \text{EQ. 2}$$

where E_i and η_i are the elastic and dissipative elements of the Weichert model and $\tau_i = \eta_i/E_i$ are the characteristic periods of each element, E_0 is the long term stiffness value and $R = D/2$ is the idler radius. In equation (2), $F(E_i, \tau_i)$ denotes a function similar to that part of equation (1) involving δ , only somewhat more complex, but explicit form. While forms of equations (1) and (2) are similar, we observe that equation (2) is explicit in the Weichert parameters, while to use equation (1), the values of E' and $\tan(\delta)$ would have to be calculated from the material parameters. The relationships for that calculation is the Prony series forms of

$$E'(\omega) = E_0 + \sum_{i=1}^n E_i \frac{\omega^2 \tau_i^2}{1 + \omega^2 \tau_i^2}$$

$$E''(\omega) = \sum_{i=1}^n E_i \frac{\omega \tau_i}{1 + \omega^2 \tau_i^2} \quad \text{EQ. 3}$$

The half space models of Hunter [3] and May [4] are difficult to extend from the SLS material to the Weichert model, but the Winkler foundation models that result in equations (1) and (2) are relatively simple to make this extension, hence allowing for more realistic rubber materials while requiring little more computational effort.

As an example, Figure 1 shows the indentation resistance results from three different deformation models with identical material models (SLS) for each. For the range of belt speeds considered, it is observed that the approach of Lodewijks provides lower values for the indentation resistance than the energy absorption approach of Jonkers, while the full two-dimensional solution of Hunter provides results which lay between the other two for lower values of belt speed. Lodewijks [5] provides a conversion factor to scale Winkler foundation results to the more exact half space models of

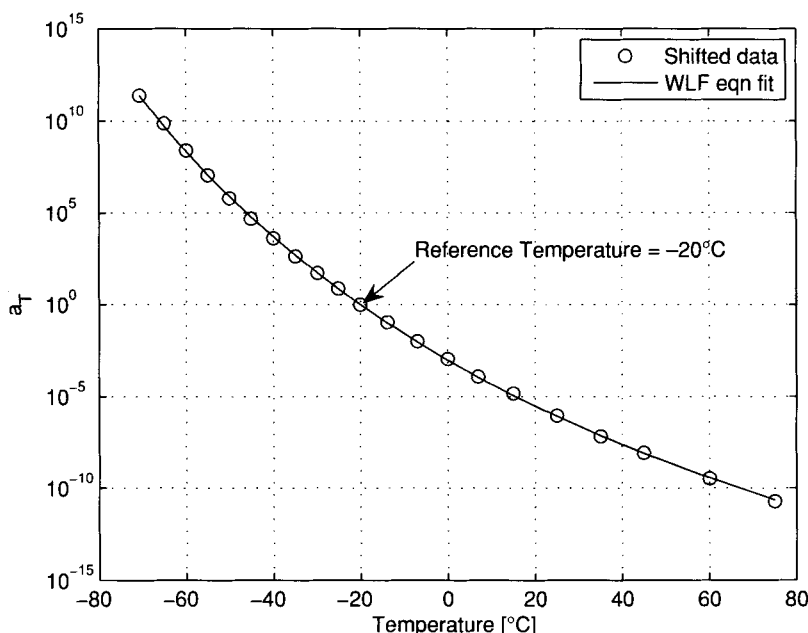


FIGURE 2 Frequency/temperature shift factor as a function of temperature

Hunter and May, which produces resistance values somewhere between the Lodewijks/Hunter curves of Figure 1.

Although the predictive models of indentation discussed above provide some variation in results, all are capable of providing relatively good estimates of the indentation resistance. The more analytically sophisticated models would logically provide better results, and to be sure, the computational solutions of Wheeler [7] and Qiu [8] would provide accurate predictions for finite backing thicknesses. Regardless of the approach, there are many aspects of the indentation phenomena that are not likely to be included, such as slippage and roughness at the interface, adhesion, etc. Similarly, the material model is likely to introduce its own assumptions and limitations. Thus, for this study, the method of Lodewijks [5], extended to the Weichert material model by Rudolph and Reicks [9], will be used as the predictive model of indentation resistance.

BACKING MATERIAL CHARACTERIZATION

The mechanical properties of viscoelastic materials are typically measured by sinusoidal imposed deformations on specimens in simple tension, shear, bending or torsion at controlled temperatures and relatively low frequencies to avoid inertial effects. The time/temperature correspondence principle (cf. refs. [10] and [11]), which relates time or speed effects to temperature, allows one to extrapolate to frequencies and load rates considerably in excess of the test frequencies. In the frequency domain, the correspondence principle implies a shift factor a_T , which is determined from test data taken at a range of frequencies and a range of temperatures and then overlaying, through frequency shifts, the data at the different temperatures to form a "master" curve for a material. Examples of these graphs for typical backing rubber compound are shown in Figures 2 and 3.

A phenomenological basis for a_T in amorphous polymers is the Williams, Landel and Ferry [12], or WLF

equation, $\log(a_T) = C_1(T - T_0)/[C_2 + (T - T_0)]$, where T is the temperature, T_0 is a reference temperature and C_1 and C_2 are constants determined by fitting the WLF equation to a_T as determined from the shifting to form the master curve. Figure 2 shows the shifted data and a least squares curve fit to the WLF equation.

The theory of linear viscoelasticity relates the stress and strain through relaxation or compliance functions and convolution integrals (adds up history effects). Standard characterization of the material by the Weichert model means determination of the constants (spectrum) E_i and $\tau_i = \eta_i/E_i$ of the Prony series of equations (3). Determination of that spectrum from experimental data, as embodied in a master curve like Figure 3, is a non-unique process, laden with several theoretical issues, but several methodologies (cf. Emery and Tschoegl [13]) have been developed to do this. Commercial software is also available for this purpose and rheological testing machines are often accompanied with data analysis software for that purpose. This issue is not the focus of this paper; it is presumed that the spectrum can be determined that faithfully reproduces the master curve data. The master curve data of Figure 3 shows the G' and G'' curves as reproduced by the spectrum developed by the author's own software—a least square, non-negative fit process at equally spaced period values τ_i through the frequency span of the data. The data represented in Figure 3 was taken by a standard rotational shear mode tests on thin tabs of the backing material.

A strong component of the indentation resistance, as evidenced in equation (1), is the material loss factor $\tan(\delta) = G''/G'$, as shown in Figure 4 for the above material. This curve is a typical shape for rubber compound properties used for belt backings in that it exhibits a fairly strong peak when plotted against the log of the frequency. Also, it is apparent that the master curve fit to the data may under or over-predict the data, due to

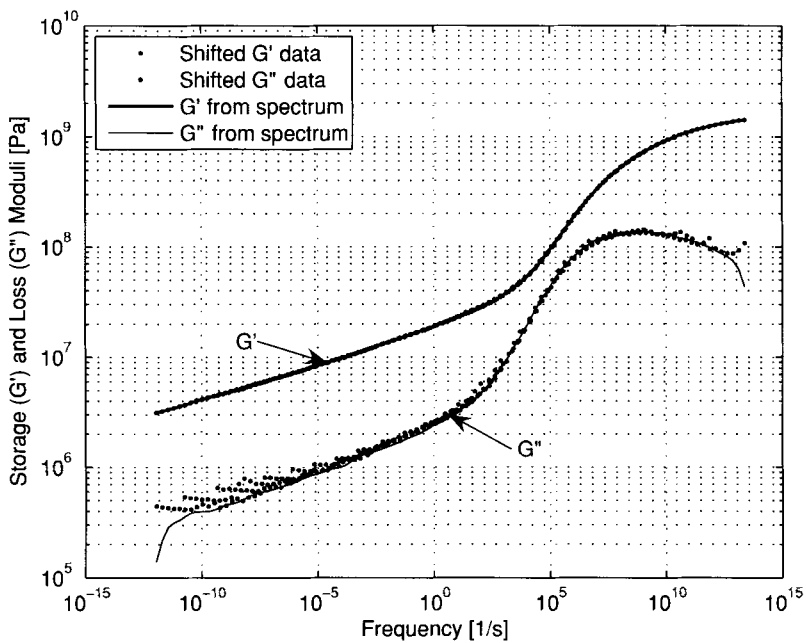


FIGURE 3 Typical master curves of shear storage and loss moduli

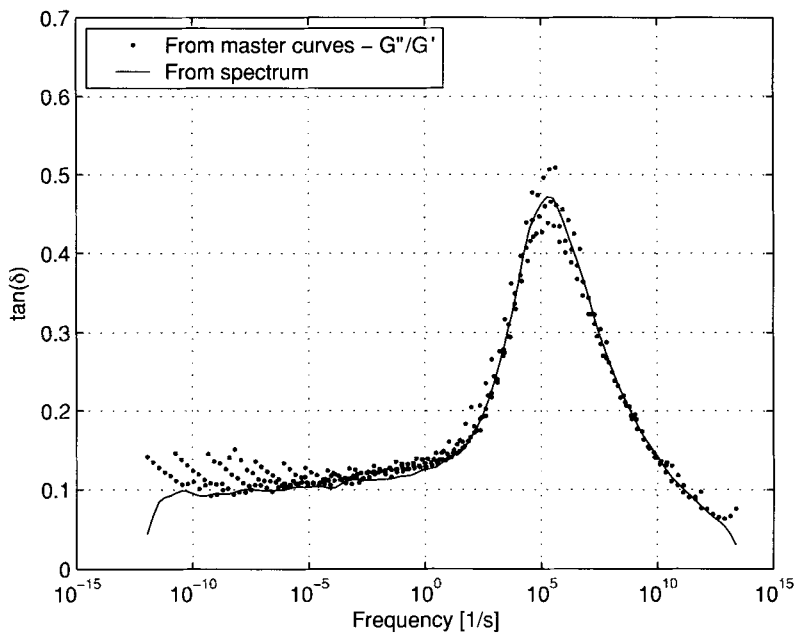


FIGURE 4 Loss tangent as a function of frequency

errors from several possible sources, but in this case is generally a good fit, which is important since the indentation resistance depends strongly on the loss tangent.

AN INDENTATION RESISTANCE EXAMPLE

The normalized indentation resistance factor $F = f/(WhE_0R^2)^{1/3}$ values for the above material as determined by both the equation of Jonkers, equation (1) and the extended method of Lodewijks, equation (2), with the Weichert material model is shown in Figure 5. The factor F

is graphed vs. va_T , since on a logarithmic scale, the a_T -shifted values overlap for the full range of belt speeds and temperature due to the linear time/temperature superposition principle. Also, to reveal where a specific temperature determines values on the speed shifted scale through the shift factor a_T , shown on the right vertical axis is a plot of $\log(v)$ vs. va_T . On the logarithmic scale, these are the nearly vertical straight lines for a given temperature, or discrete values of a_T . Thus, to determine a value of F on this graph, at a given v and T , one starts with a specific V on the right

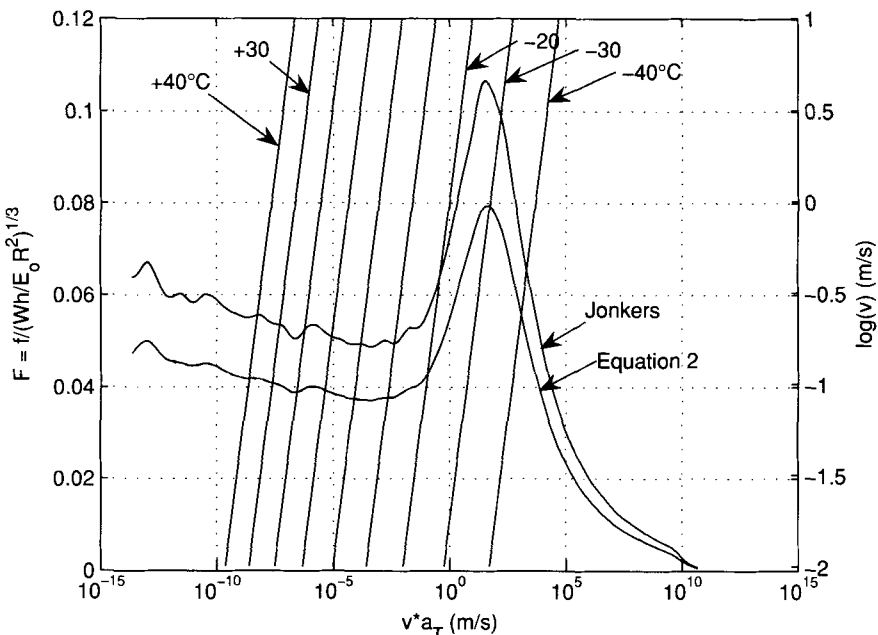


FIGURE 5 Indentation resistance as a function of belt speed and temperature

$\log(v)$ axis, follows it horizontally to the intersection of a specific temperature line of interest, then projects vertically, up or down, to the intersection with the curve to locate the F value corresponding to the given v and T . In this way, all indentation resistance values as a function of belt speed and temperatures are collapsed onto one curve.

As representative of a typical rubber backing material, it may be observed from Figure 5 that the predicted value of F , or f , at any given temperature, comes from a narrow range of the general curve, due to the nearly vertical $\log(v)$ lines. Alternately, for a given temperature, the variation in F comes from a small band on the curve as v varies, in this case, from nearly zero to 10 m/s. Thus F is relatively insensitive to v except at steep parts of the curve. We also observe the strong dependence on the loss tangent, due to the similarities of F in Figure 5 and the loss tangent $\tan(\delta)$ of Figure 4. Presumably, the determination of F by a half-space model, by analogy to the results of Figure 1, would lie somewhere between the two curves, especially to the left of the peak.

From Figure 5, observe that the upper curve peaks at about $v = 10$ m/s and -25°C . At lower temperatures and higher belt speeds, one would drop down the resistance curve to the right. For most applications, one would not expect to exceed those conditions and at higher temperatures, one would be operating on the curves to the left of the peak. Within this lower range (higher temperatures and lower speeds) there is a possible variation in F from about 0.04 to 0.08, or a factor of two. For efficient design one may want to take advantage of that broad, relatively level region of these curves to the left of the peaks, while yet not ignoring the higher values in F at the lower temperatures and higher belt speeds.

SIMPLIFIED CURVES OF INDENTATION RESISTANCE FOR DESIGN

Based on the results and foregoing logic for the above representative material, a strategy for design for indentation resistance is suggested. One could create a design

curve for F to be a simplification of Figure 5, within a practical range of interest, in the form of a "sigmoid,"

$$F = b_0 + b_1 \{ 1 + \tanh[b_2 + b_3 \log(va_T)] \} \quad \text{EQ. 4}$$

where the four constants $b_0 \dots b_3$ would be chosen to fit the normalized resistance curve in a "best" sense. Figure 6 shows such a sigmoid fit to the Jonkers' prediction of Figure 5 for use within a temperature range of about -20°C to $+20^\circ\text{C}$. A similar curve could also be fit to the less conservative values of equation (2).

From such a simple parameterized curve of F as in Figure 6, the actual resistance factor f would be determined through the conversion $f = Wh/E_0R^{2/3}F$ and the parameterized frequency/temperature shift factor a_T from Figure 2.

The F -curve parameterization process as described was performed for two other materials. Those results, fit to the equation (2) predictions, are shown in Figure 7 with the materials labeled (a), (b) and (c); material (a) being that of Figure 6. These could be considered low (a), intermediate (b) and higher (c) resistance compounds.

In this fashion, these types of generic material characteristic curves and associated parameters could then be used in a "design selection" or handbook fashion.

STRAIN AMPLITUDE EFFECTS

The effect of strain amplitude on the dissipative effects of rubber compounds is commonly known and strains larger than about 1% may often exceed the linear range (cf. Osanaiye [14]). For material (a) in the above study, along with measurements of the storage and loss moduli at low strain levels and a full range of temperatures and frequencies, the moduli were also measured at 3% strain, a frequency of 10 rad/sec and a range of temperatures. Figure 8 shows the effects on G' and G'' in a plot of each, normalized to their respective values at 0.01% strain, vs. % strain. The temperature dependent data is scattered, so there not a strict temperature

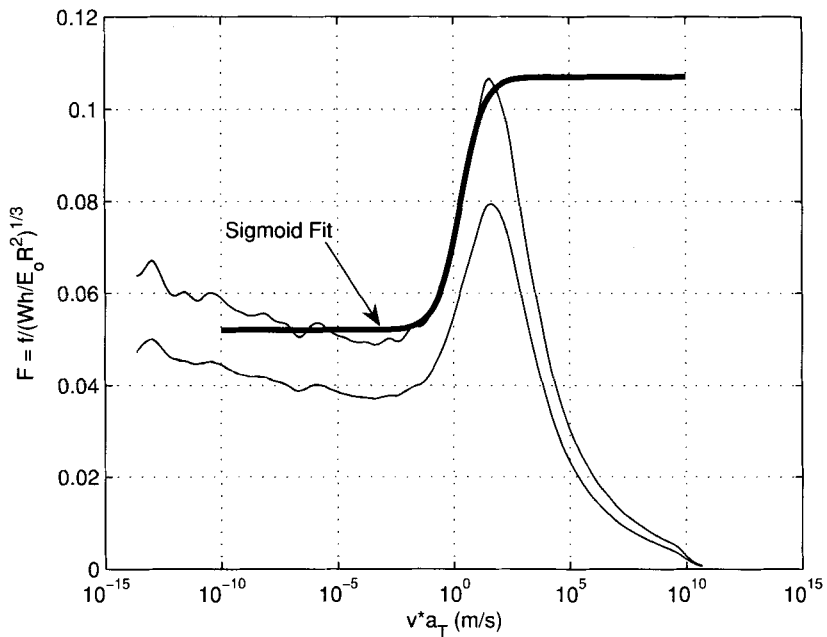


FIGURE 6 A sigmoid fit to the normalized Indentation resistance factor

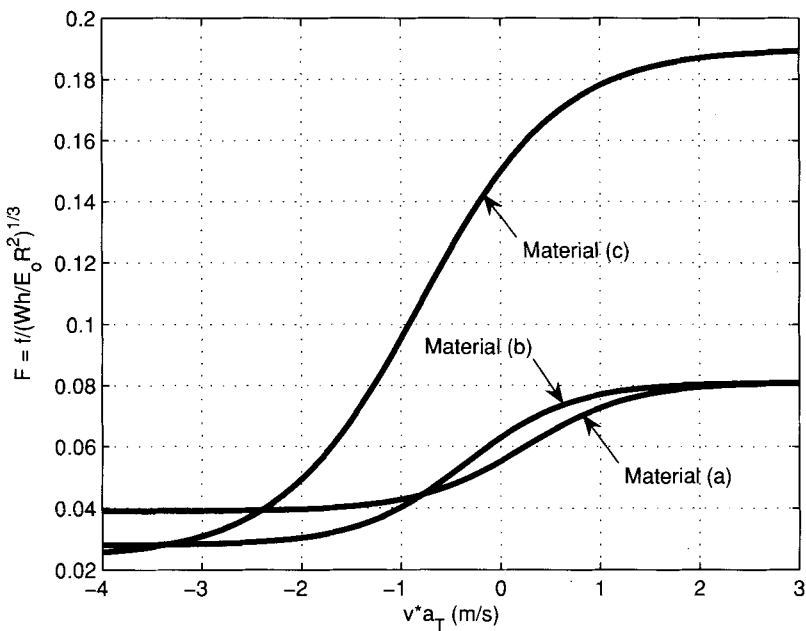


FIGURE 7 Sigmoid curves of normalized resistance factors for three materials

independence, but a polynomial is fit to both G' and G'' . From the fitted curve it is clear that for strains greater than about 1%, G' decreases dramatically and G'' increases somewhat. Of course, with this trend, $\tan(\delta) = G''/G'$ varies proportionally with G'' and inversely with G' . It would be expected then, that at higher strain levels the loss tangent $\tan(\delta) = G''/G'$ would increase considerably. From Figure 8, there would be nearly a doubling of $\tan(\delta)$ at the higher strain values. Similar trends were observed in materials (b) and (c).

With an increased $\tan(\delta)$ at higher strain levels, the effect on the indentation resistance can roughly be gauged from equation (1), i.e., to first order effect, proportional to $\tan(\delta)$. The geometric parameters of the system, R and h , and the carry weight W also determined the strain in the backing material, but to a lower order than $\tan(\delta)$.

Using again the generalized method of Lodewijks with the material properties of material (a) as exemplified in Figures 2 through 8, strain amplitude corrections to the

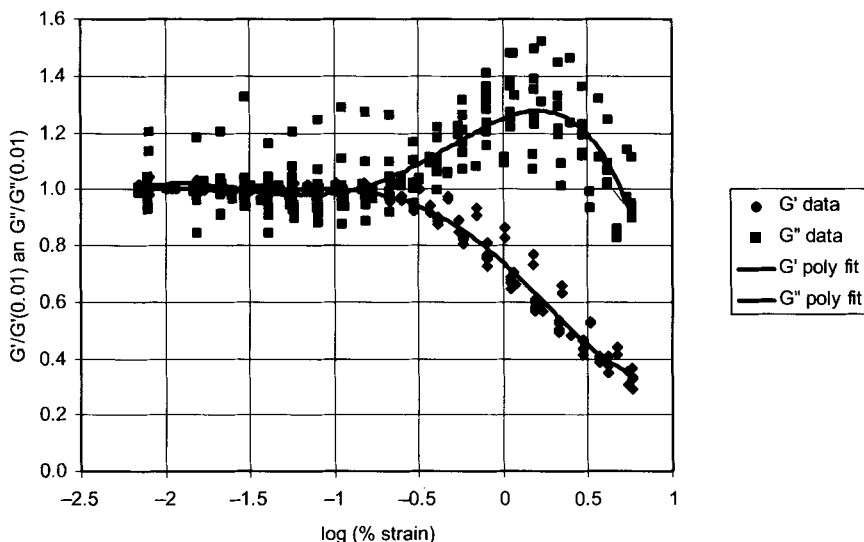


FIGURE 8 Strain amplitude effect on the shear storage and loss moduli

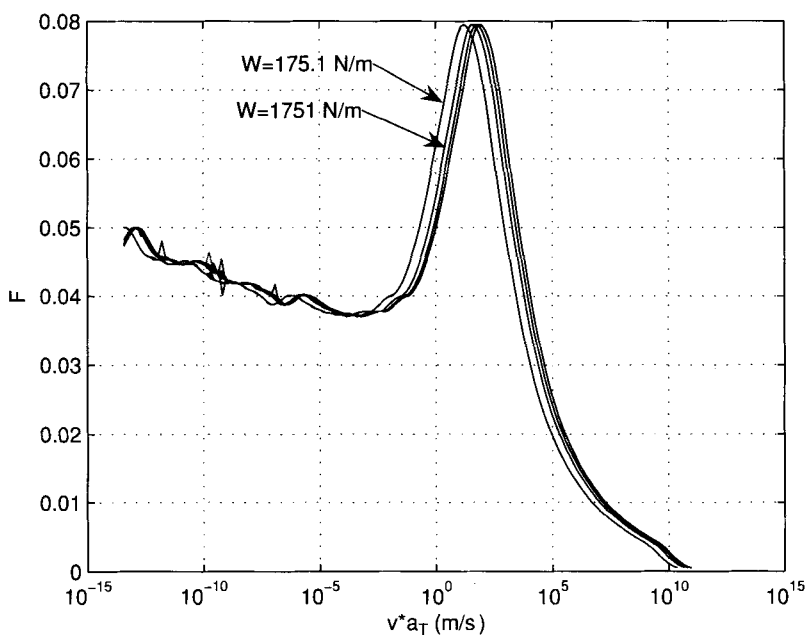


FIGURE 9 Normalized indentation resistance factor with strain amplitude correction

calculations required to evaluate the indentation resistance factor by equation (2) were performed. Now, however, as the strain is coupled to the parameters of the normalizing coefficient $(Wh/E_0R^2)^{1/3}$, i.e., W , h and R , the whole equation is evaluated. Since the maximum strain ϵ_0 of the Winkler backing increases with W , and decreases with h and R , to examine extreme values of f , the following calculations were made with small values of $h = 0.006350 \text{ m} = 0.25 \text{ in}$ and $R = 0.05080 \text{ m} = 2.0 \text{ in}$, while W takes on the four increasing values of $W = [175.1; 1,751; 4,378; 8,756] \text{ N/m} = [1, 10, 25, 50] \text{ lb/in}$. Figures 9 and 10 shows the normalized and non-normalized indentation factors resulting from the analysis.

The normalized factors are shown in Figure 9 where it is seen that four curves nearly overlap one another, except for a small shift on the horizontal axis. The curve corresponding to the smallest W lies leftmost; the others proceed in order of increasing W to the right. The similarity of these curves is a consequence of using a continuously updated value of E_0 of equation (2) for each temperature and belt speed value, as required by the strain alteration of the material moduli, and $\tan(\delta)$, as the calculation proceeds. This is to say that strain modulation of the material properties makes it essentially behave as different material, and the higher strains increase $\tan(\delta)$ so that it responds more slowly, making the contact length shorter or increasing the load

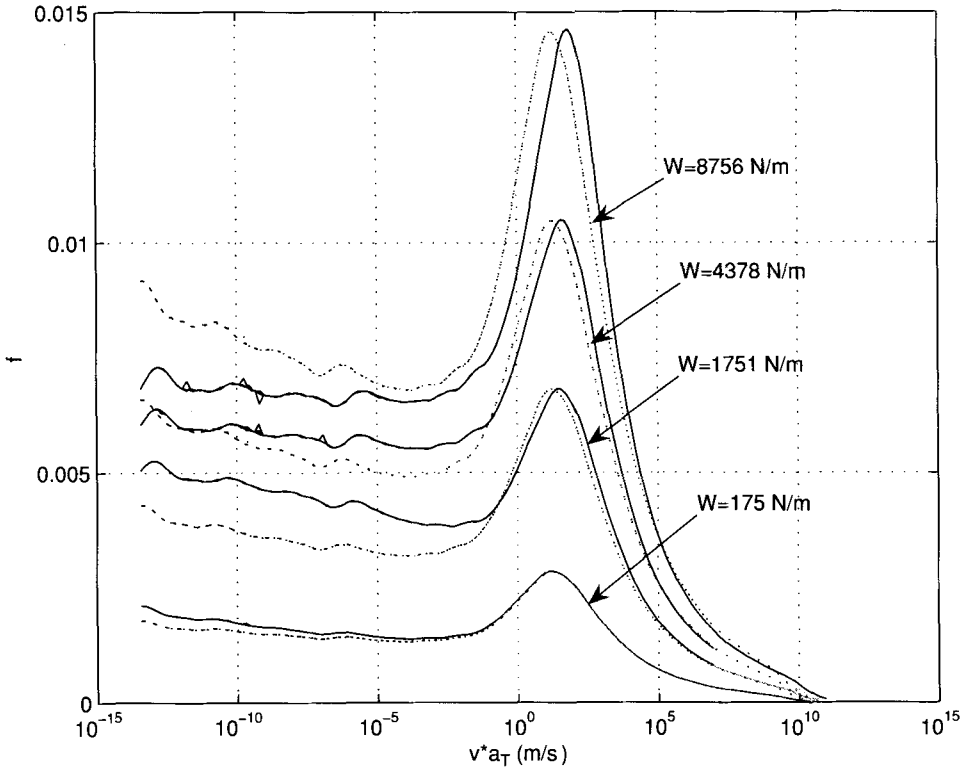


FIGURE 10 Indentation resistance factor with strain amplitude correction

frequency, shifting the curves to the right. Evidently the factor $F(E_0, \tau_i)$ of equation (2) is independent of strain amplification, other than the horizontal shift.

Figure 10 shows the un-normalized resistance factors by multiplication by $(Wh/E_0R^2)^{1/3}$ according to equation (2). The figure shows two curves for each increment in the load W . The solid lines show the values as determined by equation (2) with the continuously updated E_0 . The dashed lines show approximations to the same curves by using the low strain, normalized F curve of Figure 9 and a particular E_0 value chosen so as to produce equal values at the peak of the corresponding curves. Determination of that aligning E_0 value requires an iterative process, with strain correction, to determine the particular value of E_0 at the point where the F function peaks. Although this is nearly tantamount to direct determination of f , it has the important advantage of only requiring the one, low strain F curve of Figure 9. Further, the process is then amenable to the simplified sigmoid parameterization of Figure 7.

From the foregoing, we have then the ability to incorporate strain amplitude correction into the scheme of creating master and simplified curve for any material as in Figure 7. Values for the indentation factor f are then determined through a programmed process for any system parameters W, h and R , with the material parameters of a_T from the WLF equation for temperature location, remembering that for strain amplitude adjustment, the particular values of E_0 will also be required (an iteration, given W, h and R). Accordingly, an algorithm of small computational requirements can provide estimates

of the indentation resistance for any material where the spectral properties are known.

The aforementioned iterative process could be based on the formula taken from Jonkers [1] methodology which relates maximum strain level ϵ_0 of the Winkler foundation (strain of that element directly under the idler), to W, h, R and E' , i.e.,

$$\epsilon_0 = \left[\frac{W(\pi/2 + \delta)\cos(\delta)}{2E'\sqrt{2Rh}(1 + \sin(\delta))} \right]^{\frac{2}{3}} \quad \text{EQ. 5}$$

With this equation (5), for any given load and geometric parameters, and the strain amplification curves for the material like that of Figure 8, a small number of iterations on ϵ_0 , given an initial estimate, determines a consistent values of E' and δ , and hence E_0 for that material and strain. By sweeping through the temperature and belt speeds of interest, while monitoring for the point where $\tan(\delta)$ is maximum, the appropriate value of E_0 is determined.

SUMMARY AND CONCLUSIONS

Fairly simple mechanical models of the indentation process are capable of providing good estimates of the indentation resistance. The basic methods based on the Winkler foundation assumption are easily extended to the general Weichert material model so realistic rubber compounds can also be included in the analysis. Under the assumptions of linear viscoelasticity, and the time/temperature correspondence principle, experimentally measured values of the dynamic storage and loss moduli at relatively low temperatures and modest frequency ranges can be used to

produce sufficiently high frequency data for simulating the indentation process. This paper shows how simplified characteristic indentation resistance factors can be developed for typical backing rubber and proposes that characteristic design curves be developed with an attendant algorithm for design calculations.

Under the Winkler foundation model for the backing material, strain amplitude effects on the material process can be included, although dependence of the material moduli on strain amplitude would be a violation of the linear viscoelastic assumption. We can incorporate this simple strain amplitude dependence into the material design curve methodology with little additional burden on computation.

Of course, the results of any analysis can be no more reliable than the material properties upon which it is based and for rubber belt backing materials, there are other, perhaps more influential issues to be considered, such as accuracy and reproducibility of measured material properties, evolutionary changes of the material properties due aging, the breaking-in transient, environmental influences, etc. The issue of strain amplitude correction is also based on assumptions that stretch the validity of linear viscoelasticity. Nevertheless, as more reliable material properties become available and testing methodologies become more standardized and reproducible, then the method outlined here by development of characteristic forms for various rubber compounds would serve to provide designers the ability to take advantage of lower power loss predictions.

REFERENCES

1. C.O. Jonkers, The indentation rolling resistance of belt conveyors: A theoretical approach, *Fördern und Heben*, 30, 4 (1980) 312–317.
2. C. Spaans, The calculation of the main resistance of belt conveyors, *Bulk Solids Handling*, 11, 4 (1991) 1–16.
3. S.C. Hunter, The rolling contact of a rigid cylinder with a viscoelastic half space, *Journal of Applied Mechanics*, 28 (1961) 611–617.
4. W.D. May, E.L. Morris and D. Atack, Rolling friction of a hard cylinder over a viscoelastic material, *Journal of Applied Physics*, 30, 11 (1959) 1713–1724.
5. G. Lodewijks, The rolling resistance of conveyor belts, *Bulk Solids Handling*, 15, 1 (1995) 15–22.
6. J. Margetson, Rolling contact of a rigid cylinder over a smooth elastic or viscoelastic Layer, *Acta Mechanica*, 13, 1–9, (1972), 1–9.
7. C.A. Wheeler, Analysis of the indentation rolling resistance of belt conveyors, *Proc. 7th Int. Conf. on Bulk Materials Storage, Handling and Transportation*, The Univ. of Newcastle, Australia, 559–567, Oct., 2001.
8. X. Qiu, A full two-dimensional model for rolling resistance: Hard cylinder on viscoelastic foundation of finite thickness, *Journal Engineering Mechanics, ASCE*, 132, 11 (2006).
9. T.J. Rudolph and A.V. Reicks, Viscoelastic Indentation and Resistance to Motion of Conveyor Belts Using a Generalized Maxwell Model of the Backing Material, *Journal Rubber Chemistry and Technology*, June 2006.
10. A.S. Weinman and K.R. Rajagopal, *Mechanical Response of Polymers: An Introduction*, Cambridge University Press, Cambridge, UK, 2000.
11. J.D. Ferry, *Viscoelastic Properties of Polymers*, 3rd Edition, Wiley, New York, 1980.
12. M. Williams, R. Landel and J. Ferry, The temperature dependence of relaxation mechanisms in amorphous polymers and other glass-forming liquids, *Journal of the American Chemical Society*, 77 (1955), 3701.
13. I. Emri and N.W. Tschoegl, Generating line spectra from experimental responses. Part I: Relaxation modulus and creep compliance, *Rheologica Acta*, 32 (1993), 311–321.
14. G.J. Osanaiye, Effect of temperature and strain amplitude on dynamic properties of EPDM gum and its carbon black compounds, *Journal Applied Polymer Science*, 59, (1996), 567–575.

.....

Belt Conveyor Idler Roll Behaviors

Allen V. Reicks*

This paper reviews the impact of the idler set on the performance of belt conveyors. Idler rolls as part of the load support system and their interaction with the conveyor system will be discussed. In particular, the rotating performance of the individual idler roll concentrating on the rotating resistance and life of the bearing and seal design are addressed in detail. A basis for the development of performance specifications for use in conveyor design that takes advantage of the idler manufacturers design and manufacturing expertise is discussed.

INTRODUCTION

This paper reviews the impact of the idler set on the performance of belt conveyors as they support the weight of the belt and bulk material. Idler rolls and their assembly in sets are an integral part of belt conveyors used to transport a wide range of bulk materials and applications. Almost as much as the belt itself, they affect the behavior of the conveyed material, the power used and the overall suitability of the conveyor. Idlers have been developed to perform adequately for various installations but indentifying the most appropriate is not that clear. This paper attempts to review the impact that idlers have on conveyors, describe the range of product produced and provide insight into their selection.

The Role of the Idler in Conveyor Operation

Awareness of the ways that idlers affect the conveyor and interacts with other components is necessary for optimal selection.

The nominal role of an idler roll is to provide load support with low resistance to movement. Radial loading from belt and material over a particular idler spacing is the principal requirement of most rolls. This load also includes absorbing impact at the loading point and belt tension when located in curves. These can be a difficult load to quantify but modern conveyor designs conveyor design methods have improved the understanding and control for clearer idler implications.

Assemblies of idler rolls are created to control the belt profile, typically to form a trough or tube. This will not be discussed in depth but it should be acknowledged that the trough form, consistency and flexibility can have an

important effect on the idler roll behavior. Troughing rolls develop axial load due to being angled to vertical as wing rolls in a trough and to the belt direction to provide guiding or tracking forces. Aspects of mounting method, alignment, self cleaning etc. are important aspects of idler frame design.

External interaction with the conveyor system goes beyond the primary function of supporting a normal load to include longitudinal load or power and operating behavior.

All of the conveyor longitudinal “main” resistances are transferred via the idler rolls.

- Trampling loss power is due to reforming the material cross section. Material lifting and acceleration reactions transfer load to the wing roll from the center roll in this process. Troughing angle and idler trough influence this resistance.
- Viscoelastic belt cover indentation develops at the rollers. Larger diameter rolls can be expected to have lower losses.
- Transverse friction from roller misalignment is affected by roll mounting variations established by the frame manufacture and installation. The transverse rubbing reaction is also affected by the idler roll material and its friction to the belt.
- Nominal rolling resistance of the idler bearing and seal is a direct impact of the idler design and is discussed below. Load and manufacturing induced frame and shaft deformations affect the rolling resistance as well.

* Overland Conveyor Co. Inc., Lakewood, Colo.

In addition to the vertical support, the idler set affects the lateral belt operation in several ways.

- Alignment of the idler rolls perpendicular to the belt and parallel to one another provides a smooth running load with balanced lateral loads and good belt tracking. Imperfect orientations of the rotational axis to the local belt path causes axial friction with power and wear consequences to the belt and the idler shell. This is set by the idler frame and local belt stretch or as when garland idlers are allowed to swing in the direction of belt movement.
- When one end of a roll is ahead of the other the belt tends to be pushed in the direction of the latter. This can be used to advantage for tracking.
- The toughed or "V" return idler provides a balancing for the belt and material weight as both wing rolls funnel their weight to their lower position. Guidance through horizontal curves relies on a similar balance against the radial component of the belt tension.
- Conveyor noise and vibration are evidence that wear, damage, and additional power loss is occurring as well as being objectionable in its own right.
- Belt flap or inter idler belt vibration is driven or excited through small idler roll runout, TIR, or radial variation at the rotational frequency.
- Belt slap implies a vertical bouncing at the idler at frequencies away from the belt natural frequency. It is due to high roll TIR.
- The resonance frequency of steel roll shells can be in the audible range.
- The support frame can bounce or vibrate as affected by its stiffness in several modes.

IDLER ROLL DESIGN

The idler roll provides a basic radial support against gravity and belt tension in the case of curved belts, and to force belt bending and material cross section. In doing this the roll also allows longitudinal movement with only a small though accumulating belt tension increase part of which is attributable to the roll torsional resistance to rotation. Minimizing this resistance and matching the idler roll life to that of the conveyor are the primary design goals at a particular radial load beyond enabling a cost effective and well "behaved" rotating construction.

Construction

The idler roll design is fundamentally simple comprising a rotating outer cylindrical surface and a pair of bearings almost universally mounted on a stationary shaft. Though a wide range of shaft, bearing positioning components and outer cylinder material are used, the design can be identified nominally with a diameter, length and material, each with various impacts on the conveyor as described above. The bearing set design has the primary affect on idler performance. It can be defined as an imbedded antifriction rolling element on a stationary shaft with components locating it to the outer shell and protecting it from the outside world. The bearing load rating is fundamental to its selection.

Idler Rotating Resistance

The idlers power, a basic loss though not necessarily the major loss as described above, is due to the torsional resistance to rotation at the bearing set. This is typically

modeled to be the accumulated friction due to the (1) rolling element sliding and deformation hysteresis which is load sensitive, (2) shear of the lubricant which is primarily speed related and (3) the seal drag which varies widely with design.

Bearing Rolling Resistance. The bearings used in today's bulk material handling conveyors are virtually always precision machined, hardened, ground and polished set of elements designed and assembled to roll in similarly treated and lubricated "races." The result is to develop as close to pure rolling as possible with minimal deformation and sliding forces for low resistance to rotation and long life while resisting radial and axial displacement. Lubricant for the relatively low speed operation of idler bearings is generally provided with grease which is placed around the rotating elements and bleeds out lubricating oil to the rolling contact. The viscous grease is subject to shear and churning due to contacting various elements which causes speed and temperature varying resistance to movement and roller rotation.

Two basic bearing types are used with unique characteristics in several regards. In both, the outer ring is pressed into a bore of the rotating roller. This clamping fit prevents movement and fretting wear of the bearing outer ring. The inner ring is a small clearance slide on fit to the shaft so that the rolling elements are not preloaded. The bearing bore should be restrained from sliding or loosing on the shaft when the roll is lightly loaded.

- Ball bearing idlers use spherical rolling elements in correspondingly radiused grooves or races to distribute the contact forces and provide some axial resistance. The variation in rolling radius due to the depth of the groove causes sliding friction and wear and prevents disassembly when optimized with a full ball complement. Initial clearances between the balls and races allows for thermal expansion, slight angular misalignment and slight allowance for compression of the outer ring when pressed into the roll. Ball bearing idlers are commonly prelubricated and available equipped at the bearing plant with a precisely fitting seal. Special designs have been developed that are more tolerant of soft contaminant through the race shape and clearance.
- Roller bearings, typically with tapered rollers, have a wider contact width for lower pressures and increased radial capacity. While the use of tapered rollers additionally provides high resistance to axial forces the contact path is also not purely cylindrical with a tapered rolling radius and inevitable sliding. The wide rollers better resist transverse moments from flexible shafts and stiff roll ends but this can increase rolling pressures and reduce the allowable load. The wide roll also reacts differently with the lubricant. This can be seen with increased relubrication recommendations (SKF 1991, 2005). In addition, rolling resistance can be seen to decrease with increasing speed, counter to normal grease viscosity behavior. This is presumably due to more grease being pushed out of the roller path with the higher dynamic pressures from high speed.

Assembly Considerations. The bearing set must be thought of as including the shaft with a method of

attachment to the idler frame and a bearing axial locating feature as well as a rotating housing to transfer the support forces to the outer shell. The assembly is inevitably imperfect in aligning the bearing rolling elements with their inner and outer races. Additional deformation develops under load. Both of these displace the bearing out of the optimal purely circumferential rotation causing additional rolling element sliding with frictional loss, noise and wear as well as higher contact stress and shorter fatigue life. The product and manufacturing process designer must address the bearing needs in a number of ways to maintain the rolling action designed by the bearing with consistency and efficiency. The two bearing types used in idlers require fundamentally different axial support and assembly which must be incorporated into the design. Both must clamp the outer race to prevent movement and wear but the axial freedom varies between the two.

Grease Contribution to Rotating Resistance. Grease is identified here as a separate component since it contributes uniquely to the idler power performance. Grease is necessary for lubrication and can also be used for seal functions discussed below. In any case, as a viscous material it resists shear strain. This resistance causes idler drag that varies with strain rate, the grease stiffness or shear strength and the total shear area. These relate to the rotating speed and bearing mean diameter, the temperature and the amount of grease, respectively with all influenced by the conveyor design, the environment and the idler design. Therefore, fully understanding the impact of grease on conveyor power requires characterizing it for the possible range of speeds and temperatures for a particular design.

Grease is composed of a lower viscosity lubricating base oil that flows at the rolling contact and a higher viscosity carrier or thickener that stores the oil and releases it to the lubricate surfaces that are near it. The thickener provides the greater flow resistance as it is forced to shear between the bearing elements and seal components. Thickeners are produced in a wide range of base materials with varying strength, temperature, miscibility and cost characteristics. Unfortunately from the perspective of predicting the roll drag due to lubricant, grease is too stiff to work with common oil viscosity tests.

Instead, the apparent viscosity, often characterized through pumpability tests (NLGI, 1982), can be used. Cone viscosity instruments designed for uniform shear strain can compare torque to rotating speeds at different temperatures also demonstrate the expected performance of particular greases. Arveson (1934) was among the first to observe that the log of the apparent viscosity of grease typically varies linearly with the log of the shear strain rate. In addition, this linear relationship repeats itself as parallel lines for different temperatures. This allows Time Temperature Shifting (TTS) to conveniently characterize the viscous resistance to idler rotation for a particular idler with only a few measurements applicable to a wide range of applications. It must be acknowledged that the temperature of the grease is inevitably different than the ambient temperature and that grease is displaced differently for different stiffness's and speeds. Nonetheless, the author has found that the log linear nature of the test results maintains sufficient accuracy to use TTS to extrapolate between and beyond test conditions. These cannot be used interchangeably for steady

running and for cold startup due unless the heat transfer properties of the idler are well known.

Rotation of Bearing Seals. Finally, a seal is always provided to protect the precision bearing elements from contaminants such as fine abrasive grit and moisture that damage the precise bearing elements and the lubricant diminishing the rolling effectiveness. These will often have their own resistance to rotation both intentional and due to manufacturing variations. In addition, seal effectiveness can be thought of as a power criterion if a major part of the bearing life is spent with poor lubrication or rough rolling pathways. Several functional concepts are used to isolate the bearing from the outside environment. Though their effectiveness and drag ranges widely, the two are generally inversely related.

IDLER LIFE

Life versus design can be thought of as the maximum possible life of a loaded roll and the factors that contribute to not fully experiencing this life. The following descriptions of common idler components.

Bearing Life

The bearing life is ultimately limited by the contact stresses between the rolling element and the races that they run. Several scenarios can develop that must be addressed in the design of the bearing set.

A classic AFMBA fatigue calculation, relevant to long life under steady loading, is commonly used for sizing a bearing appropriate to the desired roll rating or radial load. While it does include useful statistical probabilities of a bearing lasting for a particular number of revolutions, this oversimplified calculation is probably given too much credence in conveyor engineering. Ultimately though, it is still worthwhile as a benchmark since the failure mode it represents implies a range of conditions which encompass others that can be much more difficult to evaluate and be sustained. When all of the loads are sufficiently understood, alternate advanced selection criteria may be relevant in the development of an idler roll but use in specification would be very difficult due to the wide range of inputs. Most bearing manufacturers publish dynamic load ratings or capacity of their product for use in this equation as well as a static load rating which serves as an allowable for infrequent overloads which could cause minor damage that accelerated fatigue failure. Lubricant life is also a limit to the applicability of the statistically possible cycle life and must be accounted for as an overriding limit or by relubrication.

Bearing sizing, friction and lubricant life can use newer methods (SKF 1991, 2005) developed by bearing manufacturers which better represent actual bearing design and materials. As with the nominal ratings, these methods should be considered specific to the bearings from the respective manufacturer.

Standards groups continue to evolve to incorporate new technology and understanding. Ref ISO 281:2007. These should be considered but can still come up short to fully represent the total operating condition so their usefulness in specifications is limited.

Though bearing size has a significant effect on cost, availability and economies of scale as well as design philosophy can influence the selection of a heavier bearing than may be "needed," especially since oversizing can reduce the importance of the various issues discussed below.

A wide range of additional bearing loads can occur which affect the actual stress in the race. These can significantly affect the accuracy of the simple radial calculation and should be included in the bearing sizing and friction assessment.

- Axial roll loads from transverse belt reaction and wing roll gravity loads.
- Angular loads that cause axial stress from shaft deflection under load.
- Axial and angular preload from assembly.
- Radial preload from press fit assembly.
- Dynamic radial loads from belt flap impact and idler runout.

Bearing race fatigue calculations implies the surfaces and lubrication are maintained substantially as manufactured. The rolling surfaces are subject to various abuses that must be prevented or tolerated with oversizing or comparison to the bearings static load capacity.

- Impact dents or brinelling of the races from handling and dynamic belt and material loads.
- False brinelling from shipping vibrations.
- Sliding between rolling elements and races due to assembly distortions.
- Contamination causing breakdown of the lubricant with subsequent sliding.
- Grit contamination scratches serve as crack initiation sites for spalling fatigue wear.

Seals for Bearing Life

The latter two identified above are major limitations to the actual life of idler rolls. Significant costs are commonly added for seals between the rotating and stationary components to isolate the bearings from external contaminants so they can function as intended. High performing seals for severe applications generally require more power. The nature of seals and their suitability range as follows.

Most idlers will have a stationary or rotating cover over the outer shaft extending to or past the bearing cavity diameter. The rotating design has a smaller diameter and therefore less open area but any material that enters this way is trapped between the bearing and this cover.

Labyrinth Designs. Labyrinth is a general term for non-contacting, frictionless isolation that creates a, bending, narrow and usually long path making it more difficult for material to pass to the bearing. Alternating rotating and stationary elements create axial and radial passages where the width of the passages is governed by the ability/cost to prevent contact and whether they are grease filled. In general, empty or grease filled, labyrinth only delay contaminant passage and can be quickly overwhelmed in very dirty applications. Circumferentially varying passages can provide a pumping action as well. Labyrinth seals are inherently frictionless though this changes dramatically when they are overloaded and fill with contaminant.

Grease filled labyrinth will have higher drag due to the grease shear discussed above but can serve to delay passage of dirt to the bearing. It will absorb contaminant and while mixing and churning, eventually transfer it to the bearing if unimpeded or isolated from clean grease. Though moisture will mix with grease over time, it can be useful to isolate incidental or wash water splash from

getting into the bearing cavity. Some, though not all, of grease filled seals include relubrication systems. In this case, the used grease is typically purged into the seal so that the dirtiest grease in the labyrinth is also purged from the roll, at least to some extent. If grease refreshment is counted on for extending the bearing life, it should be understood that the effectiveness of regreasing systems varies widely.

A specialized and effective labyrinth like design is commonly used at the entrance to the bearing cavity. These dry seals provide roof like protection and centrifugal rejection of contaminant through the shape of the rotating and stationary grooves before it enters the internal seal. Very dirty or wash down environments can overload the centrifugal rejection groove.

Another special labyrinth design with ultra small gaps is used to limit the amount and especially size of dirt migrating to the bearing to that which is relatively benign to the rolling contact. These require special construction and materials to maintain the precision of the assembly.

Contact Seals. Contacting lips of various design and materials are used to prevent ingress of contaminant. They can be rotating or stationary and axially or radially acting. Oil type rubber lip seals are common but soft radial washers of felt or foam are also used. These can absorb dirt but in the process become hard and passages develop allowing dirt ingress. A rotating seal will inherently have lower drag since the contact radius will be smaller for lower torque. It can be expected that internal seals will wear less since they are less likely to be exposed to grit. Accordingly, external contact seals can effectively exclude contaminant but are likely to wear more quickly. Seals in regreasable idlers must deflect to allow grease to pass without causing damaging high pressures.

Balances of effectiveness, wear life and drag are inherent in contact seal design since contact implies rotation of rubbing frictional surfaces. For instance, deflected seals will maintain their effectiveness as they wear though this may require higher initial drag. Thin, soft seals will deflect with less contact force and drag but have less volume for wear life.

Subcomponent and assembly variability is an important consideration implying a range of sealing performance and drag consequences.

The seal available with many ball bearings satisfies many of the issues discussed above and should be understood to often have particularly good value.

Reservoirs or dead zones can delay the passage of contaminate or provide a low pressure accumulating region. These can be useful in less dirty application outside of a contact seal so that pressure does not build up against a contact seal causing it to wear.

Additional sealing should be considered to prevent fines and water from penetrating under the stationary seal and bearing inner race. A minor seal behind the bearing is often provided to prevent bearing contamination from moisture or rust from the interior of the roll. A rear seal may also be necessary for many regreasing systems.

In some parts of the world with wide daily temperature fluctuations, a vent is provided to allow air exchange without penetration through the bearing cavity.

Roll Wear. The belt contact surface wear can also be the limit to idler life. The driving influence should be considered the belt contact and alignment of belt movement normal to the roll centerline. This can be affected by installation, frame design, belt curves or idler spacing. Analysis requires understanding of the local belt stretch as affected by belt sag or misalignment. In lieu of confidence in belt to idler alignment, the roll tube diameter, thickness or material are often selected to accommodate applications that prevent tight control of belt to roll sliding or where fugitive materials are expected that cause roll wear.

The above illustrates the range of designs that are produced. Few if any of these elements can be said to have obvious and universal benefit over their alternates especially when cost of production is considered. These costs must be understood to include the impact of economies of scale, labor, capital investment and production flexibility as well as raw material and delivery. To varying degrees bearing manufacturers have refined their product and their selection and rating methods. These technical advances should allow improved designs but also require diligence to analyze the range of loads, nominal and secondary, with the environment, external and internal, over the life, steady running and other, of the idler. Beyond the design and analysis, the total product should be understood to operate as an assembly and be proved statistically relevant to how it is manufactured and how it will be used.

IDLER SELECTION

The wide range of product design and component sizes commercially available makes the selection of the best idler for an application difficult. The selection and purchase process itself is often bewildering with many parties and possible combinations of components all deserving evaluation. Though specific design elements may be indicated for a particular application or the conveyor owner may have overriding paradigms or selection rationale, a comparison strategy is needed to obtain the lowest cost/benefit ratio meeting the minimum operating requirements of the particular project and as a basis for performance specifications. A financial comparison tool or model, with implied or specific guesstimates of the future value of the components, downtime and labor can be used with great benefit. Nonetheless, characterization of the component itself has to fit in this framework to provide a consistent decision making process.

No conveyor component, especially idlers, can be evaluated on their own because they can be used differently with various other components and practices resulting in a wide range of net conveyor performance. As is commonly understood, a conveyor is a system with balances and compromises among its components inherent in the overall design process. The best we can hope for is that these decisions are done consciously and in a manner that acknowledges the tradeoffs among the components, including how they are used in the design and how they are installed and maintained. In addition to these judgments identification of key operating categories allows commercial implications to be evaluated for the complete conveyor design. The following overlap somewhat but identifying and focusing on them for inter-

action with other design decisions can clarify how they affect the overall initial and future cost.

- Nominal **capacity** of the idler is commonly available in steps that match the commercially effective bearing offerings from bearing manufacturers. Shaft and frames will typically be designed to match the bearing capacity at specified life expectations and rotating speeds. In other cases or for optimization, the balance with these structural elements will affect the overall cost efficiency.
- Idler **life** is often associated with the statistical expectation for the bearing fatigue life with the applications load and speed. This is appropriate only for a best case or maximum starting point. In many installations, failed rolls will have experienced seal failure or roll tube wear due to difficult operating conditions, insufficient sealing, poor idler alignment, inappropriate maintenance, etc.
- **Performance** assessment is primarily a power issue through the rotating resistance of the bearing and seal. In many designs, life and drag will be inversely related. When power is critical, matching the seal design to the application is required for overall cost efficiency. In difficult environments, power must often be sacrificed as a necessary cost for satisfactory life. Therefore, idler rotating resistance is usually secondary to life since the consequence can be accepted through initial incremental expenditures for increased belt tension and conveyor power.
- Rotating **behavior** affects the conveyor through interaction with the other components and the system parameters. Roll runout and balance can have negative effects on component life, material stability and operating noise as discussed above. Idler set frame stiffness can have similar effects. Again, the acceptable level should be assessed in combination with the other elements of the system, especially belt speed, for the least compromises to the idler manufacturer's efficiency and idler cost. Roll runout and imbalance can also apply additional loads to the bearings through radial accelerations that develop while rotating.

As discussed above, various combinations of design details can provide comparable operating results so that specifying details such as bearing type or bore do not benefit the cause of value. Instead, requirements should state the application and the expectation of the product.

Paralleling the key operating parameters, the following are recommended information to be provided in addition to the fundamental parameters of belt width, trough shape and roll diameter when identifying the idler to be used for a particular application.

- The expected roll load or the various options for roll load with their costs should be clearly understood to allow optimization with belt speed and idler spacing.
- Life expectations in operating hours and the operating environment with expected installation and maintenance should be clearly stated. In some cases, test result requirements in accelerated seal tests or tubing thickness minimums may be justified.

- When critical to the overall conveyor required roll drag performance may be identified. The expected drag should always be requested to be provided with guarantees of statistically relevant proof from the actual or equivalent production lots.
- Maximum allowable roll runout and imbalance should be specified in a statistical manner relative to the proximity of a multiple of the roll rotational speed to the natural frequency of the belt flap or vibration modes and to the additional dynamic load relative to the nominal bearing load.

It should be acknowledged that the range of product details and requirements can get lost in the midst of the other selection decisions required of a conveyor design. Additionally, invaluable in depth experience is difficult to collect from the point of view of a system designer or integrator. The idler manufacturer however is in position to know their product and to collect experience if they are willing to spend the time to follow up on installations, take measurements, develop tests, investment in manufacturing flexibility, etc.

Particular insight on the roll design corresponding to the application and how it is integrated into the product design should be assessed in the final purchase decision, perhaps to fine tune the product offering and its cost.

In addition, understanding the interaction of the idler with the system and the ability to evaluate the final design

can provide a value to the conveyor designer, protect the products reputation and reduce warranty risks.

Optimally, trade groups such as the Conveyor Equipment Manufacturers Association (CEMA) in North America that are in position to develop clear language and appropriate assessments will continue to do so as they have in the past in the spirit of aiding their business by making it easier to use their product right.

CONCLUSION

Idler procurement for best value has many issues as discussed above. Understanding the purposes of the idler and the various influences on how these purposes are accomplished is clearly a benefit to the procurement process. Focused product specification aids by establishing a consistent and appropriate set of expectations for the particular application. Likewise, understanding what can go wrong and collected experiences add to the quality of the final purchase decision.

REFERENCES

- SKF (1991). General Catalog 4000.
- SKF (2005). General Catalog 5000.
- National Lubricating Grease Institute (1968, 1982). *NLGI Steady Flow Charts for Grease*.
- Arveson, M.H. (1934). Flow of Petroleum Lubricating Greases. *Industrial and Engineering Chemistry*, June, pp 628–633.

.....

PART 2

Solving Real Problems Using Numerical Analysis and Simulation

- Simulation for Equipment Sizing, Longwall to Stockpile **43**
- Simulation as a Tool to Determine Stockyard Handling Capacity **47**
- Interfacing Belt Feeders and Hoppers to Achieve Reliable Operation **53**
- Discrete Element Modeling of Sag Energy Losses in a Conveyor Belt System **65**

.....

Simulation for Equipment Sizing, Longwall to Stockpile

Edmond O'Donovan*

When longwall equipment is being specified, a nominal capacity is generally given on which to base the design of the various face and out-bye systems and components. This capacity generally comes from a nominal annual capacity requirement based on realistic utilization rates. From illustrative examples of simple system simulation, this paper sets out to show that a single nominal capacity is not sufficient to size the different systems. The manner in which the Longwall is operated and the overall system configuration and availability can have a significant impact on overall productivity.

INTRODUCTION

When a longwall is purchased, it will have a nominal capacity expressed in tonnes per hour. This is usually the cutting capacity of the shearer and is certainly the maximum average capacity that can be achieved from the system. However, sizing the coal clearance system based on this nominal capacity will always result in problems and expecting that the long term average production is closely related to this nominal capacity is also quite unrealistic. In this paper the effect of the cutting cycle on both the peak and average production rates will be examined.

The coal clearance system in a longwall operation is usually defined as starting at the Stage Loader since this is a convenient place to separate the responsibilities of the face equipment and conveyor system. While this separation is helpful for engineering and maintenance purposes, it provides a psychological barrier between two classes of equipment that in fact are complementary in the process of removing coal from the mine.

There are currently longwalls around the world with capacities of more than 5,000tph. Exactly what is meant by this is not altogether clear, but no-one expects a 5,000tph longwall to be able to produce 100,000 tonnes in a day. The difference between rated capacity and mean production is usually explained away in terms of availability, reliability, utilisation and other somewhat rubbery concepts. What is rarely appreciated is that the manner in which the longwall is operated has a major influence on the productivity of the face. Most importantly for the coal clearance system, matching the operation of the face equipment with the conveyor system can increase the mean production of the mine for little or no capital cost.

PRODUCTION RATES

For ease of understanding, it will be helpful to define what is meant by different sorts of production rates.

Shearer Cutting Rate	The rate at which the shearer cuts
AFC Clearance Rate	The rate at which coal feeds off the AFC and onto the out-bye conveyor system
Mean Production Rate	Total tonnes cut in a single shear divided by the time taken to complete a shear

To illustrate this point, a number of examples are shown.

Figure 1 shows the shearer position relative to the face of a commonly used cutting cycle. It is Full Web, Bi-Directional. This means the shearer takes the full seam height, for the full drum width as it travels along the face in both directions. The approach shown in Figure 1 has the shearer operating at the same speed in both directions for the main part of the cutting cycle, with lower speed for the stages when the shearer is cutting into the snake at either end. Figures 2 and 3 show the Shearer Cutting Rate and the AFC Clearance Rate for the above cutting cycle.

As Figure 2 shows, during the cutting cycle from both Maingate to Tailgate (M-T) and Tailgate to Maingate (T-M), the shearer cutting rate is the same. However, as Figure 3 shows, due to the speed of the AFC, the clearance rate from the AFC is significantly different when the shearer moves in different directions. The cutting rate is always 2,750tph, but the clearance rate on the M-T run is only 2,500tph, while on the T-M run is 3,000tph. While

* EJ. O'Donovan & Associates, Brisbane, Australia.

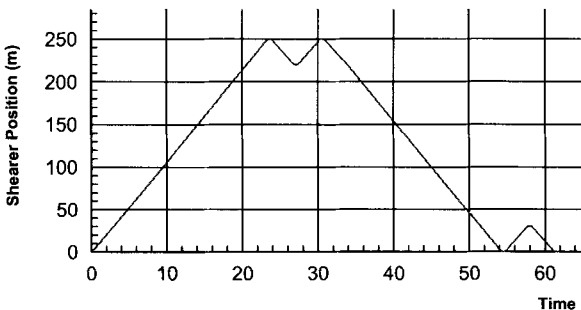


FIGURE 1 Shearer position for full web bi-directional cutting

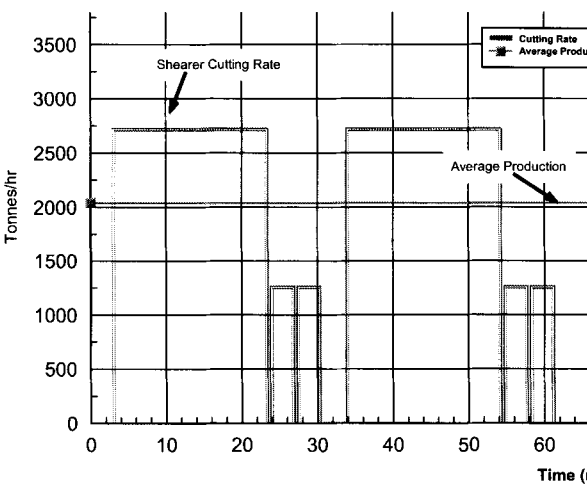


FIGURE 2 Shearer cutting rate

the shearer is only sized for 2,750tph, the AFC and conveyors must be sized for 3,000tph. It is important to notice that while the peak clearance rate is 3,000tph, the average production rate for the cycle is only 2,000tph. This means that even if everything is perfect, the conveyor system must be sized for 3,000tph and can never produce more than 2,000tph, even if there is 100% utilization and 100% availability.

If Clearance Efficiency is defined as

$$\text{Clearance Efficiency} = \text{Peak Clearance} / \text{Mean Prod}$$

then this cutting cycle has a Clearance Efficiency of 66%. In practical terms this means that the mine must capitalise for a 3,000tph coal clearance system, but even if that works perfectly with 100% availability, they will only ever get 2,000tph average production. Similarly, the Cutting Efficiency is only 73%.

Of course there are ways to improve the Clearance Efficiency and most operations make some effort in this area. The most common option to get better overall performance is to operate the shearer at different speeds on the M-T and T-M Cuts. For the system to efficiently use a 3,000tph conveyor system on both the M-T and T-M runs, then the shearer must operate significantly faster on the M-T run.

Figure 4 is a combined graph of Shearer Cutting Rate and AFC Clearance rate with the speeds adjusted to give uniform loading on the AFC in both directions.

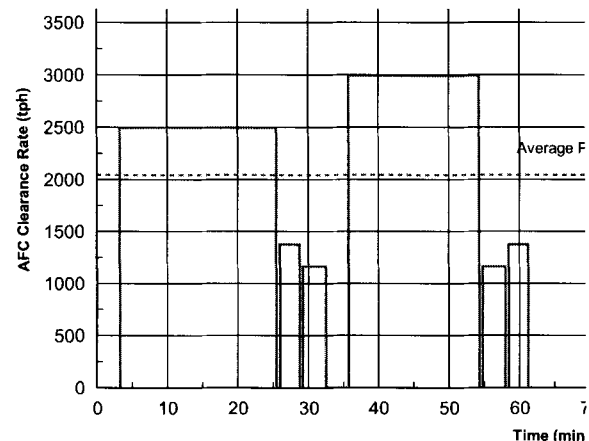


FIGURE 3 AFC clearance rate

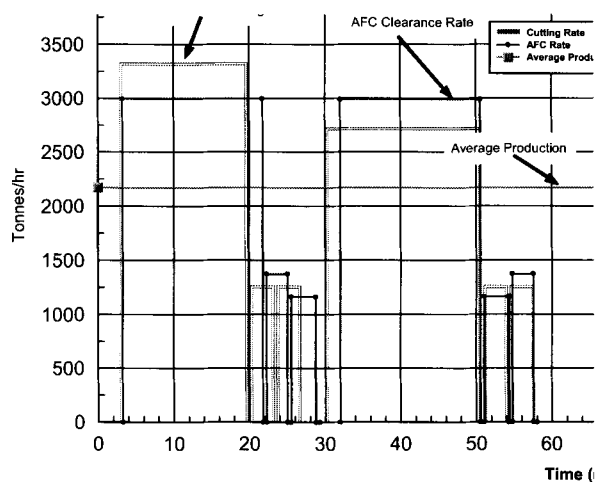


FIGURE 4 Shearer speed adjusted to give uniform AFC loading

The new arrangement gives an AFC Loading Rate of 3,000tph in both directions and an Average Production Rate of 2,200tph. This means the Clearance Efficiency is now 73%. This is a significant improvement. It does however require a shearer that can cut at a rate of 3,300tph whereas the constant speed option had a peak cutting rate of only 2,750tph. So while the Mean Production Rate has increased by 10%, the Cutting Efficiency has fallen to 67%.

While it is clear that improved Clearance Efficiency comes at the price of decreased Cutting Efficiency, it should be remembered that as a mine progresses through its life, upgrading the shearer is relatively easy, whereas upgrading the AFC and particularly the conveyor system, is usually a much bigger task.

It is interesting to note that a significant reason for the overall inefficiency of the Full Web Bi-Di Cutting Cycle, is that the shearer spends a significant portion of its time in unproductive maneuvers at the ends of the runs. These have a greater effect on narrower faces, but are still important on even very wide faces.

There are alternate cutting cycles that reduce the amount of time spent shuffling at the ends of the block and

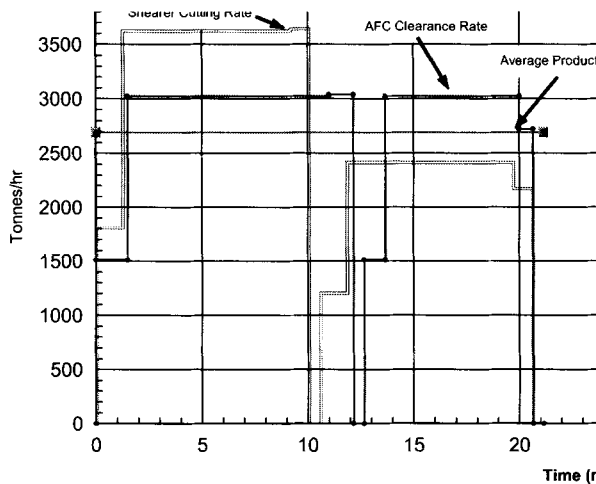


FIGURE 5 Half web bi-directional cutting

hence increase the overall efficiency of the operation. One cycle offers significant benefits referred to as Half Web, Bi-Directional. With this cutting approach, the shearer only takes a part of the Web in each direction so in one trip up and back it only takes one Web thickness. In this type of operation, the shearer will usually operate at the same speed in both directions, but regulate the load on the AFC by taking a different portion of the Web on the two different runs. The big advantage of the Half Web approach is that it requires less shuffling at the ends.

Figure 5 shows the Cutting and Clearing rates for a Half Web Bi-Di cutting cycle with the same general parameters as the Full Web examples.

For the same overall production rate, a Half Web approach requires much higher shearer speeds than a Full Web cycle. This is because in a single up and back pass, the shearer will only cut one drum width, while with the Full Web cycle, two drum widths are cut. However the Half Web option does have some significant benefits.

As can be seen in Figure 5, the performance improvement is dramatic. For the same peak clearance rate of 3,000tph, the average production is now 2,700tph while the peak cutting rate has risen to 3,600tph. These numbers give a Clearance Efficiency of 90% and a cutting efficiency of 75%, a substantial improvement in both.

The Clearance Efficiency of 90% is particularly impressive. It means that the theoretical limit on production is now 90% of the coal clearance capacity, rather than 73% for the optimized Full Web cycle, and 66% for the uniform cutting rate Full Web cycle.

These calculations show the importance of understanding the cutting approach when selecting equipment for the longwall. It is particularly important if a mine is looking for a capacity increase. The option of bigger equipment generally is always attractive and but it can be expensive and difficult to implement in an existing mine. This is particularly the case if the conveyor system needs significant upgrading. The option of a faster, higher powered shearer and a change in the cutting cycle can result in significant production increase with a relatively small capital injection.

While changes to the cutting cycle are not always simple, due to mining conditions, dust issues and all manner of other problems that beset every longwall

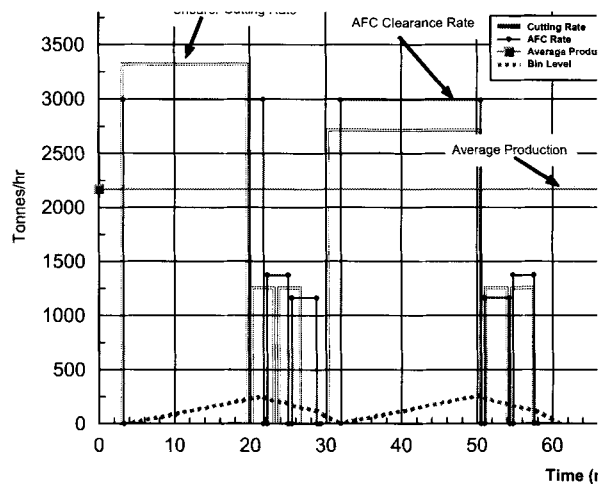


FIGURE 6 Bin level discharge at mean production rate

operation, it is an option that should be examined whenever a mine is limited by its coal clearance system.

EFFECT OF A SURGE BIN

Apart from modifications to the LW Cutting Cycle, the use of a surge bin close to the LW is another way of getting more coal out of the mine without a major upgrade to the entire coal clearance system. As mentioned before, upgrades to the longwall and panel conveyors are relatively easy as they can be done without disruption to the rest of the mining operation. It is the upgrading of the out-bye conveyors that are difficult as they continuously needed for both development and production. What a surge bin does is reduce the capacity requirement of the conveyors out-bye of it from the Peak Clearance rate to the Mean Clearance rate. For the Full Web Bi-Di example, an adequately sized bin would reduce the demand on the out-bye conveyors from the peak clearance rate of 3,000tph to the mean clearance 2,200tph. Another way to look at the issue is to say that the installation of a surge bin will enable a 2,750tph shearer to be used sensibly with a 2,200tph conveyor system.

Proper sizing of the bin is important. Whenever bins are discussed, there is always a desire to be able to hold an "entire shear." Often this extends to holding an entire shift's production. A very large bin is needed for these conditions and is almost always uneconomical. However, it is surprising how small a bin is needed to reduce the peak clearance rate to the mean clearance rate. Figure 6 is the same as Figure 4 except that it also includes a line showing the accumulation of material in a bin, if material is removed from the bin at the mean clearance rate. ie How much material will accumulate in the bin if it is feeding out of the bin at a rate of 2,200tph.

As can be seen in Figure 6, the peak accumulation in the bin is 265 tonnes. This means that a 300t surge bin would be sufficient to enable the 2,200tph out-bye conveyor system to operate with the longwall, despite there being peak clearance rates of 3,000tph.

AVAILABILITY AND RESTARTING

Another area in which the coal clearance system can have a profound influence on the productivity of a longwall operation is availability. This is particularly the case

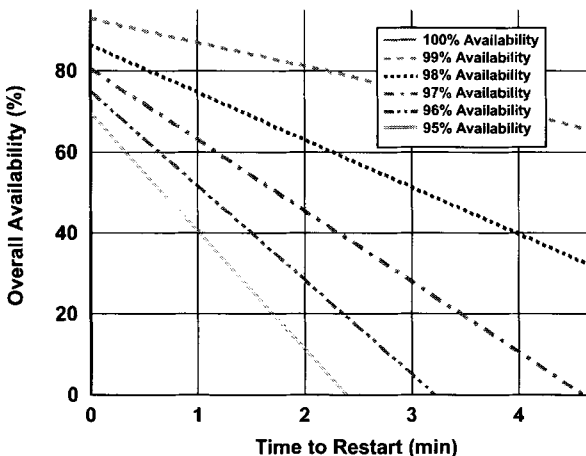


FIGURE 7 Overall system availability (Individual availability 95%–100%)

as the number of conveyor flights from the face to the stockpile increases.

While it is universally known that availability is vital, what is not appreciated so well is that all availabilities are not equal! In a multi flight system, the most out-by conveyor has a disproportionate effect on the availability of the overall system. This is due the time required to restart the system in the event of a conveyor trip. If a single flight takes one minute to start, then if the maingate conveyor trips, the overall system will only incur a delay of one minute. If the most out-by conveyor in a seven flight system trips, the overall system will incur a delay of at least seven minutes while all the conveyors restart.

Often the most out-by conveyor in a longwall operation is a small and relatively insignificant conveyor. Frequently it is a short stacking belt or similar. This makes it far less glamorous than say a multi-tripper maingate system with torque controllable drives and sophisticated controls, or a high powered, high lift drift belt. It is, nevertheless, important to be aware that these out-by conveyors have a greater influence on overall availability than in-by conveyors.

Figure 7 shows the overall availability of a seven flight conveyor system with varying availabilities of the individual flights and various restart times per conveyor. The modeling has assumed that there is one restart for each one percent of down time per flight. i.e. In a single shift, a conveyor with 99% availability will have one stop, whereas a conveyor with 97% availability will have three stops.

This figure shows a dramatic fall in availability as the number of restarts rises and is particularly worrying if the availability of individual flights falls below 99% or the restart time is more than about one minute per flight.

Figure 8 shows the same information except that that it is for availabilities of 99.5% to 100%. In this figure, the assumption is that there is one restart per shift for every 0.1% down time. (This is probably not realistic as high availability conveyors usually have very few stops, but it does illustrate the point.) The results here are even more startling. Even if the conveyors individually have excellent availability, frequent short stops, and long start times will severely effect overall availability in a multi flight system.

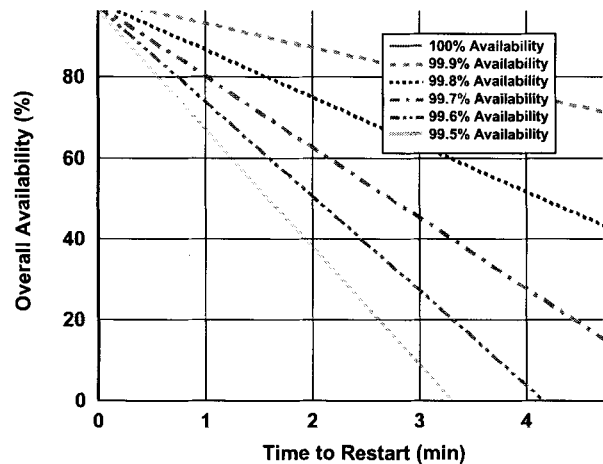


FIGURE 8 Overall system availability (Individual availability 99.5%–100%)

For many modern conveyors, the starting time can be several minutes, as the start sequence includes run up and testing of various ancillary components such as pumps, fans, brakes etc. For such systems, perhaps the time has come for new ways to provide sequence for starting the conveyors.

The usual starting sequence for a series of conveyors is the most out-by conveyor is started and once it is up to speed, a sequence command is sent to the next conveyor. It starts and when it is up to speed the sequence command is passed to the next conveyor and so on. The sequence command is often a hard wired switch, but increasingly is sent over a control network. For operations where control networks exist, there are a number of options that can significantly reduce the overall startup time. These include sending a provisional start command so that all preliminary start checks such as starting pumps and fans, pre-tensioning take-ups etc. can be achieved while other conveyors are starting. A further option that could have merit is a sequence where the conveyors start together, with the in-by conveyors never operating faster than 80% of the next conveyor.

The networks and control systems to achieve these benefits are in place in an increasing number of mines, and there are significant benefits to be gained by implementing strategies such as these.

CONCLUSIONS

The object of the paper has been to demonstrate that nominal capacities of various items involved in Longwall production are at best only one factor in estimating the actual production rate that can be expected from a system. In particular, the manner in which the longwall is operated will have a significant impact on the sizing of the coal clearance system. In operations where this is the production limiting factor, attention to the cutting cycle may be a more effective manner of increasing overall production than upgrading the conveyor system.

The use of a surge bin to better utilize the out-by conveyors has also been shown to be most effective.

As will all mechanical systems, availability is very important to overall production but in a multi-flight system, the effect of long re-start times is also very important. For operations that face this problem, strategies to reduce the impact of the starting delays have been suggested.

.....

Simulation as a Tool to Determine Stockyard Handling Capacity

Eric Monrad* and **Harry King***

Discrete event simulation modeling provides a tool to quantify the throughput capacity of stockyards. Interactions between the main equipment types (trains, dumpers, conveyors, stackers, reclaimers, shiploaders) can be captured, including route blockages, breakdowns, and planned maintenance. Simulation has been successfully used at world-class stockyard facilities to determine current capacity and to identify gains resulting from improvement projects. Recent projects have focused on iron-ore, coal, and soya facilities, but the technology is suitable to be used on any bulk material type.

INTRODUCTION

Bulk materials include commodities such as coal, iron ore, cement, grain, and wood chips. They are typically transported from the point of production via train, truck, overland conveyor, or slurry pipeline to a central terminal, where they are stockpiled. From the central terminal, they are sent to market via ship or train. This paper will consider a port operation that is fed by trains and loads ships as being representative of the other possible combinations.

A typical problem faced by port planners when planning port operations is to determine the current throughput capacity of the port and to determine the infrastructure improvements necessary in order to achieve a higher targeted throughput.

Determining the capacity of a system can be complex. The operation includes interactions between a variety of equipment types with buffer storage in different areas. Complexity is also added when there are requirements to track several product grades for blending or if there is additional processing done at the port. A final complexity is the introduction of random events such as equipment breakdowns or weather downtime.

Simulation modeling is a tool that can be used to evaluate these complexities, to determine port capacities, and to confirm infrastructure requirements for expansion. It can take into account all of the interactions between the pieces of equipment as well as the random influences, which allows a realistic assessment of the capacity to be made.

RULE-OF-THUMB APPROACH

In the past, ports were designed using rules of thumb or very simplified calculations. For example, stockyard capacities could be specified to be 10% of the annual throughput (that is, for a 5.0 Mt/y operation, the stockyard requirements would be estimated to be 500,000 tonnes). This approach is intended to capture the storage requirements that result from seasonal peaking in production, late ships, breakdowns of equipment, and weather downtime and is based on past experience.

The shortcoming of the approach is that it often either results in overly-conservative designs or else it neglects site-specific conditions that result in different requirements than previously experienced. The benefit of this approach is that it is very fast and can be accurate if it captures valid past experience for a particular operation.

SPREADSHEET OR HAND CALCULATION APPROACH

A more detailed approach than rule-of-thumb is to perform some calculations, by hand or through a spreadsheet, to estimate requirements more carefully. Continuing with the stockyard capacity example, such factors as annual seasonality, expected late arrivals of ships, and desired buffer stock might be included in a calculation to estimate the required stockyard capacity.

This approach requires some more time and effort than the rule-of-thumb approach, but is still quite fast. The shortcoming of this approach is that random variability and interactions between the equipment areas are not taken into account. It can be very difficult to capture interactions, randomness, and such effects as weather

* Sandwell Engineering, Vancouver, British Columbia, Canada.

downtime in a manageable spreadsheet. As more complex spreadsheets are made to capture some of these effects, it also increases the opportunity for a mistake to be made and makes auditing difficult.

SIMULATION MODELING APPROACH

Recent increases in computational power have allowed a much more detailed approach to be taken. Simulation modeling explicitly incorporates the elements that are implicitly allowed for in the rule-of-thumb or calculation approaches. Significant factors may still be overlooked as the model is developed, but it is less likely for two reasons. First, the act of creating the simulation model requires the details of the operation, such as connectivity, rates, and downtime, to be explicitly defined and matched to reality. Second, the model results can sometimes uncover unexpected, but true, relationships between operations.

In a discrete-event simulation model, a representation of an operating system is created and modeled through time. The basic building block of a simulation model is the “object.” Objects are created by the modeller to represent equipment and processes in the system, such as trains, conveyors, and stockpiles. Each objects has parameters that specify its qualities. A reclainer, for example, would have parameters such as peak rate, average rate, physical location, and travel speed. Logical rules govern the interactions between the objects. For example, stackers and reclaimers located on a shared conveyor can not pass each other.

External events such as weather and production variation (due to ore hardness, for example) can be included in the model. Random events, such as equipment breakdowns and variation in activity time, can also be included. Simulating external and random events over a long period of simulated time allows a detailed and quantitative understanding of the expected operation of the system to be gained.

EQUIPMENT CAPACITY

Individual pieces of equipment have a throughput capacity. In some cases, there is a clear bottleneck to an operation and the capacity of the system as a whole is equal to the capacity of the bottleneck piece of equipment. In other operations, the capacity of the system as a whole is less than the capacity of any individual piece of equipment due to interactions between sub-operations. This section describes a methodology to calculate the capacity of individual pieces of equipment based on historical operating data. Simulation is required to determine the throughput capacity of the operation as a whole, including interactions between the sub-operations.

The main equipment types used in a port stockyard are: train dumper, conveyors, stackers, reclaimers, and shiploaders. Each piece of equipment has a design rate, normally expressed in tonnes per hour. The first step in determining the capacity of a particular piece of equipment is to analyse operating data for that piece of equipment to determine the actual average rate achieved in a particular operation. The average rate can be affected by site conditions, operator efficiency, and mechanical efficiency. For new pieces of equipment or green-field sites, performance data for similar pieces of equipment and sites can be used.

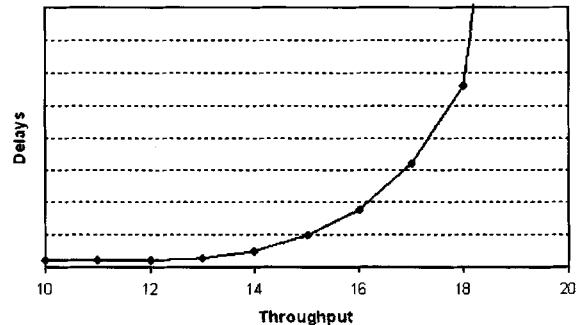


FIGURE 1 Exponential increase of parameter as throughput Increases

The next step is to determine the amount of time per year that the piece of equipment will not be available to work for any of the following reasons: scheduled maintenance, unscheduled maintenance (breakdowns), “blocked upstream” (an example of “blocked upstream” is the time a stacker would not be available to stack due to a conveyor or dumper breakdown that occurs while a train is unloading), and “blocked downstream” (an example of “blocked downstream” is the time a reclainer would not be available to reclaim due to a conveyor or shiploader breakdown that occurs while a ship is loading).

The time in which a piece of equipment is not working and is not in one of the above states is classified as idle time.

The term “commitment” is defined to include all time for a piece of equipment except its idle time. Commitment is similar to the term “utilisation” that is in more common use. A weakness of utilisation is that there are several interpretations of its formula, depending on the person using it or the application it is being used for. Commitment has a theoretical maximum at 100% while utilisation typically has a theoretical maximum of something less than 100%, depending on the formula being used.

As a piece of equipment or an operation reaches high commitment/utilisation levels, negative effects will occur. The negative effects typically manifest as queuing upstream of the high-commitment area and these queues translate into system delays, decreased capacity, and in some cases (such as demurrage) direct costs. As the throughput through a piece of equipment increases, its commitment will increase linearly, but the effects of high commitment will increase rapidly to a vertical asymptote as 100% commitment is approached. Figure 1 demonstrates the rapid increase in delays as throughput increases.

While the theoretical maximum commitment of a system is 100%, the practical maximum is somewhat less. The benefits of increased throughput, such as increased revenue, must be balanced against the negative effects of high commitment, such as increased demurrage. A key decision that has to be made that is specific to individual operations is the level of commitment that is considered to be the capacity of the piece of equipment or operation. For example, to reach a targeted

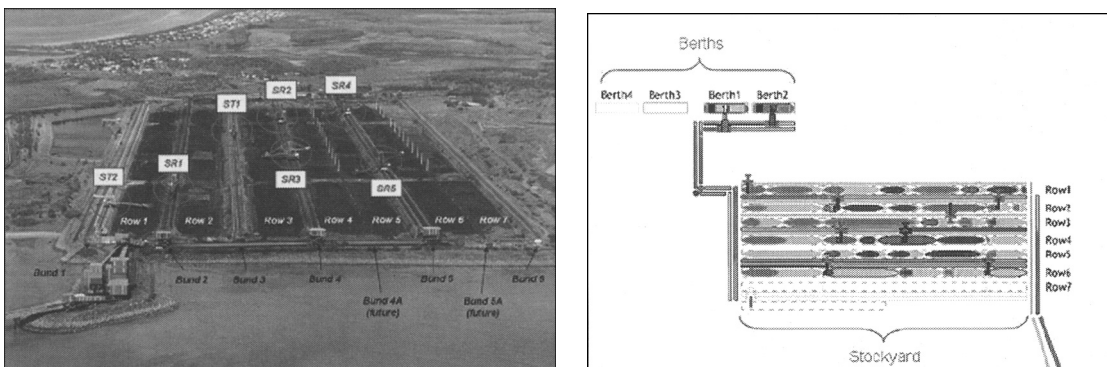


FIGURE 2 Coal terminal layout (actual and modeled)

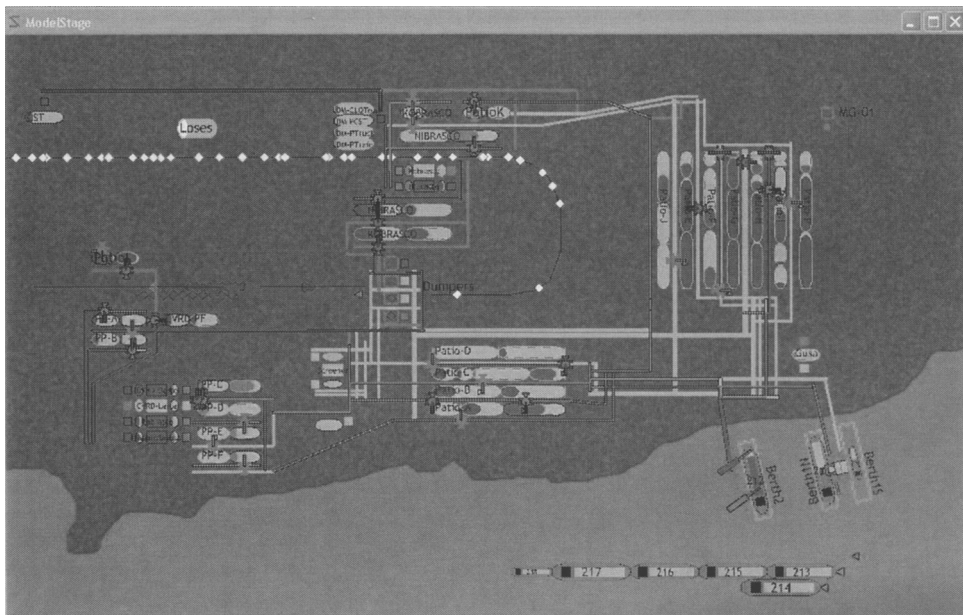


FIGURE 3 Graphical representation of model of complex iron-ore export port

future throughput, a port with two berths might forecast a commitment of 90% with significant annual demurrage costs. If a third berth were built, at some capital cost, the commitment would be reduced to 70% and the demurrage costs would be negligible.

Typically, commitment levels of 80–85% are used for design capacities—equipment and systems will normally run smoothly at this level without significant operational costs. Higher commitments can be achieved and may be desirable—the revenue generated by extra throughputs may offset the operational costs. In some cases, generally those with high variability or unusual restrictions, capacity may be reached at lower commitments.

CASE STUDIES

The following case studies are intended to show the variety of applications simulation can be used for and the types of decisions it can aid in.

Case Study 1—Port Capacity Analysis

The focus of this model was the marine terminal, so the mine and rail operations included only minimal detail, such as the average production rate, number of trains, average train capacity, and the average travel time to an from the terminal. The terminal itself was modeled in considerable detail. Production flows from the mines for each grade of coal to the mine stockpiles, where it is taken via train to the marine terminal. Train dumpers unload the trains and conveyors feed to either the stockyard (for stacking into piles) or to the berths (for direct loading onto ships). An actual view of the port stockyard as well as a view of the simulation model graphics are shown in Figure 2.

In the model, the movements of trains and ships in the model are coordinated in the following steps:

1. The main driver for the model's logistics is mine production. Annual production for each mine and grade are entered as inputs to the model.

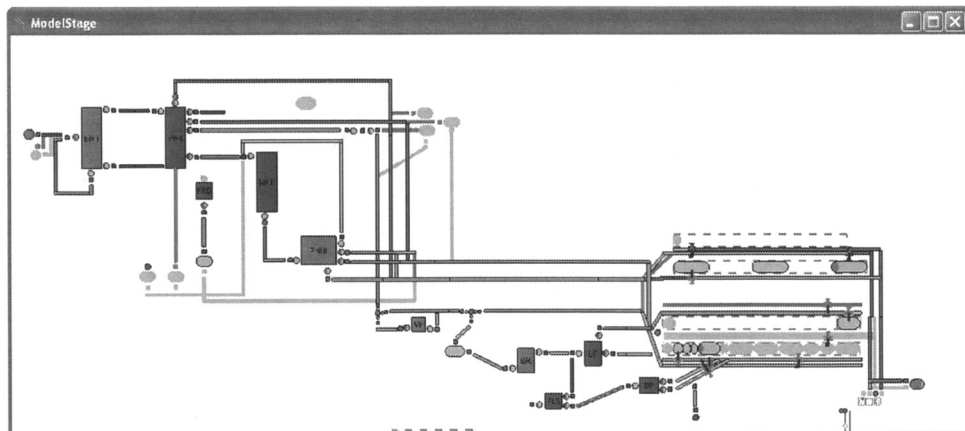


FIGURE 4 Graphical representation of a beneficiation plant

2. Ships are chartered with stem dates (i.e., scheduled arrival dates) that match the availability of coal for each parcel. The size and number of parcels for each ship are selected appropriately from the historical distributions for each grade.
3. The actual arrival time for each ship is selected randomly in a window around its scheduled time based on historical ship arrival data for a similar bulk terminal.
4. Coal is moved by rail from the mines to the terminal on a just-in-time basis, to match ship arrival times over the next ten days. Only the amounts needed for the ships' cargoes (plus any extra amount needed to make up full train loads) are railed to the terminal. If sufficient trains and stock-yard space are available, the model accumulates the full amount for each of the ship's parcels two days ahead of its arrival time at the terminal.

The operation was modeled at increasing levels of throughput to determine the port capacity. Capacity was determined by the utilization of the inloading and outloading components of the port. When utilization reaches an impractical level, queuing of trains and/or ships will occur, resulting in high demurrage costs and, ultimately, a shortfall from the target throughput level.

Stepped infrastructure cases can be modeled to determine the optimal path forward to meet future throughput targets.

Case Study 2—Port Capacity Analysis

This port is shown to demonstrate that even the most complex ports can be modeled with relative ease. The port shown in Figure 3 includes four dumpers, seven pelletization and screening plants, and recirculation of product through several stockyard areas.

Case Study 3—Process Bottleneck Analysis

Generic processes can also be analysed using simulation. An example is a beneficiation plant used by an iron-ore exporter. The modeled representation of the process is shown in Figure 4.

The beneficiation process included several steps, with the bottleneck being the secondary crushing. At increasing

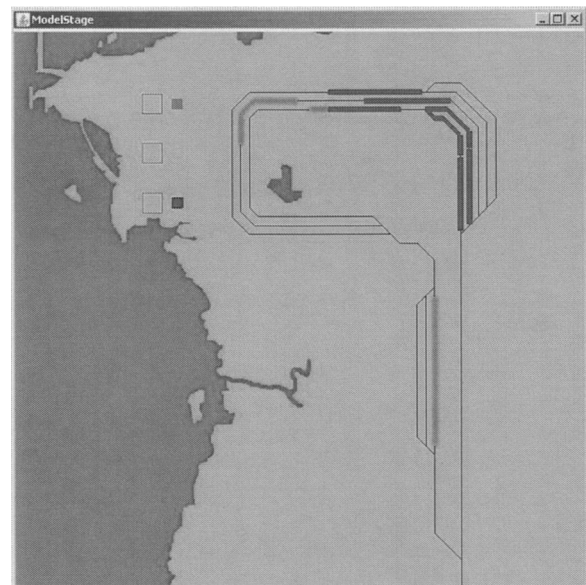


FIGURE 5 Graphical representation of modeled railyard

throughputs, buffer storage and processing rate requirements throughout the plant were determined.

Case Study 4—Railyard Operations

Rail capacity is often limited by complex operations at the rail-yard. The rail yard shown in Figure 5 included the movements of trains as they entered the yard, split into two sub-units, and proceeded to one of three dumpers. Through the simulation, railyard bottlenecks and capacity could be found.

Case Study 5—Operational Synergy

After an acquisition, two iron-ore export facilities were owned by the same parent company. A simulation study was performed to determine the synergies that could be obtained by operating the two ports as a single unit. A view of the combined operation is shown in Figure 6.

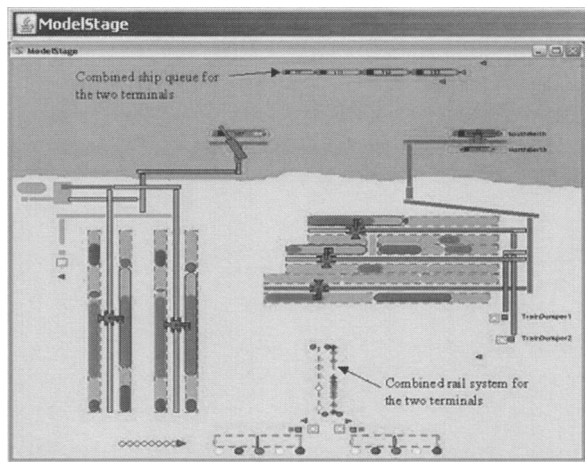


FIGURE 6 Graphical representation of modeled ports

CONCLUSIONS

The rapid increase in computing capacity and processing speed has made it possible to prepare simulation models that include much greater detail and realism than was possible in the past.

The application of simulation to commodity transportation systems has allowed capacity planning to be performed to a high level of detail. Simulation modeling is currently used in a wide variety of applications in the commodity industries including rail, port, pipeline and sea operations; materials such as coal, iron-ore, and soya; and a wide variety of throughput levels and physical environments.

As computing power continues to increase, it is expected that the use of simulation will become a standard tool widely used to improve operations and to plan infrastructure investments.

.....

Interfacing Belt Feeders and Hoppers to Achieve Reliable Operation

John Carson,* Francisco Cabrejos,† and Michael Rulff‡

Belt feeders are commonly used to meter the flow of bulk solids from bins and hoppers. If the interface between the hopper outlet and belt feeder is not designed correctly, flow from the bin may be severely compromised, resulting in problems of no-flow, segregation, flooding, etc. By knowing the flow characteristics of the bulk solid being handled and applying proven design techniques, such problems can be avoided.

Relevant bulk solids flow characteristics are identified, along with measurement techniques. Design procedures for correcting problems with existing feeders as well as proper design of new feeders are presented, along with case histories of successful application of these procedures.

INTRODUCTION

A belt feeder is an extremely important element in many bulk material handling systems, since it is the means by which the rate of solids flow from a storage vessel (bin, silo, bunker, bore hole, hopper, etc.) or stockpile is controlled. When a belt feeder stops, solids flow should cease. When the feeder is running, there should be a close correlation between its speed of operation and the rate of discharge of the bulk solid.

Belt feeders differ from belt conveyors in that the latter are only capable of transporting material, not modulating the volumetric or mass flow rate. Throughput of a belt conveyor is set by the rate of solids flow onto it, so changing belt speed only changes the depth of material, not the belt's capacity. Because a belt feeder is flood loaded by the hopper located above it, changing belt speed changes the amount of material discharged per unit time.

For elongated hopper outlets, the primary feeder choices are: screw, belt, apron and vibrating pan. Plant personnel often have a preference for one or the other because of past experience, availability of spare parts, or to maintain consistency to make maintenance easier throughout the plant. However, there are reasons to choose one over the other depending on specifics of the application.

A screw feeder is often a better choice than a belt feeder if containment of the bulk solid is important—due, for example, to concerns about dust generation, spillage, etc. Screws are also capable of sealing the hopper outlet from downstream pressure if feeding into a higher-than-atmospheric pressure environment. Using a belt feeder in such an application requires a standpipe.

Screw feeders typically have a lower maximum capacity than belt feeders, and they have a limited length-to-diameter ratio within which increasing capacity can be reliably achieved. This value (typical 6:1 or so) is set by tolerances of fabrication of the screw. No such limit exists for belt feeders.

An apron feeder is sometimes used in applications involving abrasive bulk solids and/or when there is concern about damage due to impact of a falling stream when the bin is empty. The design basis for an apron feeder is very similar to that for a flat belt.

Vibrating pan feeders are sometimes used under elongated outlet bins. Unfortunately it is seldom possible to obtain uniform withdrawal over the entire outlet area with such a feeder unless the pan is oriented perpendicular to the major axis of the slot.

This last requirement (uniform withdrawal over the entire outlet area) is often essential if one is to avoid flow problems in a storage bin, as discussed below. Hence, feeder design and operation become critical in the performance of the bin.

* Jenike & Johanson, Inc., Tyngsboro, Mass.

† Jenike & Johanson Chile S.A., Viña del Mar, Chile.

‡ Jenike & Johanson, Ltd., Mississauga, Ontario, Canada.

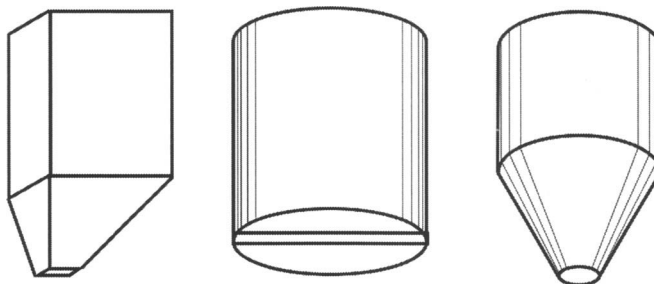


FIGURE 1 Examples of funnel flow bins

TYPICAL BIN FLOW PROBLEMS

To design an efficient storage bin and feeder, the engineer must be aware of problems that can arise during storage and flow of bulk solids:

- No flow. A stable arch or pipe (rathole) develops within the bulk solid and flow ceases.
- Erratic flow. Momentary arches form, or ratholes empty out partly and then collapse.
- Flooding. Powders can become aerated and flow uncontrollably through a bin outlet.
- Lack of design capacity. Much of the stored material remains stable around a rathole. A flow aid (e.g., vibrator, air cannon, sledge hammer) may be required to restore flow.
- Segregation. Particles of different sizes, shape or specific gravity tend to separate from each other creating zones in a storage system that vary in these properties. The zones may discharge at different times, resulting in quality control problems.
- Product degradation. Spoilage, caking, oxidation or attrition may occur when a material remains in a bin too long. This is usually caused by a first-in-last-out flow sequence. In some bins, the bulk solid is not discharged from the bottom until the bin is completely empty.
- Level control. Measuring the amount of material left in a bin is difficult if a rathole develops. In one portion of the bin the level control device may indicate the bin is full; in another portion, it may indicate the bin is empty.

BIN FLOW PATTERNS

All bin flow problems can be minimized or prevented by suitable design of the bin and feeder unit. This involves knowing the flow properties of the bulk solid, described below, and then choosing the appropriate type of bin and feeder.

One of three solids flow patterns may occur in a bin: funnel flow, mass flow or expanded flow. *Funnel Flow* is a phenomenon in which some of the material is stationary while the rest is in motion. Examples of funnel flow in bins are shown in Figure 1.

Characteristics of funnel flow bins are

- Low headroom. A bin with a flat bottom or shallow hopper has large storage capacity with minimal bin height.

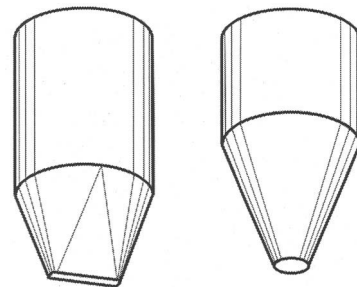


FIGURE 2 Examples of mass flow bins

- First-in-last-out flow sequence. The first material put into the bin is the last to be withdrawn, because the flow pattern allows material to channel in the region above the outlet. This is a problem if the bulk solid degrades with time.
- Ratholes may develop. Depending on the size of the flow channel, a rathole will develop if the material has sufficient cohesive strength.
- Erratic flow. Once a rathole becomes partially or completely empty, it may collapse. The impact may cause a stable arch to form or flow to be erratic.
- Flooding. Collapsing ratholes allow powders to become aerated.
- Segregation. Segregation problems are often made worse.

Funnel flow bins are only suitable for coarse, free flowing, nondegrading solids, when segregation is not important.

Mass flow is a bin flow pattern in which all the material is in motion whenever anything is withdrawn. Characteristics of mass flow bins, examples of which are shown in Figure 2, are

- Smooth steep hoppers. The hopper walls have to be steep and low enough in friction to force particles to slide along them.
- First-in first-out flow sequence. The first material put into the bin is the first material withdrawn, thus eliminating problems with product degradation.
- Fine powders deaerate. Allowing material to deaerate eliminates the problem of flooding.
- Segregation problems generally minimized. As material is withdrawn it is pulled from the sidewalls as well as along the centerline of the bin, causing the bulk solid to remix.

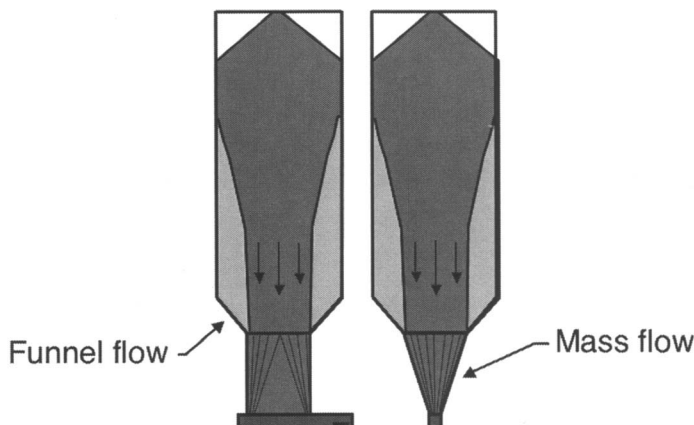


FIGURE 3 Example of expanded flow bin

- Material fed uniformly at constant density. Because all the material undergoes the same amount of compaction as it flows through the hopper, its bulk density and rate of flow through the outlet are essentially independent of bin level.
- Abrasive wear of hopper walls. Because particles are flowing along the walls, this is more likely than when using a funnel flow bin. Wear can be a significant problem when handling hard, angular particles in large bins at high throughput.

Mass flow bins are suitable, and in fact preferable, for cohesive solids, solids that degrade with time, and when segregation needs to be minimized.

Expanded flow combines some of the solids flow advantages of mass flow and the economics of funnel flow. A mass flow hopper is used at the bottom to expand the flow pattern into the upper funnel flow section thereby overcoming ratholing. An example of an expanded flow bin is shown in Figure 3.

BULK MATERIAL FLOW CHARACTERISTICS

The first step in solving or preventing a bulk solids flow problem is to measure the flow properties of a representative sample of the bulk solid. These tests must be run under conditions that accurately simulate how the solid is handled. They can be conducted on site if the solid's properties change rapidly with time or if special precautions must be taken.

The most important flow properties are described below.

Flow Function

A bulk solid's cohesive strength as a function of consolidating pressure is usually measured on a Jenike shear tester or comparable device (Jenike 1964; ASTM D6182-06, 2006; ASTM D6773-02, 2002). The test procedure involves applying compressive loads to a sample of the bulk solid and then shearing the sample to determine its cohesive strength. Minimum outlet dimensions required to ensure reliable flow are calculated from these measurements.

Cohesive strength of a given material is primarily affected by moisture content, particle size distribution, and storage time without movement. Strength typically increases as the bulk solid's moisture content increases,

its particle size decreases, or its storage time lengthens. Temperature also may affect a material's flow properties, particularly if chemical or physical changes occur.

Effective Angle of Internal Friction, δ

This is determined as part of the data analysis to develop a flow function.

Compressibility

The relationship between a material's bulk density and consolidation pressure is determined by a test in which a known mass of material is compressed under increasing consolidating pressures (ASTM D6683-01, 2001).

A material's bulk density at the pressures exerted at a hopper's outlet just above the feeder must be known in order to calculate minimum outlet dimensions required to ensure flow. This material property must also be known when determining loads applied to bin walls and feeders by a bulk solid, and when estimating feeder speed range needed to achieve a desired throughput.

Wall Friction

The smoothness of the wall surface affects wall friction (Jenike 1964; ASTM D6182-06, 2006; ASTM D6773-02, 2002). Generally, the smoother the surface (e.g., new, smooth vs. rusted carbon steel) the less frictional resistance to most bulk solids. Lower friction allows less steep hopper walls to achieve mass flow.

The bulk solid's moisture content, particle size, temperature, and storage time also affect wall friction. Moisture can migrate within bulk solids if there is a temperature gradient. A high amount of moisture on the walls can cause solids to freeze during the winter or become more frictional. In some cases moisture lubricates the surface and reduces friction. Rough, jagged particles are almost always more frictional than smooth, round ones.

Permeability

The ability of air or gas to flow through the voids between particles is measured by passing a gas through a column of material that is compacted to various bulk densities (Carson and Marinelli 1994). The test results are used to predict critical, steady state discharge rates of fine powders and determine the amount of gas that is required for an air permeation system to overcome those

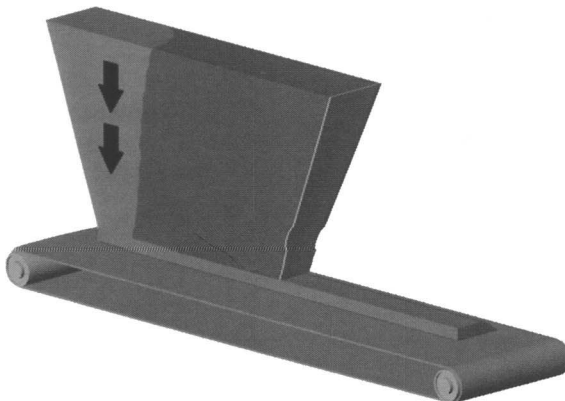


FIGURE 4 Example of improper belt feeder interface that allows feed from the back

rates. In addition, deaeration times and flooding (flushing) conditions can be analyzed.

Abrasiveness

The rate at which a bulk solid wears out a hopper or chute surface is a function of the pressures exerted on the surface, the total amount of material that travels across the surface, and the particles' size, shape, and relative hardness. Laboratory tests can determine the life expectancy of a bin or chute liner, or other material handling equipment (Johanson and Royal 1982; Johanson and Royal 1984).

Friability

Friable materials break down because of high pressures, high velocities or both. For instance, mechanical or pneumatic conveying can break bulk solid particles. Attrition tests can predict the pressure at which particle breakage occurs (Carson and Marinelli 1994).

Angle of Surcharge

This is the slope that forms as a bulk solid is conveyed on a belt. Strictly speaking it is not a flow property but the result of flow properties.

Particle Size

Both maximum particle size and particle size distribution are important for sizing bin outlets and belt feeder interfaces.

CRITERIA FOR BELT FEEDER DESIGN

A belt feeder should provide the following:

- Reliable and uninterrupted flow of material from some upstream device (typically a bin or hopper).
- The desired degree of discharge flow rate control over the necessary range.
- Uniform withdrawal of material from the outlet of the upstream device. This is particularly important if a mass flow pattern is desired, perhaps in order to control segregation, deliver uniform residence time, or to minimize caking or spoilage in dead regions.
- Minimal loads acting on the belt from the upstream device. This minimizes the power required to operate the feeder, as well as minimizes particle attrition and abrasive wear of feeder components.

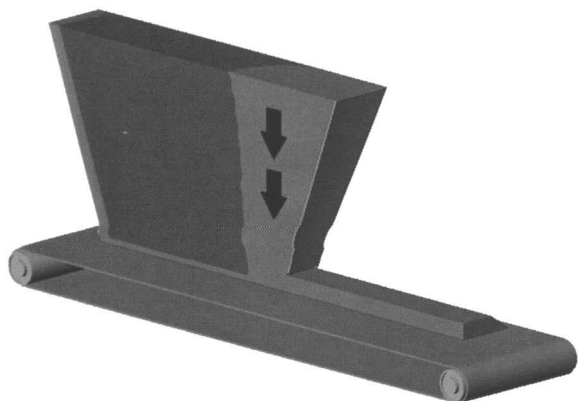


FIGURE 5 Example of improper belt feeder interface that allows feed from the front

PROBLEMS TO AVOID WHEN USING BELT FEEDERS

Flow Issues

If the outlet through which the bulk solid is expected to flow is too narrow, arching due to interlocking of large particles or cohesive strength of smaller particles can prevent material from discharging. If the interface between the hopper and belt feeder is not properly designed to discharge material uniformly over the entire cross section, a funnel flow pattern will develop with the additional potential problem of ratholing.

With fine powders, the discharge rate may be limited if the belt feeder is operating at a speed greater than the bulk solid's critical steady state rate of discharge. Similarly, flooding of fine powders is a common problem if the interface is not designed for uniform withdrawal and/or the bin is not designed for mass flow.

Channeling of material in the bin is possible if the interface is not properly designed. Unlike screw feeders, which, if they channel, do so at the back end of the outlet, an improperly designed belt feeder interface can result in channeling at either the back or front end depending on the front gate opening. See Figures 4 and 5.

Mechanical Design Issues

Sometimes the power required to shear material and operate a belt feeder is greater than the available power. This problem is usually the result of an improperly designed interface that does not allow uniform withdrawal over the entire cross section of the outlet. Also, if the interface is not structurally designed and reinforced to withstand the pressures exerted by the bulk solid against it, it will deform in such a way that significantly higher forces are needed to shear the material (Jenike & Johanson 1983). Another cause of excess power is differential settlement between a bin and an independently supported feeder, which compacts material above the feeder. A fourth cause is excessive belt sag between idlers.

Sometimes belts wear out prematurely. This is usually the result of an improperly designed interface or an interface too close to the belt. Another problem is choosing the wrong belt carcass for the material being handled.

A third mechanical design issue is belt slipping on the head pulley. This is usually an indication that the belt is not tensioned properly.

Operational Issues

Excessive spillage and/or dust generation create house-keeping and environmental concerns. Particles falling onto the top of the return portion of the belt may create tracking problems and premature belt and idler wear.

Belt sag between idlers can allow particles to escape, increase idler loads and increase skirt wear. Sag can also excite the bin to vibrate at one of its resonant frequencies, which may damage the structure (Purutyan et al. 1994).

BELT FEEDER SIZING AND DESIGN

Belt feeders can be ideal for handling friable, coarse, fibrous, elastic, sticky, or very cohesive materials. They can even be used with fine powders provided careful attention is given to the design of the bin and feeder (Reed and Johanson 1972). Since belting is commonly available in widths up to 3 m (10 ft) and unrestricted lengths, belt feeders can be designed for much larger outlets than most any other type of feeder.

If the gap between the bin interface and belt is constant along the length of the outlet with capacity set by the opening of a front gate, material will be withdrawn preferentially from one end of the outlet. Various methods of providing an increase in belt capacity with length have been tried (Bridge and Carson 1987), including:

- Taper in plan achieved by varying the elevation of the intersection of the cylinder (i.e., vertical-sided section of bin) and hopper. This is not recommended for most materials because the narrow back is prone to having arches form over it.
- Taper in elevation achieved by varying the elevation of the intersection of the cylinder and hopper sections. This is a useful configuration; however, it will tend to withdraw material at a greater rate at the downstream end of the outlet due to the angle of surcharge on the belt.
- Taper in both plan and elevation, restricted by vertical side walls, with capacity set by front gate opening. This geometry can be achieved by maintaining a constant elevation of the intersection of the cylinder and hopper sections. Uniform withdrawal is possible provided the gate is properly adjusted (Rademacher 1982). Unfortunately, operators are likely to move the gate to adjust output, thereby preventing uniform material withdrawal.

Proper sizing of a bin outlet/feeder inlet is usually dictated by the needs to prevent a stable flow obstruction (i.e., an arch) from forming, prevent ratholing in the bin above, and deliver the required discharge rate. A rectangular bin outlet is a good design choice when using a belt feeder because it has the advantages over a circular or square outlet of:

- Reducing the minimum opening size required to prevent arching by a factor of approximately two. For example, if a certain bulk solid requires a minimum outlet diameter of 600 mm to prevent arching in a conical hopper, it will require only a 300 mm wide (by at least 900 mm long) rectangular slot outlet to prevent arching.

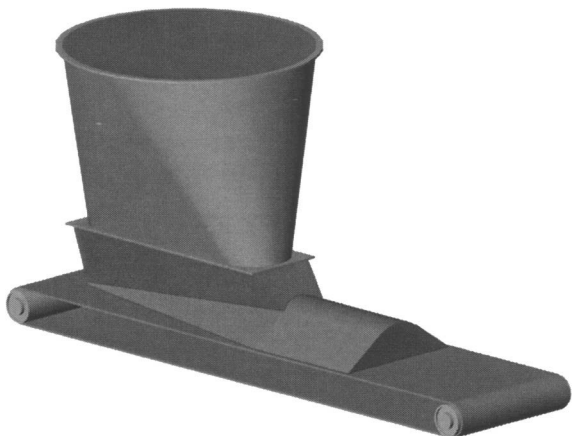


FIGURE 6 Example of mass flow belt feeder Interface

- Allowing mass flow to occur with less steep hopper walls. A conical hopper must be at least 10° to 12° steeper than the side walls of a wedge or chisel-shaped hopper to allow mass flow with the same wall surface.
- Minimizing or eliminating ratholing in a funnel flow bin because the size of the flow channel can be substantially increased by simply lengthening the outlet without increasing its width.
- Increasing the maximum steady state discharge rate.

A proven design that eliminates most of the problems described above is shown in Figure 6.

The minimum outlet width at the rear of the interface must be greater than or equal to the value required to prevent a stable arch from forming. The sloping side walls must be at least as steep as the hopper wall slope required for mass flow. Often there is an advantage to using a much steeper angle (10° to 20° from vertical is often used). This can reduce belt width and power consumption at a small expense of headroom, but may increase the risk of arching for some materials. Both the minimum outlet width and required hopper angle can be calculated from measured flow properties.

The slot length should be at least three times the width in order to realize the benefits of a rectangular outlet. Often it is advantageous to use a much longer slot with large silos or with wedge or chisel-shaped hoppers containing vertical end walls. The latter are useful geometries if the bulk solid being handled is very frictional and/or cohesive.

There is considerable latitude in choosing the remaining variables since, for example, there are tradeoffs in both capital and operating costs between a wide belt operating at low speed compared to a smaller belt operating at higher speed. Each component of the wider belt is likely to initially cost more; however, since abrasive wear of a belt is a function of both the belt's speed and the stress exerted on it by the material, the effect of varying belt width is difficult to generalize. A wider belt will have higher solids stresses acting on it, but may experience less wear because of its lower speed. A slowly running belt may deliver uneven discharge (e.g., the result of material sloughing off the end of a belt). This

problem can sometimes be overcome by installing a rotating cutter near the discharge end of the belt.

Another consideration is the power consumption of different belt sizes. Wider belts require more belt tension but may require less power if the speed is reduced sufficiently. Low speed belts require high ratio gear reducers, which have more drive loss than standard units. Other tradeoffs are possible in the choice of idlers, vertical gap between the belt and interface section at the discharge end, and minimum slot taper. The latter determines the maximum slot length for a given belt width.

For most situations, a practical approach is to start with standard 20° picking idlers with the center roll wider than the interface at the front. This sets an initial belt width. A reasonable gap between the interface and belt is then chosen, as described below. Using a conservative (i.e., shallow) angle of surcharge, one can quickly determine whether a wider belt is required to prevent spillage or allow a slower belt speed. An ideal maximum speed for a belt feeder is 0.25 m/s (50 fpm), particularly when handling abrasive materials. Generally, a practical upper limit to belt speed is about 1 m/s (200 fpm), but this should only be used for nonabrasive bulk solids.

Another variable is the angle of the side idlers. Typically, 0° (flat), 20°, 35° and 45° are available for most belt sizes. Flat idlers are generally not recommended unless the belt width is less than about 610 mm (24 in.) and/or the belt is to be operated in gravimetric mode. Otherwise, excessive wear and power consumption as well as induced resonant bin vibrations may result. Idlers with 45° outer rolls often result in large belt carcass stresses and long transition lengths at the head and tail pulleys.

Taper of the slot in elevation must be sufficient for particles to freely form an angle of surcharge on the belt. Unfortunately, model tests and/or experience are often necessary to set the minimum taper since there are no verified guidelines, and taper is not simply a function of maximum or average particle size. For example, a fine material such as -12 mesh sand requires a minimum taper of about 0.02 (e.g.),* even if there is a small percentage of much larger particles. On the other hand, closely sized particles that have the same average particle size as the sand may not flow evenly from the same interface. A coarse material such as -150/+50 mm ore may require a taper of as much as 0.3. Whatever the case, the absolute minimum gap between the interface and the belt at the discharge end must be at least three times the normal maximum particle size, and this gap must be greater than the maximum possible particle size. Long particles or tramp material such as stray pipe or a 2x4 will tend to enter the interface vertically due to velocity gradients in the bin and lay down as material is pulled from the interface.

Once a discharge end gap has been selected for the desired slot length, the belt's size and speed can be estimated. This process can then be repeated with a different belt size, type of belt, type of idler, or slot length to obtain an optimal configuration.

Other important aspects of belt design include

- A slanted “nose” with an arch-shaped cutout to provide stress relief and prevent stagnation at the discharge end.

- Capacity set by belt speed, not by an adjustable front gate.
- A flexible rubber or plastic buffer at the back end to allow a typical 12 mm gap for uniform material withdrawal without belt or interface damage.
- Spillage skirts that expand slightly in the direction of belt travel and that are remote from the feeder interface. This prevents the skirts from interfering with uniform material withdrawal. Ideally, spillage skirts are only used to contain unusual fluctuations in the surcharge angle or near the discharge pulley to prevent spillage as a troughed belt flattens. Skirts may not be necessary with flexible sidewall belts or some apron feeders.
- Replacing side rolls with slider bars within the hopper interface region to eliminate uneven skirt wear, spillage due to belt sag, and high idler loads.
- Properly designed and well-maintained belt scrapers, which are critical to minimizing the amount of spillage due to carryback.

Transverse triangular inserts are sometimes used to manipulate drawdown (Strydom 2006). Such inserts are also helpful in reinforcing hopper and interface sidewalls to prevent them from bowing out.

It is often desirable to minimize the distance between the hopper interface and head and tail pulleys. At the tail end, troughing of the belt, if necessary, can be accomplished beneath the hopper interface with transition idlers. This allows the centerline of the tail pulley to be located as close as only a few inches behind the rear end of the interface. The belt line work point should be the top of the idlers and pulleys, so as to avoid belt lift when starting up the feeder. Detroughing of the belt can start a short distance downstream of the interface; however, the centerline of the discharge pulley must be located beyond a point formed by the material's angle of surcharge from the top of the interface in order to prevent leakage.

CEMA (Conveyor Equipment Manufacturers Association, 2002) outlines a satisfactory method for calculating the appropriate trajectory of a discharge stream. However, the velocity of fine powders will be retarded by air viscosity and thus fall short of the calculated path. On the other hand, large dense particles will tend to concentrate near the top of the material bed on the belt and therefore travel much further than the calculated path. Stream splitters and samplers must be designed to account for these variations.

Collecting chutes should be designed so that the stream trajectory contacts the surface tangentially (Stuart-Dick and Royal 1992). This minimizes turbulence, which generates dust. It also minimizes impact stress, which can cause material adhesion, particle attrition, and abrasive wear of the chute. Beyond the point of impact, chute sections must be designed to smoothly accelerate the particles.

MATERIAL LOAD CONSIDERATIONS

Knowledge of the material loads acting on the portion of a belt feeder below a hopper outlet is an essential component in determining drive details. The first factor is the vertical material load acting on the belt, which is used for

* This could be achieved, for example, by tapering the slot at least $\frac{1}{4}$ in. per ft length.

determining belt support requirements and the required tension in the belt to overcome drag of the supports (e.g., idler friction). The second factor is the force (belt tension) required to shear the material from beneath the interface. Both of these loads are sensitive to interface geometry and loading conditions; consequently, the approach developed by CEMA for belt conveyors does not apply to belt feeders.

Using an approach based on the work of Jenike (1964) and assuming that the bin and belt feeder interface provide mass flow, the vertical load can be expressed as

$$A \times F + B \quad \text{EQ. 1}$$

where

A = integrated vertical material force at the shear plane (generally assumed to be at the bottom of the interface)

F = dimensionless multiplier used to correct for different loading conditions

B = weight of material between shear plane and belt

The shear load can be approximated as

$$C \times F \quad \text{EQ. 2}$$

where

C = Value A multiplied by the effective coefficient of internal friction, usually taken as ($\sin d$).

A proprietary, two-phase flow computer program can be used to calculate values of vertical force acting on the shear plane. In addition to describing bin geometry, fill level, and top and bottom boundary conditions of solids and gas pressure, the following variables describing the bulk solid must be entered:

- Wall friction angle, ϕ'
- Minimum outlet width to prevent arching
- Effective angle of internal friction, d
- Bulk density/consolidating pressure relationship
- Minimum bulk density
- Permeability/bulk density relationship
- Specific gravity of particles

As an example of the results of using this program, consider the bin shown in Figure 7.

It has a 6 m diameter by 12 m tall cylinder, below which is a mass flow transition hopper converging to a 1,200 mm by 3,600 mm outlet. Below this is a 500 mm tall spool piece (for a slide gate or spile bars), then an interface to a 1,220 mm (48 in.) wide belt feeder. The material has a bulk density of approximately 1,600 kg/m³.

Values of major principal stress in the hopper section during initial fill and discharge are shown in Figure 8.

Initial fill stresses occur after the bin is filled from empty with the feeder off and no material discharge. Flow stresses, which occur just after the material has started to be discharged, are higher than initial fill stresses near the top of the hopper but much lower throughout most of the hopper sections below this. The ratio of major principal stress at the shear plane during initial fill to its value during flow in this example is 3.1. Once discharge has occurred, flow stresses remain even when flow is stopped. The flow stress field is only altered

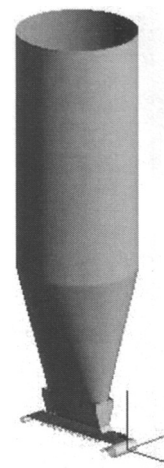


FIGURE 7 Mass flow bin used for analysis. See text for description.

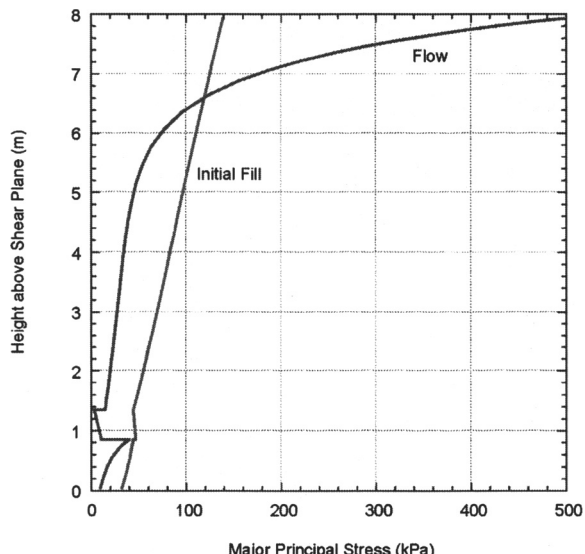


FIGURE 8 Calculated initial and flow stresses in hopper section and below

by completely emptying the bin and refilling it from empty without any discharge.

Since this is a mass flow bin, material level in the cylinder has little to no effect on stresses from roughly the midlevel in the transition hopper down to the outlet. The value of this stress at the shear plane is used to calculate loads acting on the belt (Roberts 2001).

The effect of interface angle is shown in Figure 9.

For this analysis we fixed the top and bottom dimensions of interface, so its height changed as the angle changed. Note that as the interface angle becomes less steep there is less stress acting on the shear plane.

The effect of flow rate is shown in Figure 10.

Here we used typical values for the permeability and bulk density relationships. As discharge rate increases, upward air flow through the outlet provides increasing

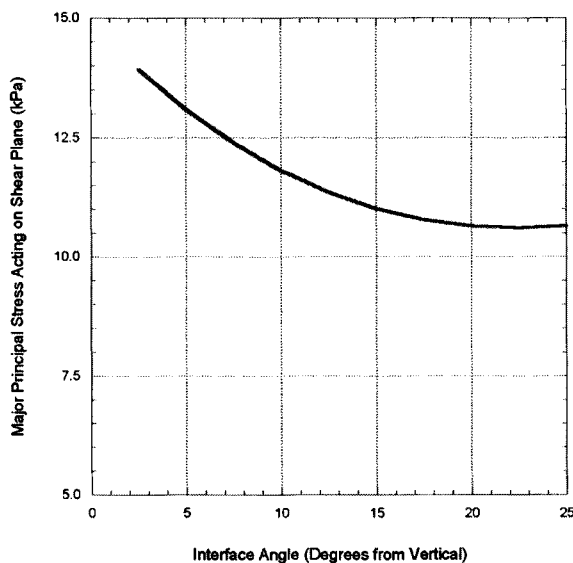


FIGURE 9 Typical effect of interface angle on major principal stress acting on shear plane

support for the material and thereby reduces stress on the shear plane.

The value of dimensionless multiplier F is close to 1 during steady state running conditions but can easily exceed a value of 3 during startup, particularly if there is significant relative deflection between the hopper interface and feeder. Other factors that influence F include outward deflection of the interface walls (Jenike & Johanson 1983), belt sag between idlers, and filling of the bin from empty.

It is common to find that the value of F dominates the material loads acting on a belt feeder; consequently, design details and experience are critical. One approach to minimizing material loads is to maintain a sufficient heel (i.e., minimum material level) above the belt. This will help to isolate the belt from overpressures developed during refilling of the bin and prevent excessive belt wear due to impact of hard particles. Another approach, which can be used in conjunction with a material heel, consists of mounting the belt interface rigidly to the feeder frame and using a connection that allows vertical slip between the hopper and interface in order to isolate the belt from any relative deflection. The location of this connection must be approximately one outlet width or more above the bottom of the interface in order to be fully effective. A similar effect can be achieved by operating the belt whenever material is added to the bin or by mounting the belt on flexible supports (e.g., Belleville washers) that deflect as the vertical load on the feeder increases. If the belt feeder is small, it can often be supported from the interface so that if the interface deflects at all, the feeder will do likewise.

ADDITIONAL CONSIDERATIONS

Drive Types

Two main drive types are available: electrical/mechanical and hydraulic. Electrical/mechanical drives are capable of operating over a 10:1 speed range by varying the motor frequency. However, the drive's output torque,

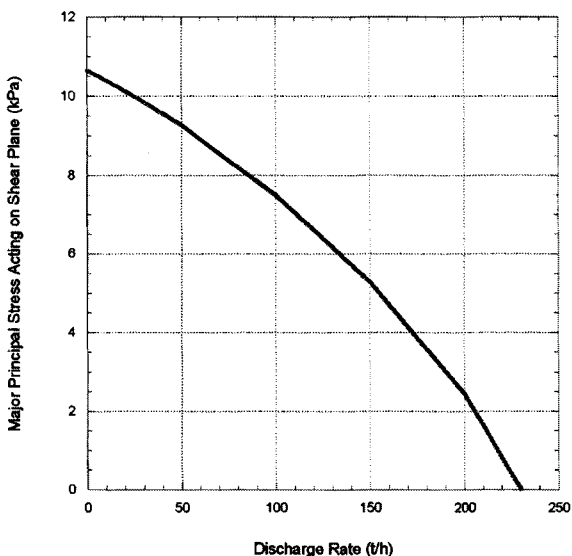


FIGURE 10 Typical example showing effect of discharge rate on major principal stress acting on shear plane

efficiency and temperature will change with frequency, which must be considered in the design of the drive. Electrical/mechanical drives can deliver up to 300% of their rated torque during startup, which helps to overcome feeder startup loads. Hydraulic drives have constant output torque from 0–100% of design speed, thus providing a larger operating range. Hydraulic drives are compact, shaft-mounted units, usually smaller than an equivalent electrical/mechanical drive. This is particularly important with slow speed drives since they require large gearboxes to provide the desired output speed.

Gates

A gate is used to isolate a feeder from the storage system above. This facilitates routine maintenance and is required when replacing belting. Closing the gate when filling an empty storage system protects the feeder from direct impact and reduces feeder startup loads, since the bulk solid is not compacted in the interface.

Many bulk solids gain strength when stored at rest. A gate can be used to lengthen the time that a bulk solid can be left at rest before flow stoppages occur due to cohesive arching. By closing the gate and emptying the interface, the smallest opening becomes the top of the gate rather than the bottom of the interface.

If a gate is used below a mass flow hopper, the gate must be either fully open or fully closed. A partially opened gate creates a flow obstruction and will convert what would otherwise be a mass flow design into funnel flow. It is equally important that the gate be selected carefully to ensure that the actual opening size is larger than the hopper outlet opening, so that there are no protruding lips or ledges that would impede flow. Similarly, the interface should be sized slightly larger than the actual gate opening above it.

A rod (pin) gate involves less capital cost than a mechanized slide gate, but it will be more difficult to add and remove the rods than to close a slide gate, and the outlet will never be completely closed off. There is also a tendency to leave some rods in, which is less likely if a

slide gate is used. A slide gate must be structurally robust and designed such that it does not racking as it is operated.

Developments In Belt Technology

The useful operating range of belts has been expanded significantly over the years. Improved carcasses and covers have increased load ratings to over 1,500 PIW,^{*} improved troughing characteristics, and increased useful life. Covers capable of temperatures from -50°C to 200°C are available.

Belt Splicing

To facilitate belt replacement, there must be an accessible length of feeder between the hopper and one of the pulleys for splicing. This is typically 50% greater than the belt width.

Safety

As with any piece of rotational equipment, belt feeders have pinch points, which can cause serious injury. At a minimum, permanent guards must be placed around drive belts, drive chains, gear drives, and rotary shafts. In addition, guards and/or interlocks must be utilized in order to prevent someone reaching into the feeder while it is operating. Safe cleaning procedures with proper lock out/tag out are a must. All applicable ANSI and OSHA standards must be followed.

SPECIAL APPLICATIONS

The design flexibility of belts allows them to be used in various ways. Some special applications are described below.

Weigh Feeders

Belt feeders can be operated in gravimetric mode, where the weight per unit time is monitored and controlled. Generally in order to achieve the type of feed rate accuracies expected of such devices, the belt must be flat, not troughed. Small belt feeders are sometimes mounted completely on a weight sensing device. This is satisfactory if the material pressures at the bottom of the interface are constant.

If a precise measurement of instantaneous flow rate is not required, a weigh idler can be used with either flat or troughed belts to measure the total weight of material going across the belt in a given period of time. In this case, the weigh idler is placed on the conveying portion of the belt at some point beyond the material's angle of surcharge from the bin outlet. This idler must also be upstream of any detroughing section, since the stiffness of a belt changes rapidly over this region.

Sloped Belts

Inclined belts can be designed to feed material uniformly from a slotted outlet as long as the coefficient of friction between the belt and material is great enough to prevent slippage and the slope is less steep than the material's angle of surcharge. In some cases, shallow belt cleats can be used to prevent slippage. This may be necessary with wet materials that lubricate the belt or freeze and slide off. For inclined belts, the additional power required to elevate the material must be taken into consideration. For declined belts, the interface may need to be tilted

downwards in order to prevent the slot from narrowing in the direction of belt travel.

Multiple Feed and/or Discharge Points

The optimum interface cannot accept material from more than one hopper outlet; consequently, it is better to use individual belt feeders for each outlet and use a common collecting conveyor. In some instances, such as self-unloading ships, feed from more than one hopper opening onto a single belt is necessary, and this can be achieved using a special gate and interface design (Hargreaves 1985). Multiple discharge can be accomplished using a reversing belt with a pivoting interface, a side discharge plow on a flat portion of the conveying section, a splitter in the trajectory stream, or a downstream splitter.

CASE HISTORIES

Feeding Calcine Dust Using a Belt Feeder

Feeding a dry ground iron ore calcine dust with 80% -325 mesh and a Blane number of 2,200 at 60 t/h and 70°C can be a problem. The first inclination was to use a pneumatic system for handling such a fine dry powder. This solution was not feasible because of the high capacity required and because immediately from storage the dust was to be mixed with water in preparation for balling. Another possibility was to use a rotary airlock or star valve. However, at the rate of 60 t/h the size (and resulting cost) of such a device would be prohibitive and the uniformity of feed rate questionable. A screw feeder was ruled out because of anticipated extreme wear and maintenance problems at the required high tonnages. A belt feeder appeared to be the most economical and best solution.

Belt feeders had been used at this plant before for feeding similar ground ores. Unfortunately, earlier attempts often resulted in surging and flooding onto the belt feeder with ore pouring over the belt. At times the ore was forced out with sufficient velocity to squirt 8 m or so with only a 300 to 600 mm horizontal drop. These conditions are typical when handling fine powders at high flow rates using an improperly designed belt feeder interface.

In order to provide for future expansion the ground calcine bin and feeder were designed for a flow rate of 90 t/h on each of two 760 mm (30 in.) wide belt feeders. The width of the belt interface varies from 230 mm at the back to about 255 mm at the front over a length of 5.5 m. The total bin height is 11.6 m. Air is injected at several predetermined levels by a special air permeation system to provide a consistent flow rate of the dust.

This bin went into operation in 1970 (Reed and Johanson 1972). After an initial adjustment of the gap between the belt and hopper outlet, the bin has operated many years without flooding or even dusting with short-term rates as high as 90 t/h. The initial design called for sealing skirts on the belt to contain any possible dusting or flooding. These were found to be unnecessary. Good volumetric feed controlled by belt speed is maintained as long as the calcine level in the bin is kept above the converging part of the bin. The bed of dust on the belt comes out consistently compacted.

* Load rating expressed as lb per in. width of belt.

Operating experience has shown that, if an air injection port is closed off, the volumetric feed control is not as uniform. This illustrates the importance of the air permeation system.

Underground Bin and Feeder for Trona Ore

The world's largest known source of natural sodium carbonate (trona) lies in the Green River formation in southwest Wyoming. FMC Wyoming is the largest of four companies operating in the region, which together mine roughly 15 million tonne of trona each year and produce over 8 million tonne of soda ash, which is roughly 80% of the soda ash produced worldwide from natural sodium carbonate.

The primary deposits in the Green River formation are found in depths of 120 to 1,070 m (400 to 3,500 ft) in beds that range from 1.2 to 3.7 m (4 to 12 ft) in thickness. Approximately 1,300 km² (500 mi²) of deposits contain high quality ore, but occasional pockets of insoluble impurities are common even in high quality ore deposits. When these unpredictably high levels of insoluble materials enter the process stream they reduce yields and drive up production costs. To smooth out these variations in the ore, FMC engineers wanted to detect the troublesome ore and divert it from the process stream, then meter it back into the process in a controlled way.

FMC found they could use an on-line analyzer to detect the level of insolubles in the ore as it moves on a conveyor belt from the mine face to the hoist. In order to segregate the high-insol ore and control its delivery, a large underground storage and handling system was needed. Another benefit of underground storage was that it would allow operators to better control the flow of ore to the surface. With limited underground storage and miles of conveyors, matching the mine output to the hoisting capacity was a challenge. The additional storage would give the system a greater ability to adjust to surges from the mine face and maintain a constant flow of ore to the surface.

Flow properties tests on the trona confirmed what most operators know: when stored at rest, trona crystals grow together and form a hard, solid mass. Surface moisture accelerates the process and results in high strength. The tests provided the information necessary to design the two 1,180 tonne bins for mass flow, which prevents stagnant, nonflowing regions where the trona could cake together.

Building two 7.6 m diameter bins and a 60 m conveyor system at a depth of nearly 600 m below the surface involved many challenges. See Figure 11.

It was necessary to evaluate materials of construction for abrasive wear, calculate loads on the structure and 1.8 m (72 in.) belt feeder, and design a unique diverter for the in-feed conveyor system. Since startup in early 1998, the system has been operating reliably and has allowed the mine and processing plant to work together more efficiently, thereby reducing production costs (Jenike & Johanson 2000).

Belt Feeders in Chilean Mining Applications

BHP Billiton recently opened the new Spence copper mine, the latest large-scale, greenfield mining project developed in Chile in the past few years. This project is located at an elevation of 1,700 m in the Atacama Desert, 150 km northeast of the port of Antofagasta. This one

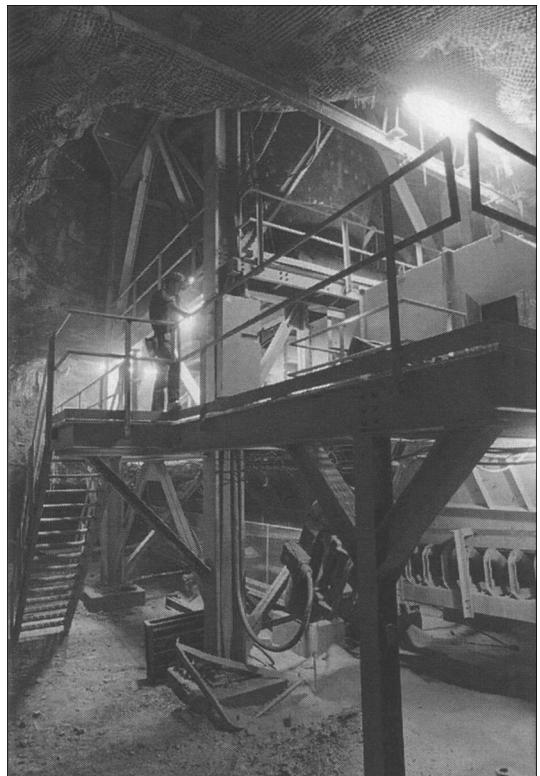


FIGURE 11. Underground trona bin and 1.8 m (72 in.) belt feeder at FMC Wyoming

billion dollar, open pit, heap lixiviation/solvent extraction/electrowining (Lx-Sx-Ew) project has a design capacity of 200,000 t/y of copper in the form of cathodes, for a lifetime of 19 years.

Minera Spence uses conventional open pit mining methods with a nominal daily throughput of 50,000 t/d, operating 365 days per year and 24 hours per day, running separate campaigns of oxide and sulphide ores. The run-of-mine ore is transported by trucks to a gyratory crusher to produce a coarse ore 100%–200 mm. The primary crushed ore is stored in a surge bin directly under the crusher, with two reclaim belt feeders, and is transported to the crushing/screening plant by two belt conveyors. In the plant, the ore is crushed to a final product 100%–19 mm and stored in a fine ore silo to feed the agglomerator.

During the design phase of the plant, tests were run to determine flow properties of representative samples of crushed ore to be handled under conditions similar to those expected to exist in the plant. The influences of moisture content, storage time at rest, fines and/or clays content were studied. Based on this data, functional design recommendations were developed to safely and effectively handle, store and feed the crushed ore in the primary crusher surge bin, tertiary crusher surge bins, tertiary screen feed bins and fine ore silo, including their corresponding reclaim systems using belt feeders.

The plant commenced production in January 2007 and is currently running in excess of design capacity. A total of fourteen hoppers and belt feeders were designed and built for this project in accordance with the principles

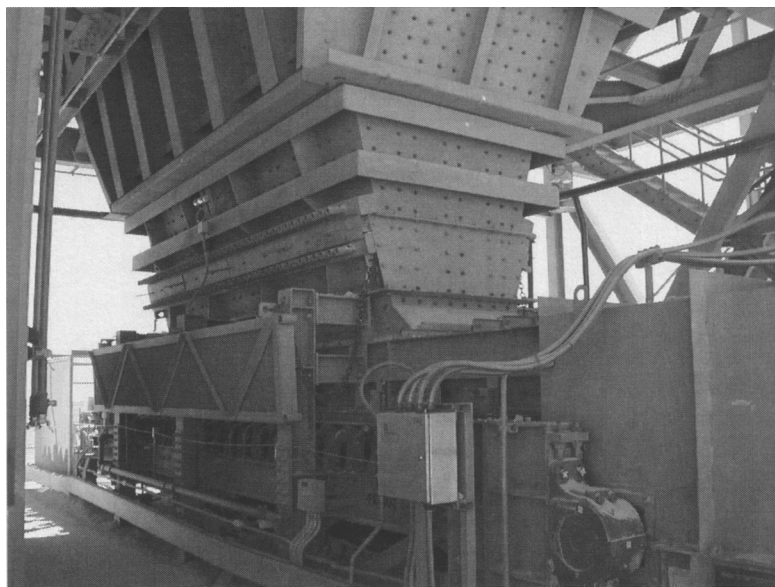


FIGURE 12 Reclaim hopper and 1.8 m belt feeder of the tertiary screen feed bins at Minera Spence

outlined in this paper, and all are performing as designed. An example is shown in Figure 12, which is one of the reclaim hoppers of the tertiary screen feed bins. Each of these belt feeders is 1.8 m wide by 7.5 m long and operates at 1,300 t/h capacity.

REFERENCES

- ASTM D6182-06. 2006. *Standard test method for shear testing of bulk solids using the Jenike shear cell*. West Conshohocken, PA: ASTM International. Available from www.astm.org.
- ASTM D6683-01. 2001. *Standard test method for measuring bulk density values of powders and other bulk solids*, West Conshohocken, PA: ASTM International. Available from www.astm.org.
- ASTM D6773-02. 2002. *Standard shear testing method for bulk solids using Schulze ring shear tester*, West Conshohocken, PA: ASTM International. Available from www.astm.org.
- Bridge, D.T. and Carson, J.W. 1987. How to design efficient screw and belt feeders for bulk solids. In *Proceedings of Powder & Bulk Solids Conference*, Rosemont, IL. May:159–180.
- Carson, J.W. and Marinelli, J. 1994. Characterize bulk solids to ensure smooth flow. *Chemical Engineering*. 101(4):78–90.
- Conveyor Equipment Manufacturers Association (CEMA). 2002. *Belt Conveyors for Bulk Material*. 5th ed. July.
- Hargreaves, D. 1985. Regional survey—ASEAN coal self-unloader delivered. *Int. Bulk J.* 5(7).
- Jenike, A.W. 1964. *Storage and Flow of Solids*, Bulletin No. 123, Salt Lake City: University of Utah Engineering Experiment Station.
- Jenike & Johanson. 1983. *Beware of hopper wall deflections*. Flow-of-Solids® Newsletter. III(2).
- . 1985. *New design of emergency shut-off gates*. Flow-of-Solids® Newsletter. V(2).
- . 2000. *Quality and Reliability in Handling Trona Ore*. Flow-of-Solids® Newsletter. Spring.
- Johanson, J.R. and Royal, T.A. 1982. Measuring and use of wear properties for predicting life of bulk materials handling equipment. *Bulk Solids Handling* 2:517–523.
- . 1984. Abrasive Wear Tester. U.S. Patent 4,446,717. May 8.
- Purutyan, H., Bengtson, K.E., and Carson, J.W. 1994. Identifying and controlling silo vibration mechanisms: Part I. *Powder and Bulk Engineering*. 8(11):58–65.
- Rademacher, F.M.C. 1982. Reclaim power and geometry of bin interfaces in belt and apron feeders. *Bulk Solids Handling*. 2(1):281–294.
- Reed, G.B. and Johanson, J.R. 1972. Feeding calcine dust with a belt feeder at Falconbridge. *Trans. ASME, J. Eng. for Industry*. Feb.:72–74.
- Roberts, A.W. 2001. An overview of feeder design focusing on belt and apron feeders. *Bulk Solids Handling*. 21(1): 13–25.
- Strydom, E. 2006. The challenges and advances in belt feeder and hopper design. *Bulk Solids Handling*. 26(2):106–115.
- Stuart-Dick, D. and Royal, T.A. 1992. Design principles for chutes to handle bulk solids, *Bulk Solids Handling*. 12(3):447–450.

.....

Discrete Element Modeling of Sag Energy Losses in a Conveyor Belt System

Graham G.W. Mustoe^{*} and Ren Bin[†]

Energy losses are important factors in a conveyor's performance and design. A significant energy loss due to belt sag within a conveyor system occurs when shearing motion between the bulk material particles occurs as the material moves along the belt.

An initial analysis of these phenomena was performed using the discrete element method, which is a general-purpose numerical modeling technique for analyzing the mechanical behavior of particulate materials. The software used in this work was Overland Conveyor Company's, Chute Analyst Professional, a discrete element computer code designed specifically for analyzing bulk materials transportation and handling problems.

INTRODUCTION

This sag energy loss has been studied previously using analytical mechanical methods that employ several simplifying approximations such as: (a) dry bulk material, (b) assumed pressure distributions between the bulk material and belt, and (c) inertial effects within the bulk material and belt, etc. For further details of these studies see Spaans 1999, Brands 2001, and Wheeler 2003, 2005.

The current work employs a discrete element method (DEM) modeling approach eliminating the need for many of the simplifying assumptions required in previous analyses. See the DEM conference proceedings Mustoe et al. 1989, and Williams and Mustoe 1993 for a detailed description of the discrete element method. Furthermore, a DEM algorithm specifically designed for bulk solids analysis is described in Hustrulid, and Mustoe, 1996.

The DEM method models: (a) the bulk material as a discrete system of particles with a specified size distribution, and interaction laws for dry and wet materials, and (b) the belt geometry shape with a detailed 3D CAD description. In this paper the effects of belt sag are studied for a dry bulk material.

TECHNICAL APPROACH

In the work described here the discrete element method is used to analyze the conveyor belt sag problem. This type of analysis provides a detailed prediction of the motion of the bulk material and its interaction with the conveyor belt.

The DEM model of the conveyor system employed simulates the mechanical behavior of a region between two sets of adjacent idlers on the belt. The configuration for this study and is a three-roll system with a 60 in. wide belt, a 20 in. center flat region, with two inclined rolls at 35° to the horizontal direction. The belt is loaded to approximately 80% of its capacity with coal material and the belt speed is defined as 120 in/s. The coal material is modeled as a system of 2 in. diameter particles, with a mass density of 1.064×10^{-4} lb-s²/in, a coefficient of friction of 0.3, and a coefficient of restitution of 0.2.

The geometry of the conveyor belt surface has a deformed shape defined by equations developed from a semi-analytical approach described in Spaans 1999. The longitudinal vertical sag displacement function is defined by:

$$u_z(x) = C_1 \left[x^2 + C_2 \frac{x}{\sinh(C_3 x)} (1 - \cosh(C_3 x)) \right] \quad \text{EQ. 1}$$

where

$$C_1 = 3.54 \times 10^{-4}$$

$$C_2 = 57.9$$

$$C_3 = 0.184$$

Note, these parameter values were determined for the specific DEM conveyor model described above.

^{*} Colorado School of Mines, Golden, Colo.

[†] Colorado School of Mines, Golden, Colo., and Overland Conveyor Co., Lakewood, Colo.

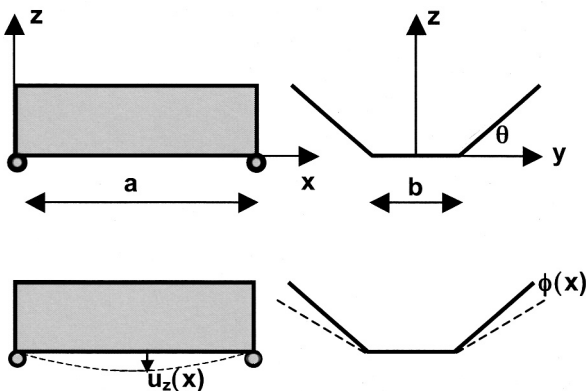


FIGURE 1 Geometry definition of the conveyor belt model, and the vertical sag displacement and bulge angle

The bulging of the belt between the idlers is approximated by assuming the maximum belt opening at the belt edge is equal to the maximum vertical sag displacement. The corresponding bulging angle function is defined by:

$$\phi(x) = \phi_{max} u_z(x) / u_{max} \quad \text{EQ. 2}$$

where $u_{max} = u_z(a/2)$ and $\phi_{max} = u_{max}/R$ are the maximum values of vertical sag displacement and bulging angle respectively. Figure 1 shows the model geometry and the definitions of $u_z(x)$ and $\phi(x)$ respectively.

The DEM model consist of the following components:

1. A three-dimensional CAD model of the conveyor belt surface between sets of adjacent idlers, discretized with 3-noded and 4-noded planar boundaries.
2. The bulk material is modeled as a system of spherical particles.

DEM SIMULATIONS AND RESULTS

Figure 2 shows the DEM model geometries with different sags. Figure 2A shows the belt shape defined by the sag deformation and bulge angle equation defined with the values of C_1 , C_2 and C_3 specified above. Figure 2B shows the belt shape defined by increasing C_1 by a factor of 2, and Figure 2C shows the belt shape defined by increasing C_1 by a factor of 3.

Figure 3 illustrates the average stress acting on the coal particles for each of the three DEM Models with different sag deformations. Note that red particles have low stresses and blue particle have maximum compressive values. These figures clearly show the increase in compressive stresses acting on the coal particles that are near the downstream idler set adjacent to the belt surface. Note animation of the material flow in these DEM models, shows the reversal of the active and passive stress states in the coal material particles as the belt opens and closes between idler sets.

Figure 3C also shows that the DEM model with the largest mid-span bulging and vertical sag, compresses the coal particles near the downstream idler set to a much higher degree than predicted in other two DEM models with smaller sag deformations (see Figures 3A and 3B).

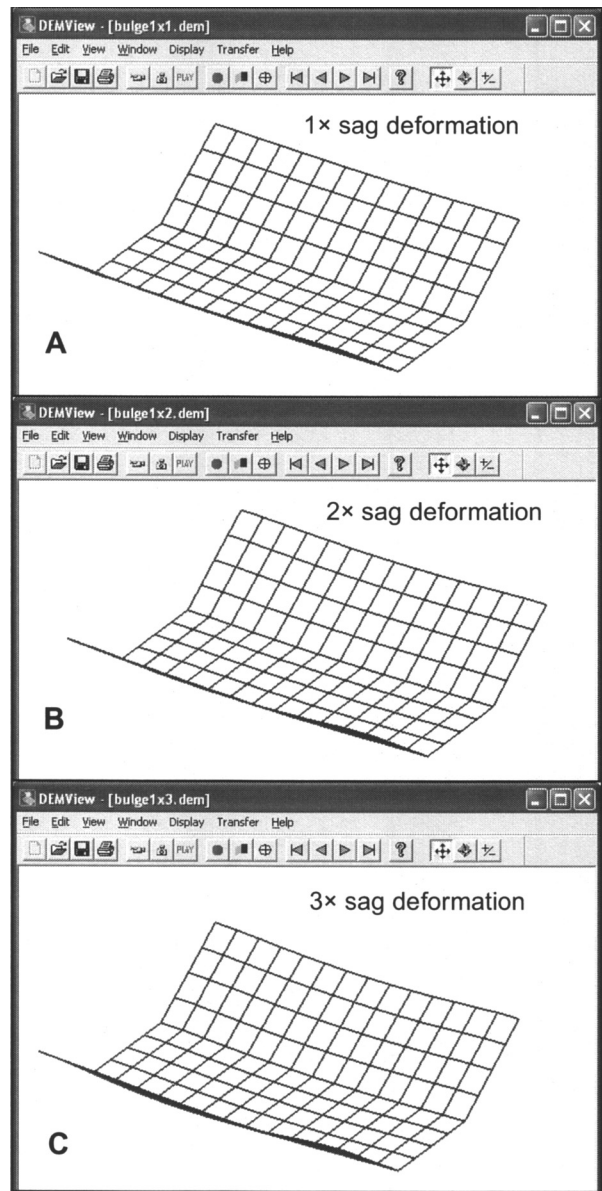


FIGURE 2 3D belt geometry of the DEM models with different sag

The average power requirements computed from the DEM models are reported in a non-dimensional format in Table 1. Note the power values in Table 1 are normalized with respect to the power requirements of the conveyor belt model (1 x sag) with the sag defined by the original values of C_1 , C_2 and C_3 .

CONCLUDING REMARKS

The initial DEM calculations reported show its applicability to the analysis of energy losses because of sag deformations in conveyor belts. The DEM results agree with previous studies and show that power requirements increase significantly as the magnitude of sag deformations increases. Further results using this DEM model will be presented at the conference.

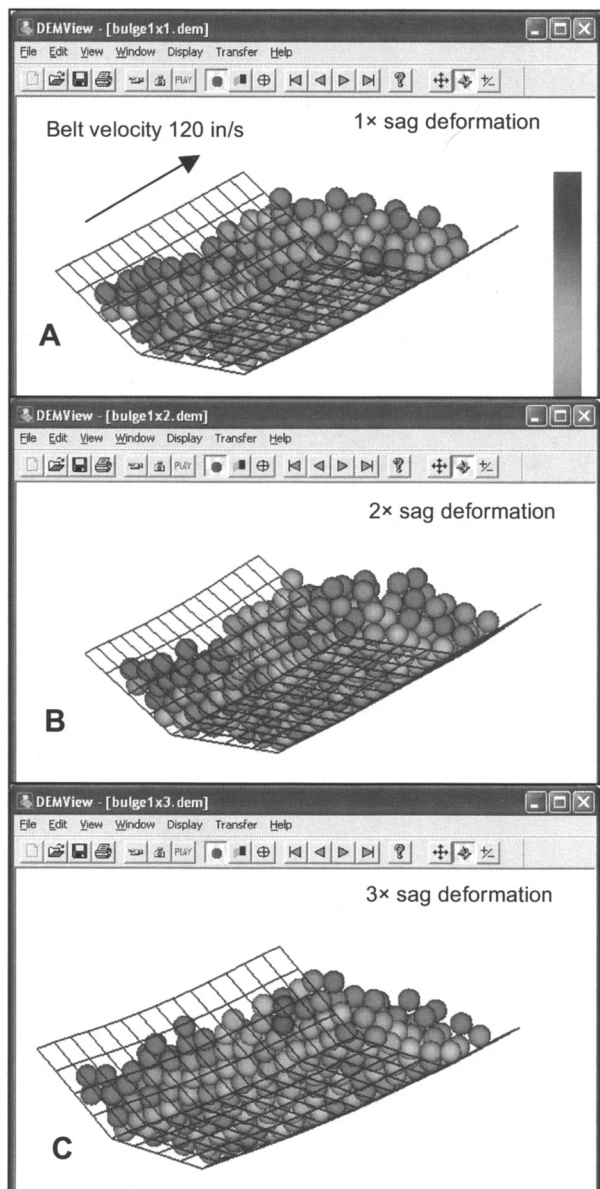


FIGURE 3 Average particle stresses in DEM models with different sag

TABLE 1 Normal power for DEM models with different sag deformations

DEM Model	Normalized Power
(1x sag)	1.00
(2x sag)	2.45
(3x sag)	3.92

ACKNOWLEDGMENT

The authors wish to thank Overland Conveyor Company for access to their discrete element analysis software, and support for the work presented in this paper.

REFERENCES

- Brands, J.M.A.M. 2001, Optimising Belt Conveyor Design to Reduce Power Consumption. *Bulk Solids Handling*, 21(5), October.
- Spaans, C. 1999, The Calculations of the Main Resistance of Belt Conveyors. *Bulk Solids Handling*, 11(4), November.
- Wheeler, C. 2003, Analysis of the Main Resistance of Belt Conveyors. PhD Thesis, University of Newcastle, Australia.
- Wheeler, C. 2005, Bulk Solid Flexure Resistance. *Bulk Solids Handling*, 25(4), November.
- Mustoe, G.G.W., Huttlemaier, H.-P., and Henriksen M. 1989, *Proceedings of 1st. U.S. Conference on Discrete Element Methods*, Colorado School of Mines, Golden, CO, October.
- Williams, J.R. and Mustoe, G.G.W. 1993, *Proceedings of 2nd International Conference on Discrete Element Methods*, M.I.T., Cambridge, MA, March.
- Hustrulid, A.I. and Mustoe, G.G.W. 1996, Engineering Analysis of Transfer Points Using Discrete Element Analysis. In *Proceedings of the Annual Meeting of the Society of Mining Engineers*, Phoenix, AZ, March.

.....

PART 3

Case Studies of Large Belt Conveyance Projects

- Alcoa Rockdale, Texas: 11.9-Mile-Long Overland Conveyor **71**
- Increasing Kaltim Prima Coal Overland Conveyor Speed to 8.5 mps **71**
- Limestone Transportation by 17-km Cross-Border Long Belt Conveyor for Lafarge Surma Cement Limited **77**
- Cadman Downhill Overland Conveyor, Blending into the Washington State Forest Area **83**
- Thirty-Year-Old Transfer Point Challenge **89**
- Large-Scale Stacking System at the Freeport-McMoRan Safford Mine **93**

.....

Increasing Kaltim Prima Coal Overland Conveyor Speed to 8.5 mps

Poltak Sinaga*

PT Kaltim Prima Coal's 13.1km overland conveyor was commissioned in 1991. It is of conventional 3 roller 350 troughed belt type. Cost and performance optimisation during initial design ended up with 5.4m/s belt speed, 1,000mm belt width to convey 1,350tph, and 7mtpa of coal.

Despite high initial figure, the belt speed was lifted to 6.5 mps in 1996 to accommodate mine throughput increase. In 2002, new low loss ST2100 1,100mm wide belt replaced the old ST2250 due for change-out.

An upgrade project was initiated at the end of 2003 to further increase the belt speed to 8.5 mps, hence to increase the OLC capacity to 30mtpa. Performance data, experience of site personnel, site observation and tests, benchmarking, and information from equipment manufacturers were major inputs to the design review. The project fast track was another challenge in addition to executing modifications on a production lifeline. The project was completed within fifteen months and the OLC was successfully commissioned at 8.5 mps belt speed in February 2005. The OLC has been to date conveying 4200tph satisfactorily.

INTRODUCTION

Belt conveyors have become a common choice for long distance transport of bulk materials in mining operation. In comparison with other modes of transport, such as rail and haul truck, belt conveyors offer more reliable system at least cost.

PT Kaltim Prima Coal (KPC) built an overland conveyor (OLC) to transport coal from Coal Preparation Plant to Coal Terminal over a distance of 13.1 km. The OLC has been in operation since 1991. It was originally designed to convey 1,350 tph (ton per hour) and 7 mtpa (million ton per annum). Industry research showed narrow and fast belt is the optimum designs both technically and economically; therefore, the OLC initial design speed was set at 5.31m/s while 1,000mm was selected as the belt width. The belt speed was already at the limit of industry at that time.

To cope with the growth in mine throughput, in late 1995 the OLC was upgraded to convey 12 mtpa at an average rate of 1,800tph and a peak of 2,100tph. Major changes included the change of gear ratio for facilitating the speed increase to 6.68 m/s and additional 1MW drive to add the existing 2x1 MW drives. The upgraded belt speed was again at the limit of industry practice at that

time. It was considered that a speed beyond that of "typical" industry practice would require the existing ST 2250 belting replaced with stronger belting, which was not economic.

In early 2002 the new belting was installed to replace the old belting whose warranty life had lasted. KPC used this replacement opportunity to fit slightly wider belting, i.e., 1,100mm belt width.

BASIC DESIGN OF CONVEYOR

Figure 1 shows a basic configuration of a conveyor belt showing the main components of the system.

The conveying capacity is determined by three design parameters namely the belt speed, belt width and troughing angle.

From Figure 2,

$$\text{Throughput } Q = \rho A v$$

where:

$$\begin{aligned}\rho &= \text{bulk density of bulk solid} \\ v &= \text{belt velocity}\end{aligned}$$

"A" represents the cross-sectional area of the bulk solid on the belt and is given by:

* PT Kaltim Prima Coal, Kalimantan Timur, Indonesia.

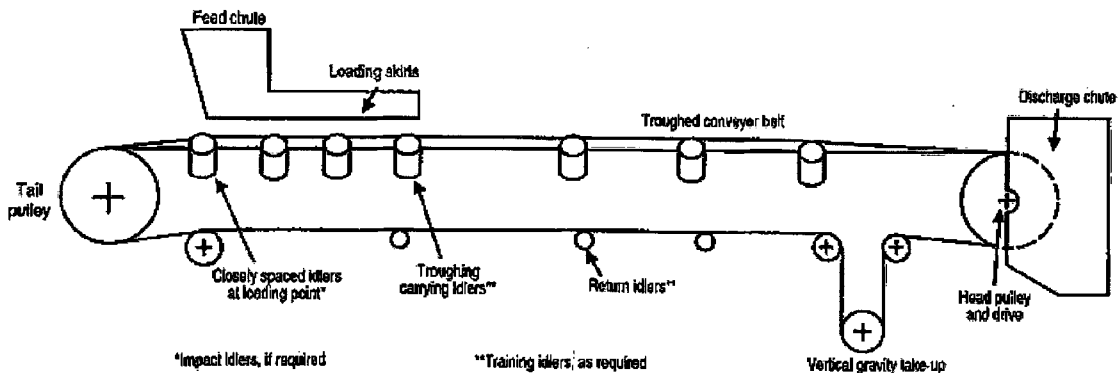


FIGURE 1 Basic conveyor

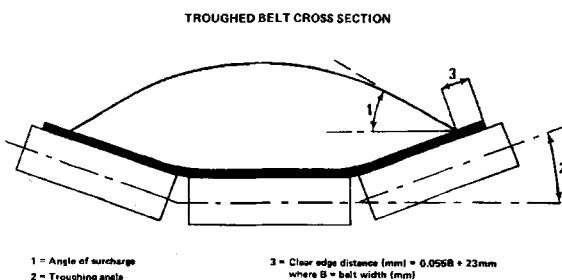


FIGURE 2 Belt capacity determining factors

$$A = Ub^2$$

where:

- U = non-dimensional cross-sectional area shape factor
- b = contact or "wetted" perimeter

The belt width $B > b$ to allow for edge effects.

Shape factors for various idler troughing configurations are available in manufacturers' handbooks or current design standards.

BELT TENSION AND POWER

Belt calculation starts with static type analysis assuming a steady state operation. Formulas for calculating belt resistance, belt tension, power, and belt rating are available on manufacturers' handbooks or current design standards. Current practice is to adopt high factors-of-safety of the order of 7:1 to account for unknown dynamic effects and uncertain belt splice efficiencies. This was the approach that used for KPC OLC original specification.

Significant improvements in conveyor belt technology have occurred over recent years. There is now a much better understanding of the dynamic behavior of belts during starting and stopping, as well as during operation. Such dynamic analysis results in design optimization and lower factors-of-safety.

DESCRIPTION OF KPC'S OLC

The OLC is 13.1 km long with an almost zero change in elevation between the loading point and head end discharge. The conveyor passes hilly terrain and over a

total of 6.5 km of swamp zones. The belt is driven by two drive pulleys situated at the conveyor's head end (Figure 3). A take-up system is also located at the head end.

The OLC discharges the coal onto two receiving yard conveyors at Coal Terminal.

The conveyor consists of modules. The modules have a line stand every 3 m (Figure 4). A line stand consists of two legs bolted to the carry and return idler frames and a concrete sleeper. The line stands are held upright by two purlins. These purlins support the roof and the conveyor power and control wires.

The idler spacings for the full length of the conveyor are 3 m and 6 m for the carry and return respectively. All idlers are at right angles to the belt in side elevation.

UPGRADE PROJECT BACKGROUND

At the end of 2003, KPC decided to increase the mine output to 30 mtpa. This demand required another upgrade of the OLC. The upgrade was the less cost option compared to building another overland conveyor. It was also directed that the upgrade had to be realized as soon as practicable.

There are several ways for KPC to get more capacity onto the OLC:

1. Feed more coal onto the existing belt and reduce the edge clearance
2. Increase the belt speed using the existing belt width
3. Increase the belt width
4. Increase the belt width and speed

Feeding more coal onto the OLC was not possible, as this approach had been actually taken place since the previous upgrade. The belting had been operating at 100% cross-sectional capacity with a minimum allowance for belt edge clearance. More feed would cause excessive spillage when belt mistracking occurs and might damage the belting.

Increasing the belt width would mean massive structural changes. Not only the cost for such change become a consideration but also the down time required for executing the changes. KPC is only operating one overland conveyor.

Therefore the only left is to increase the conveying speed further. This was a real challenge. The existing speed was already on the industry limit.

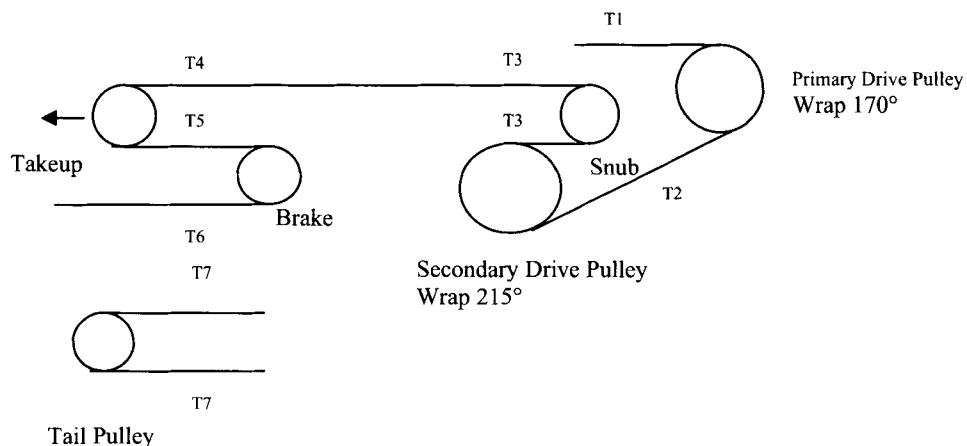


FIGURE 3 OLC pulleys

BENCHMARKING

When the project started, the project team tried to find information regarding overland conveyor operating at high speed. Unfortunately there was no information regarding long overland conveyor except short in plant conveyor. Therefore, when developing the upgrade design the project team did not have any relevant benchmark.

SITE EXPERIENCE

From the beginning of operation, KPC has progressively explored the potential of OLC operating beyond the nameplate. An upgrade could be justified only after the last ton of capacity was squeezed through the system. From the beginning of operation, KPC has progressively explored the potential of OLC operating beyond the nameplate. An upgrade could be justified only after the last ton of capacity was squeezed through the system.

It has been an approach of KPC operation that design figures will have some extra margin due to allowances in the design criteria. Site observation and measurement would become verification for the extra margin. When the extra margin could be demonstrated, it would be utilized to crank up the capacity of OLC.

As the result of those exercises, some initial design criteria were adjusted. The adjusted values were used for the upgrade design.

Original design of OLC was based on Bulk Density of 820kg/m³ for volumetric design and a Surcharge Angle of 5°. For the first upgrade in 1995 the OLC design was based on Bulk Density of 820kg/m³ for volumetric design and a Surcharge Angle of 15°.

Prior to the last upgrade, subsequent measurements of coal profile at several locations along the conveyor line were conducted. The coal appears to load at a higher surcharge angle than the 25°. The coal appears to load onto the OLC at a higher density than the 900kg/m³. The coal packs down and becomes more dense as it travels the 13.1km from Coal Preparation Plant to Coal Terminal.

Based on the test result, the design parameters for the last upgrade was established on Bulk Density of 900kg/m³ and a Surcharge Angle of 25° because loading at surcharge angles of greater than 25° consistently is

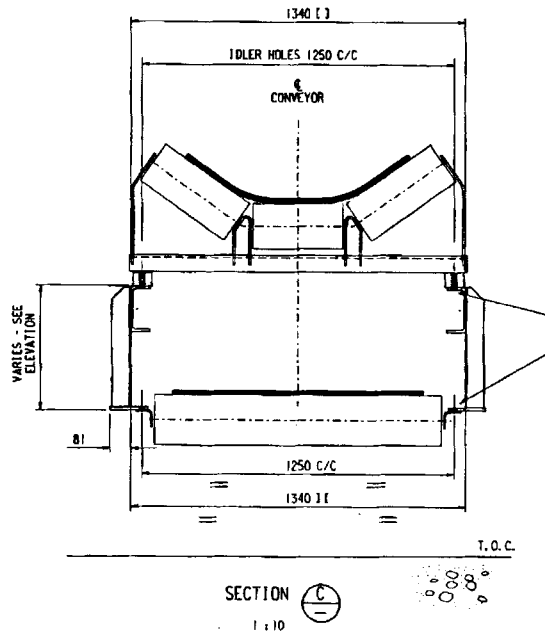


FIGURE 4 Cross section of conveyor modules

considered optimistic and if the density does increase it would only widen the edge clearance margin.

Verification was also carried out to obtain actual friction experienced by the belting. Data of actual power consumption was used for back calculation. The result showed the actual friction is less than previously used as design parameter. The adjusted friction value was then used as the basis for the upgrade design.

The load cases used as design basis was also adjusted as the result of long experience of operating the OLC. Previously the worst partial load case used was all down-hills along the OLC are unloaded while all up-hills are loaded during start-up. The adjusted partial load case used for the upgrade is with the conveyor full over its full length and only the largest hill unloaded which is considered a short term events.

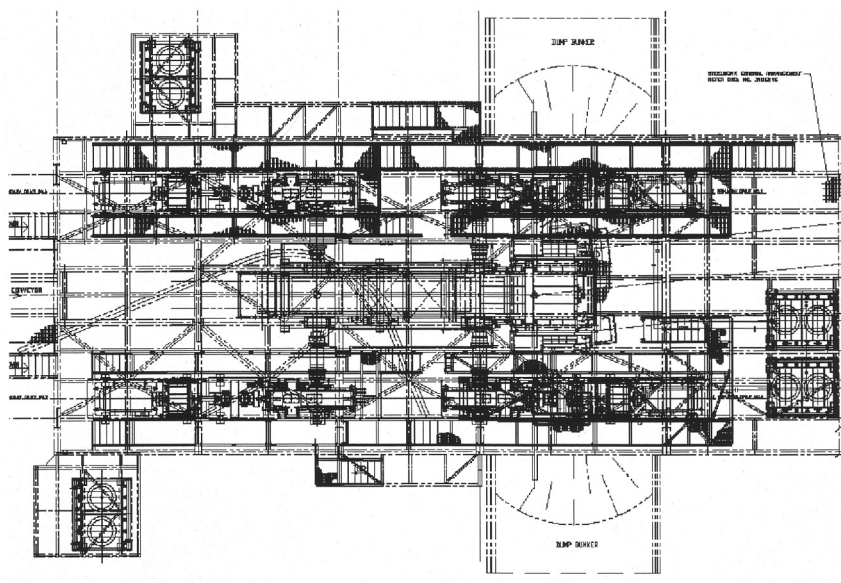


FIGURE 5 Arrangement of OLC drives

ESTABLISHMENT OF BELT SPEED

To achieve 30mtpa capacity, the OLC shall run at average rate of 4,000tph over 7,500 hours a year. Considering rate fluctuation from the feeder, a capacity of 4,500tph was established as upgrade design peak. Using ISO 5048 as the basis for edge clearance and cross-sectional area calculations and the information of conveyor drive gear ratio from the manufacturer, an increase in the belt speed from 6.68 m/s to 8.48 m/s is required to realize 4,500tph as the design peak capacity of the OLC.

The conveyor drive gear ratios shall be altered to provide the increase in the belt speed. The belt speed increase allows the conveying capacity to increase, and maintains the belt loading (kg/m) at the existing operating values. Therefore the belt forces are increased by a negligible amount under steady state running conditions.

MAJOR DESIGN CHANGES

The belt speed increase requires modification to the existing system. Following are the major changes that were executed for the upgrade.

DRIVES

Drive train consists of an electric motor, a variable fluid coupling, a flywheel, and a gear reducer (Figure 5). The gear reducers are connected to the Drive Pulleys. The gear sets of existing three drives were changed to increase the belt speed from 6.68 m/s to 8.56 m/s. The analysis showed requirement for additional 1 MW drive as the power demand of the OLC will increase in direct proportion to the belt speed increase. Therefore, the fourth identical drive was fitted to the Secondary Drive Pulley. Previously the Secondary Drive Pulley was driven only by one drive while the Primary Drive Pulley had already driven by two drives.

During the upgrade design development the Project Team assessed the possibility to replace the Fluid Coupling with VVVF (Variable Voltage Variable Frequency) recently become trend in the industry, to

facilitate soft starting. However, the capital and down time consequences did not justify this option.

An improvement on drive foundation was also executed as part of the upgrade (Figure 6). Previously the drive base plate was supported from the foundation by a pivot and load cell. Site experience concluded that such support had been contributing to the high vibration.

STARTING

The start time of the conveyor was increased to 560 seconds in the PLC acceleration program controlling the fluid coupling scoop actuators in order that the peak dynamic tension in the conveyor belt during starting does not exceed the safety limit set by the original belting specification.

The analysis showed that the upgrade capacity generating heat in the fluid coupling close to the limit.

This was experienced during the commissioning where failed start occurred due to fluid temperature increased beyond the protection limit. To manage this issue, the drives were limited to 6 evenly spaced starts/hour and the cooling system would operate first prior to OLC start up.

BELTING

Analysis showed the speed increase would increase the dynamic tensions under starting and partial loading of the belting. The belting manufacturer was consulted regarding the upgrade of the conveyor and any effects on the belting warranty. Results of the wear monitoring by KPC on the belting, power consumption and the tonnage passed by the OLC to date were used in negotiating the warranty.

The manufacturer confirmed that the tensions generated by the capacity increase in various operating scenario were still below the belting limitations. No change is required to the belting.

For full load case, the minimum safety factor is 4.45 for steady running and 3.9 for start-up. For partial load case with only one largest downhill unloaded the minimum safety factor is 4.1 for steady running and 3.6

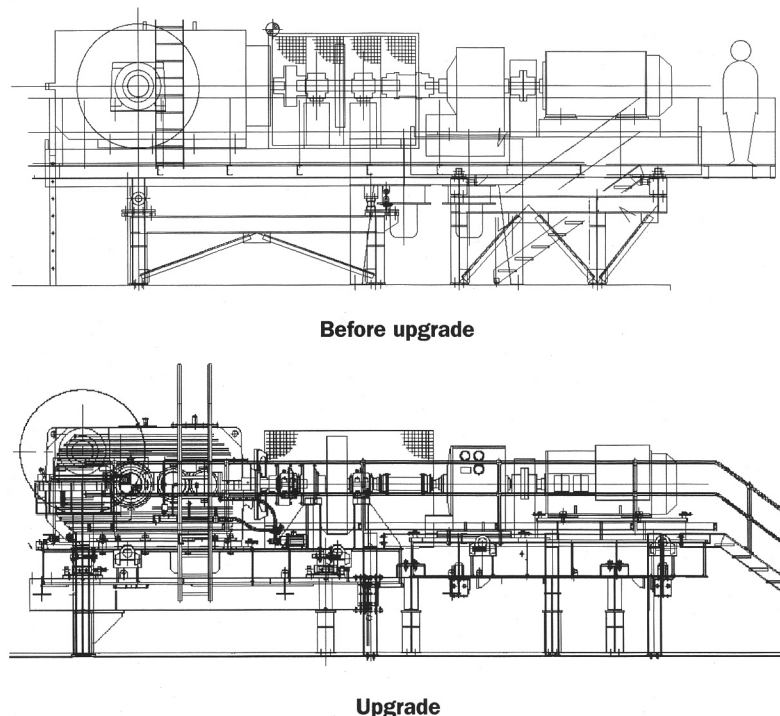


FIGURE 6 Improvement of drive bases

for start-up. The safety factor used is far below the safety factor normally used. As described in the earlier part, comprehensive dynamic analysis made the use of lower safety factor justifiable.

OLC DISCHARGE CHUTES

The old chute could not be modified whatsoever to cope with the new belt speed. It was replaced with a newly designed chute (Figure 7). The flop gate used in the old chute to split the coal from OLC onto two yard conveyors was replaced by a diverter.

FEED TO THE OVERLAND CONVEYOR

Previously the OLC was fed by vibrating feeder from a surge bin receiving coal from a CPP Reclaim Conveyor. As part of 30mtpa expansion, KPC built a new CPP directing coal to OLC from a new Surge Bin. The vibrating feeder was removed and the flow from the old surge bin is directed to new surge bin via a transfer conveyor. Therefore, only the new surges bin through belt feeder feeds the OLC to realize a single loading point.

PULLEYS

New Secondary Drive Pulley with double ended drive shafts was fitted to allow the Secondary Drive Pulley to accept two off 1 MW drives. Due to the increase belt speed, the belting working tension on pulleys also increase. New pulleys with larger shaft diameter on locking element were fitted to replace the old pulleys.

IDLERS AND IDLERS FRAME

Lifetime calculation concluded that the bearings of original OLC idlers will have shorter life time below the KPC requirement of 65,000 hours B10 life. Therefore, all idlers shall be uprated with higher rating bearings. As the

OLC has more than 17,000 idlers, the strategy adopted was a progressive replacement. During the upgrade 4,000 idlers on high tension location were replaced. After that progressively failed idlers being replaced with higher rating idlers. There was no change on idler frames. The only change is the adjustment of transition length both at discharge and tail end of the conveyor to cope with higher speed.

TAKE-UP

No change is required to the take-up as the analysis concluded the existing take up tension is still sufficient for the upgrade task.

STRUCTURAL

The integrity of OLC Drive Support Structure was checked against upgraded load case and additional weight due to additional equipment installed on the platform. As a result, the following modifications were executed:

- Structural reinforcement.
- Extension of the platform to support and provide access to fluid coupling oil coolers relocation.
- Modifications to existing steelwork to support the fourth drive.
- Modifications of platforms, stairs and ladders
- Extension of the roof.

The tail pulley foundation was strengthened to cope with increased tension.

The increase in belt speed also require that alignment and tracking be accurate. During the upgrade, an alignment was carried out by adjusting the level of some modules.

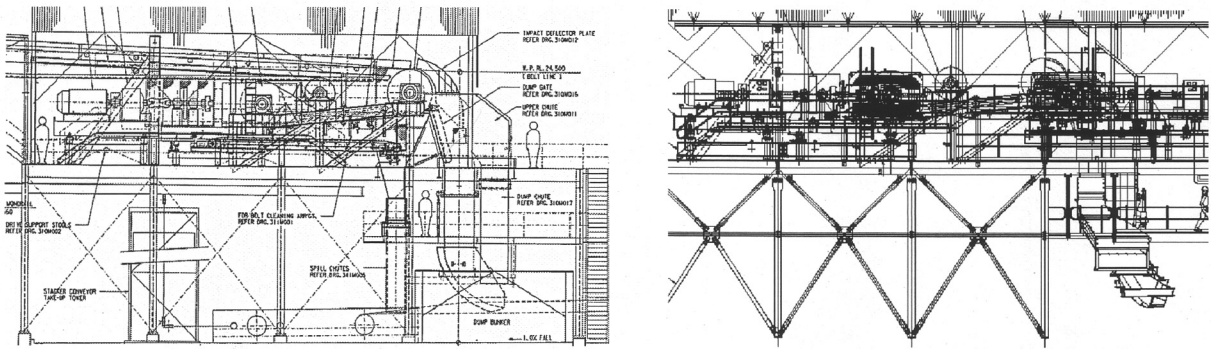


FIGURE 7 Old (left) and new (right) OLC discharge chute

PROJECT IMPLEMENTATION

The upgrade project was fully managed by in house engineering resources. Due to requirement for realizing the upgrade capacity quickly, a fast track approach was employed. Engineering and design was being progressed in parallel with procurement and site execution. The whole project was started in November 2004 and the upgrade capacity was realized in February 2005.

ENGINEERING AND DESIGN

A few numbers of specialists were engaged. They include the original belt conveyor designer, control system specialist and structural consultant. The adequacy of components of the OLC upgrade capacity were assessed to determine whether or not the existing one needs to be replaced with higher rating components. Adjustments were designed for the PLC control system to modify the starting time and other parameters as required by the changes made on the system.

PROCUREMENT

Procurement of long lead item such as gearbox, motor, fluid coupling, pulleys, idlers, and transfer chute determined the project schedule. Therefore, as soon as engineering review completed for those component, purchase was made and expedited.

SITE CONSTRUCTION

The site execution was carried out with minimum down time of OLC to minimize disruption to KPC production. The strategy implemented was to distribute the tasks over the 10 hours monthly scheduled maintenance shutdown of OLC with final upgrade installation was executed over 10 days shutdown of OLC in February 2005.

OLC UPGRADE PERFORMANCE

Soon the upgrade installation completed, the OLC was successfully commissioned to run at the new speed. Belt was tracking good. Progressively after the commissioning the OLC was taken to feeding set point of 4,200tph.

The upgrade successfully cranked up the KPC's throughput as can be shown from the following statistic.

Year	Coal Conveyed to Coal terminal	Remarks
2004	21.4 million tonnes	Before upgrade
2005	26.4 million tonnes	Upgrade took place in February 2005
2006	29.5 million tonnes	

REFERENCES

- Stickland, F.T., The Influence of Design Options on the Capital and Operating Costs of Overland Conveyors, *IIR Conference Proceeding*, 1997.
- Hager, M., Hintz, A., The Energy-Saving Design of Belts for Long Conveyor Systems, *Bulk Solids Handling*, Vol. 13 (1993), No. 1, pp. 749–758.
- James, G.L., Design of a 13.1 km Overland Conveyor, *Bulk Solids Handling*, Vol. 12 (1992), No. 539–545, pp. 99–104.
- Roberts, A.W., Harrison, A. and Hayes, J.W., Economic Factors Relating to the Design of Belt Conveyors for Long Distance Transportation of Bulk Solids, *Int. Jnl. of Bulk Solids Handling*, Vol. 5, No. 6, December 1985 (pp. 1143–1149).
- Harrison, A. and Roberts, A.W., Technical Requirements for Operating Conveyor Belts at High Speed, *Bulk Solids Handling*, Vol. 4 (1984), No. 1, pp. 99–104.
- Roberts, A.W., Hayes, J.W. and Scott, O.J., Optimum Design of Continuous Conveyors, *Bulk Solids Handling*, Vol. 1 (1981), No. 2, pp. 255–264.
- Beckley, D.E., Belt Conveyor Transition Geometry, *Bulk Solids Handling*, Vol. 2 (1982), No. 4, pp. 143–147.

Limestone Transportation by 17-km Cross-Border Long Belt Conveyor for Lafarge Surma Cement Limited

Kumar Vikram * and Pabak Mukhopadhyay *

Rich reserve of prime quality limestone in east khasi hills of India and abundant quantity of low-cost fuel (Natural Gas) in Bangladesh made Lafarge Surma cement limited a joint venture company of Lafarge France and Cementos Molins Spain to envisage an integrated cement plant at Chatak (District-Sylhet) a bordering town of Bangladesh. Since April 2006 the single flight 17 km Long Belt Conveyor (LBC) built by M/S Larsen & Toubro Ltd. (L&T), ECC Division an engineering and construction company of India, is feeding limestone/shale to the Lafarge Surma cement plant. This engineering marvel was created on a turnkey basis with technology support of M/S Aumund France.

CONCEPT TO COMMISSIONING

L&T submitted the feasibility report in December 1998, bid against international competitors in December 2000. The contract was awarded in September 2002 and received notice to proceed in July 2003. The LBC commissioned in December 2005 when fire damaged a 1.2 km stretch. The conveyor was re-commissioned against tight timelines in April 2006 and the system is running successfully since then.

TRANS-BORDER CONVEYOR—THE COMPLEXITIES

Crossing of an international border has immigration, logistic, commercial, legal and security-related issues. Two countries are governed by different rules and regulation. However, L&T overcame these hurdles by their following innovative solutions:

- The conveyor was installed at an elevated level and without walkway. Two Maintenance Vehicles run over the conveyor gallery for carrying maintenance personnel, tools/tackles to attend the conveyor. Each vehicle will run from either end up to the international border and will cross with special permission in case of emergency. The gallery bottom is maintained at minimum 5.5 M height from ground level.
- Design the LBC with drive and control at both ends. Provide independent power supply of each country to the two drive station with control located at two ends. The two control system to communicate with each other for controlling the drives as well as the conveyor.

■ Supply and construct portion of the conveyor in each country as two separate conveyors. (Special permission was arranged for working in International border area during survey and construction of foundation for few days).

- Erect the portion of the conveyor in each country independently and make final connectivity at border to make it a single conveyor. (Special permission was arranged for working in international border for few days while establishing the continuity of structural gallery, fiber optic cable and jointing the steel cord belt).
- Commission the conveyor with data communication between the two control rooms located in two countries thro Process control system. All mechanical checking being carried out from Maintenance Vehicle of each country.

TECHNICAL PARAMETERS OF THE CONVEYOR

This single flight conveyor is 17 km long out of which 7 km is in India, 10 km is in Bangladesh. The conveyor starts from the hill of Meghalaya, India, climbs down by 59M in first 1.5 km and rest of the conveyor is in plain land (Figure 1). It is a 35 deg. trough belt conveyor, Capacity 800TPH, 800mm wide steel cord belt, 4m/sec speed, 10 no's of Horizontal and vertical curve, 2 no's 630 KW drive at head end Bangladesh 1 no 630 KW drive at tail end India, conventional horizontal gravity type take up used. Belt turn over arrangement at both end provided for better performance. The conveyor civil design takes care of the local soil condition and seismic

* Larsen & Toubro, Ltd., Chennai, India.



FIGURE 1 The LBC crossing three hills

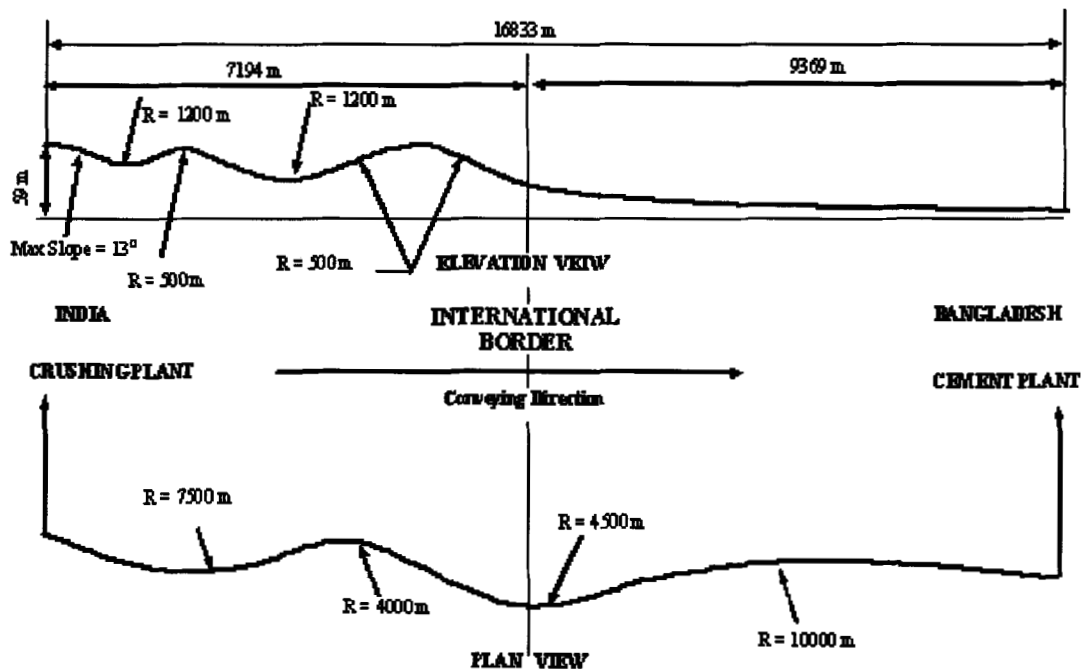


FIGURE 2 Belt profile

condition for the geological fault zone. RCC trestles have been provided for the plain land area whereas structural steel trestles are provided in hill area for ease of erection and better flexibility. The belt profile of the conveyor is shown in Figure 2.

SPECIAL DESIGN FEATURES: FEEDING ARRANGEMENT TO THE LBC

A small conveyor (sacrificial conveyor) feeds the material in the same line of the LBC travel direction. Uniform

feeding to LBC is ensured by variable speed apron feeder taking material from hopper mounted with load cell. Arrangement is shown in Figure 3.

Gallery Design

Gallery length of 24.5 M found to be the optimum solution. It was designed for 195 km/hr wind speed, two maintenance vehicle load, conveyor load of 800ton/hr and temperature variation of 35 deg. All galleries of hill area is with one end hinge and one end sliding support.

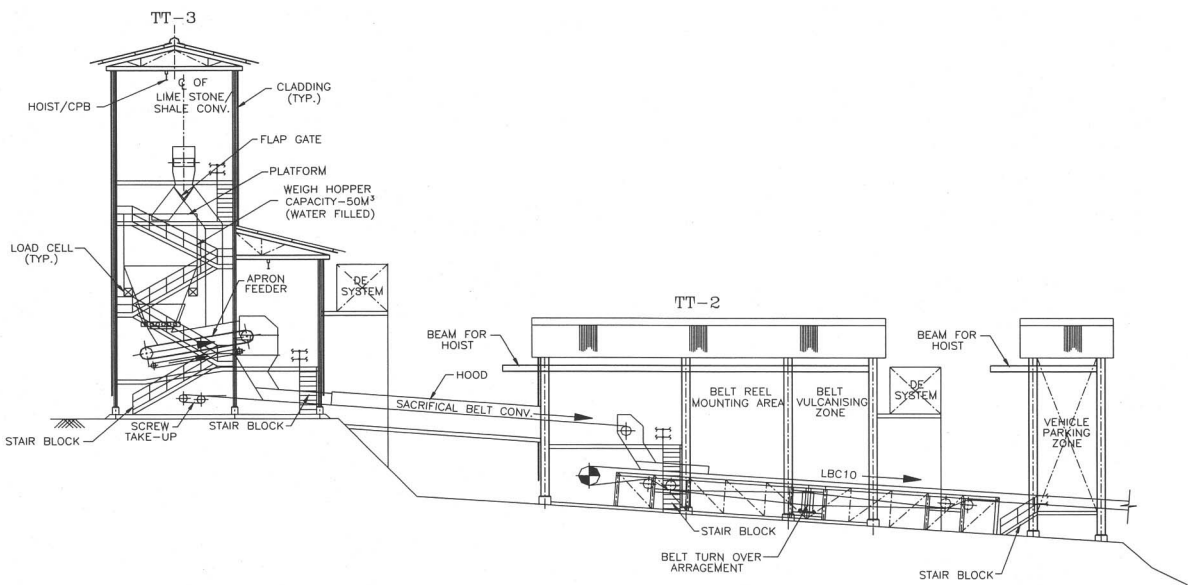


FIGURE 3 Feeding arrangement

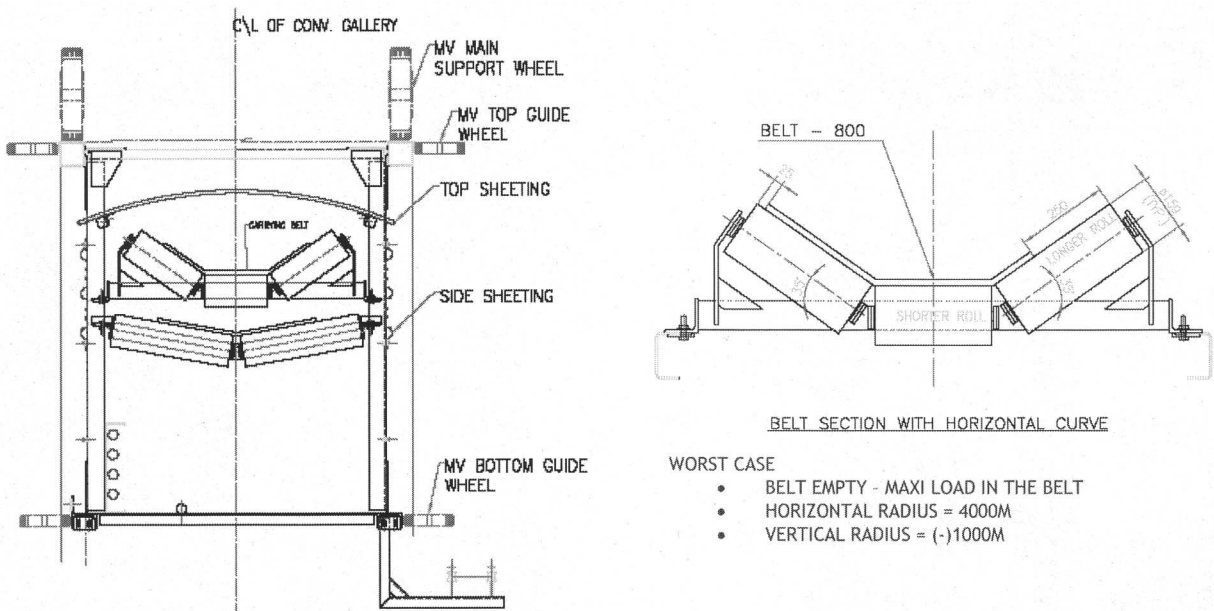


FIGURE 4 Gallery cross section

In plain area sliding supports provided at every 100 M. The top and bottom chord of each gallery is designed to take care of expansion due to temperature variation. Colour coated roof sheeting and side sheeting provided in the gallery to protect the environment from dust and the raw material from rain water. Gallery Cross Section is shown in Figure 4.

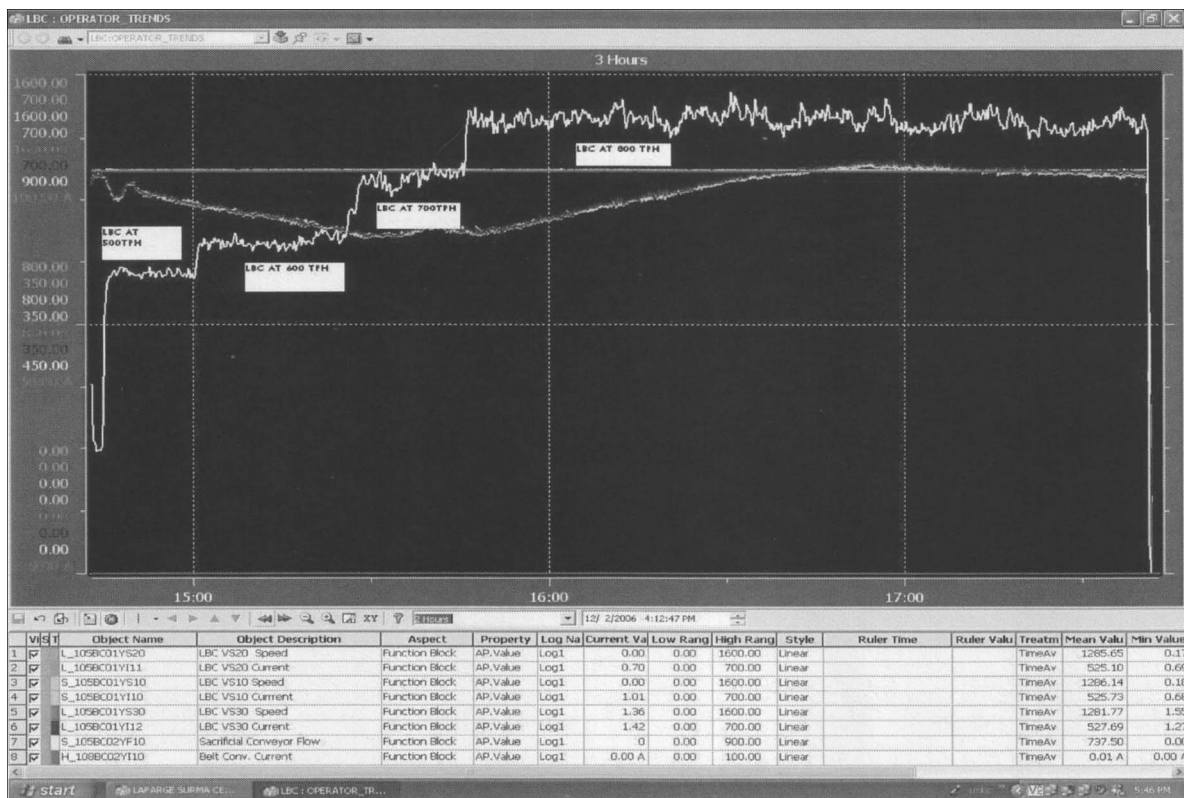
Design of the Idler

Idlers used are base mounted 35 deg conventional type. The bracket is designed such that in case any roll is dropped belt will not get damaged by any sharp edge of the bracket. At curve zone the wing rolls are longer and

idle are erected skewed. Design also takes care of condensation problem due to high humidity and high temperature variation of 35 deg.

Conveyor Control Systems

The conveyor is driven by three drive motors (630 KW each) two at discharge end and one at tail end. The speed of the conveyor is varied by VSD 6.6/0.69 KV. The conveyor is controlled by the main PCS from central control room located at cement plant in Bangladesh. The data network is through field buses (profibus) Further two PLCs are located, one close to Drive Station in Bangladesh and the other close to the

**FIGURE 5** Conveyor control system interface

Tail Station in Meghalaya (India). The two PLCs communicate with each other through fiber optic cable for speed synchronization of the drives. Safety Interlocks and Safety Switches are provided to make the system full proof. The conveyor can be stopped from either of the Maintenance Vehicle by pressing the Emergency Stop Push Button which operates on a closed loop system of signal being transmitted through wired network (Figure 5).

The Details of Maintenance Vehicle

The Maintenance Vehicle provided in this project is state of the art design (Figures 6 and 7). It can carry 5 persons (375 kg), Maintenance Tools and Tackles (200 kg). The vehicle has a variable long travel speed and can move at 5 kmph in hill area and up to 15 kmph in plain land area. Fail safe Rack and Pinion arrangement provided for the drive system for hill area only. The vehicle is powered by two diesel engines, one working and other stand by. The long travel system is through variable speed hydraulic motor with fail safe disc brake. For worst eventuality provision kept to move the vehicle by manual hydraulic pump. The vehicle is fully rain protected and ensures maintenance access below the return belt using fold down side platforms. Safety interlocks provided to disable travel of vehicle when platforms are extended. A diesel generator provided in the vehicle to supply electric power for lighting, welding, material hoisting, power tools. The following tools and attachments are also provided within the vehicle:

- Working bay on both sides of the conveyor.
- Belt hoisting device.
- A microphone system to monitor noise difference between running idlers.
- Electric hoist to lift spares/tools up to 500 kg.
- Lighting of vehicle including flood light for maintenance and head light.
- A safety escape ladder with fall prevention system.
- Space for storage of idlers for replacement.
- Storm clamp for securing the vehicle with conveyor structures.
- Tool box
- Mirror to inspect the return idlers rotation.

CONSTRUCTIONAL CHALLENGES

The Indian portion of the site is very close to Cherrapunji, the highest rainfall area of the world. The monsoon duration is from May to September with an average monthly rain fall of 1.5 M to 2M and maximum rain fall in a day around 500mm. The natural ground level of the site in India is at higher elevation than Bangladesh resulting flow of all rain water to Bangladesh and submerging the conveyor corridor under water for four months. Thus leaving 7 to 8 months time for carrying out site activity in a calendar year.

Site Welding of the Prefabricated Gallery and Final Painting

The gallery was fabricated in workshop to achieve the required tolerance. Then dismantled, prime painted and



FIGURE 6 LBC with maintenance vehicle

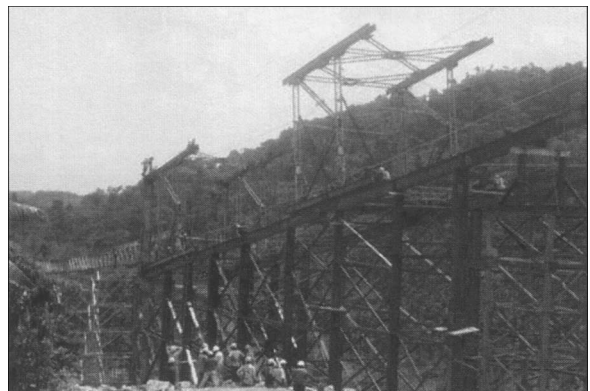


FIGURE 9 Erection of 100M-long bridge over geologic fault

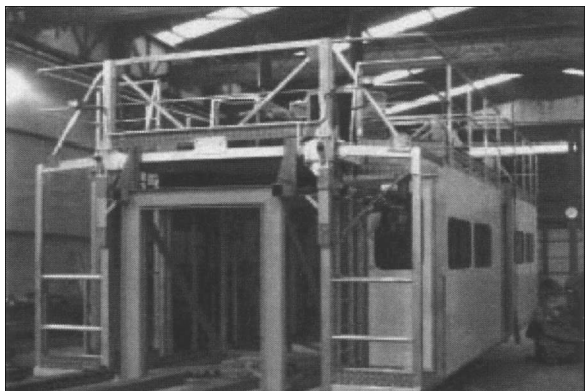


FIGURE 7 Maintenance vehicle



FIGURE 10 Difficulties of transportation along conveyor corridor

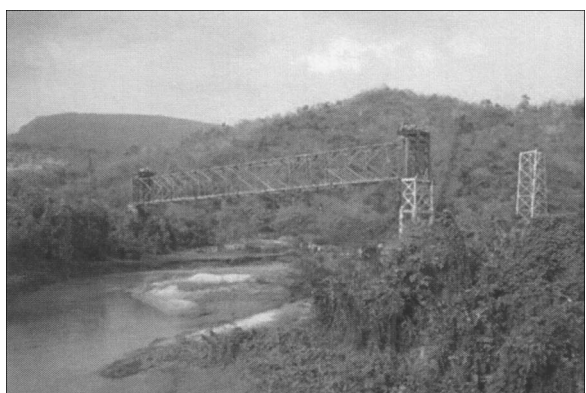


FIGURE 8 100M-long bridge over Moula River

dispatched in framed packed condition. It is reassembled, final welded and painted before erection at site.

Erection of the Two Long Span Bridges in Difficult to Reach Places Were the Toughest Task

Conveyor crosses places like river, road, etc. where trestle cannot be put at normal interval thereby requiring long span galleries. Since Maintenance Vehicle moves over the conveyor gallery, bridges were required to support the conveyor gallery with extended span. There were six bridges in India and six bridges in Bangladesh.

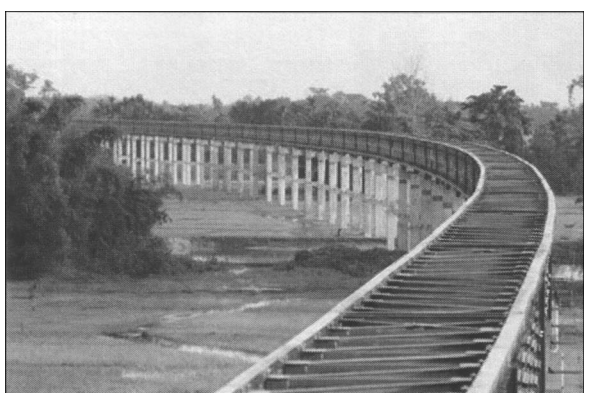


FIGURE 11 LBC with horizontal curve

One long span bridge of 100M long over Moula River (Figure 8) was assembled at ground level with special arrangement and subsequently lifted the entire bridge with the help of strand jack equipment. Long span bridge (100m) located in geological fault line and weighing about 150 MT was erected by segment launching method successfully (Figure 9).

Transportation of material up to site both in Bangladesh and in Meghalaya, India, and subsequent distribution along the corridor for 17 km was the greatest

Notice to Proceed: 25.07.2003

Commissioned Date: 06.12.05

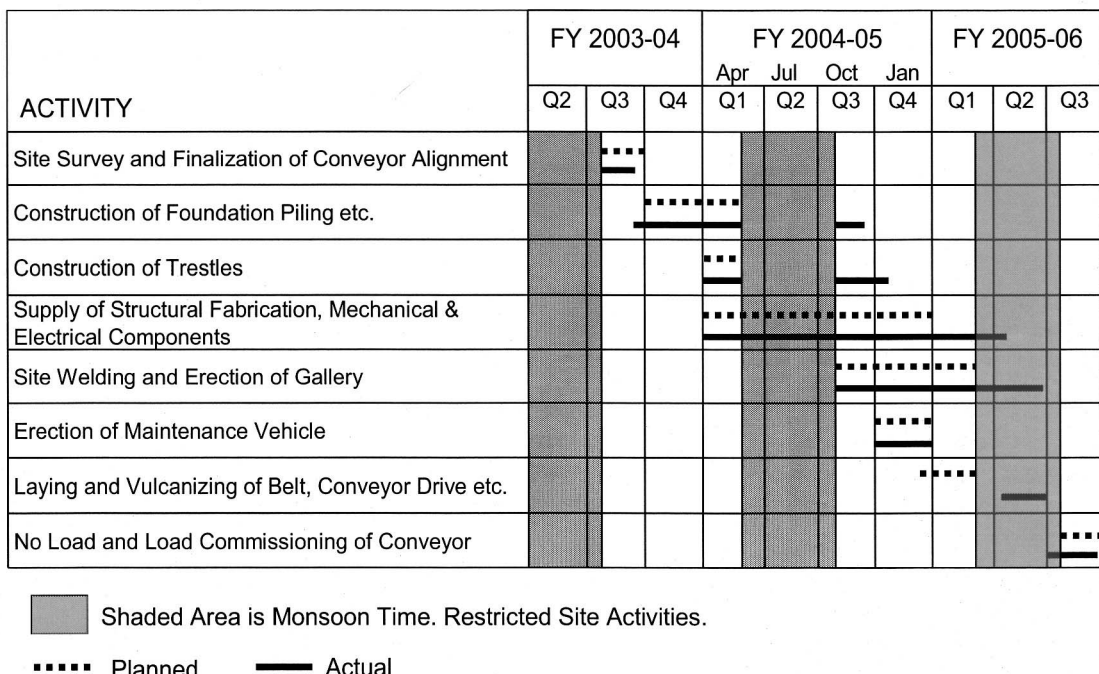


FIGURE 12 LBC schedule of major activities

challenge (Figure 10). The Indian portion of the site is very remote area. The hilly road connectivity leaded to a transportation limitation of 9 ton weight and 12M length in any consignment. River route by barge is the only mode of transportation of material to Bangladesh. The nonavailability of barge and slushy conveyor corridor affected the receipt of supply materials to site location.

Laying of the Belt and Belt Jointing

This conveyor being first of its kind in the world (Figure 11), the finalization of the belt laying scheme, equipment selection to carry out the job with a consensus of the designer was a difficult task. Finally our ability to develop the right scheme within the time available is the main reason for the success of this project.

THE RACE AGAINST TIME

The Construction Schedule

Notice to proceed for procurement and construction was received in July 2003 when the total Bangladesh stretch of the site was submerged with water; however we planned the activity such that the conveyor can be commissioned by December 2005, fulfilling customer's requirement.

Occurrence of Natural Calamity

It rained unprecedented during March 2004 and Oct 2004, causing flash flood and destroying the construction approach road, damaging construction equipment. This affected the planned programme of the job.

Implementation of Catch-up Plan

The effect of natural calamity and delay due to the same left almost no time for the belt laying activity. The belt laying plan was totally revised as per the prevailing site condition and belt jointing was carried out at multi vulcanization station without compromising the quality. Catch-up plan was drawn up and monitored on daily basis. Additional equipment mobilized to achieve extra productivity. Extra attention during erection, alignment checking of idler paid rich dividend during no load commissioning of the conveyor. Finally the conveyor was commissioned two weeks before the due date. The project scheduled as planned and as carried out is shown in Figure 12.

CONCLUSION

The commissioning of Lafarge LBC has established that conveying of raw material to longer distance through troughed belt conveyor without environmental pollution is an economically viable solution.

Cadman Downhill Overland Conveyor, Blending into the Washington State Forest Area

Bill Sayer,* Manuel Mendez,† and Peter Sehl†

INTRODUCTION

Cadman, a wholly owned subsidiary of Heidelberg Cement, is a leading supplier of sand and gravel as well as ready mix concrete in the greater Seattle area in western Washington State. Cadman's aggregate mine is located in North Bend, 34 miles east of Seattle, WA, and consists of a "Lower Pit" and an "Upper Pit."

In 2005, Cadman planned the upgrade of the North Bend mine operation as follows:

Upper Pit (Figure 1):

1. Crushing Plant, Stacker and Stockpile
2. Storage Reclaim Belt Feeders
3. Feed Conveyor
4. Downhill Overland Conveyor

Lower Pit (Figure 2, Photo 12):

1. Radial Stacker
2. Storage Reclaim and Truck Load-out

ThyssenKrupp Robins Inc., Colorado (TKRI), received in 2006 the turn-key contract to design, fabricate and install the Overland Conveyor that transports sand & gravel product from the upper mine site downhill to the lower pit, for transport to a processing site.

The 36 inch wide conveyor belt has a rated capacity of 1,000 stph and is 1.2 miles long with an elevation drop of 900 ft.

The design includes provisions for simultaneous transportation in the future of filter cake material uphill.

The project design team was faced with the challenge of building a conveyor that follows a complex route and maintains a "low-profile" design, which is minimally obtrusive to the environment. Environmental challenges included noise impacts, visual impacts and the effect on local wildlife, such as elk and deer.

The downhill inertia of the loaded conveyor generates energy and is used to offset the power needs of the crusher and feeder conveyors.

The installation started in the summer of 2006 and the performance test was successfully completed in March 2007.

Unique Features

- Simultaneous downhill and uphill conveyance.
- "Low profile design" to follow hill contours.
- 16 vertical curves (radii: 500–4,500 ft).
- 2 horizontal curves (radii: 5,000–7,500 ft).
- Conveyor decline: up to 18°.
- Ground grade decline: up to 22°.
- Regenerative drive system, using VFDs.
- Controlled mechanical braking system (backup for VFD).
- Guarding along entire conveyor length for safety and wind protection.
- Belt turn-over stations.

SYSTEM DESCRIPTION

General Design Requirements

The Overland Conveyance System had to follow the planned vertical and horizontal alignment as defined during pre-bid studies and in accordance with local community and governmental regulatory agency requirements. An obtrusive profile with long and high-elevated truss sections would not have been acceptable.

To satisfy these requirements a pipe conveyor design was initially considered, but ultimately rejected due to the cost implications.

Conveyor Module Design (Figure 3, Photo 1)

TKRI chose a modular low-profile conveyor design utilizing hat channels mounted on concrete sleepers to minimize the visual impact and optimize cost of construction. The standard modules needed to have provisions to adjust the individual idler banking within a range ±15°. Dual holding down bolt mountings allowed for compensation of grade elevation variances and vertical sleeper misalignment.

* Cadman Inc., Redmond, Wash.

† ThyssenKrupp Robins, Inc., Denver, Colo.

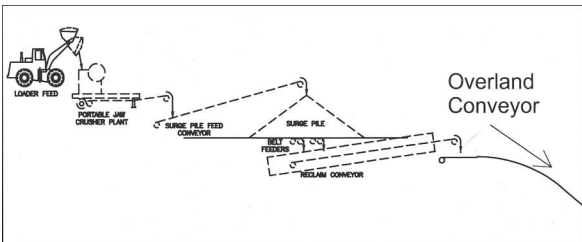


FIGURE 1 Plant overview—upper mine location

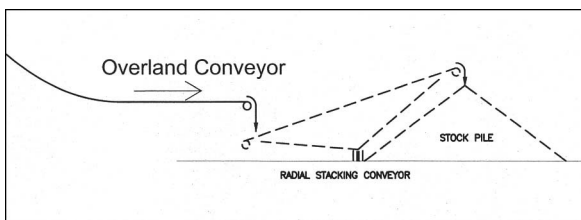


FIGURE 2 Plant overview—lower mine location

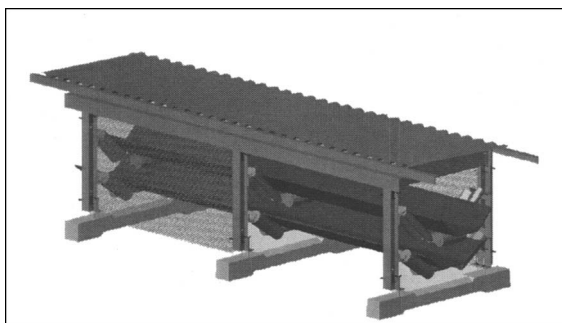


FIGURE 3 Standard conveyor module

Non-typical modules (Photo 2) with longer mounting feet were used in the transition areas to connect standard ground modules with the short elevated truss sections. The entire conveyor is guarded using expanded metal powder-coated sheets to provide an installation with a high degree of safety and that also serve as a wind break.

CONVEYOR ALIGNMENT (Photos 4, 5, and 6)

Figure 4 shows the plan view of the overland conveyor routing which was defined during the pre-bid study. In order to not disturb the existence of a historic wagon trail, portions of the conveyor had to be routed through pre-cast concrete culverts.

The upper culvert installation shown in Figure 4 and Photo 3 proved to be a critical area for proper belt tracking, where the conveyor runs through a 5,000 feet horizontal curve, a 7,500 feet vertical curve at an inclination of 18° (Figure 5).

In certain unfavorable loading scenarios and with the higher belt tensions during starting/stopping the belt has the tendency to move sideways to the inside of the curve. To limit the possibilities for this adverse situation, loading procedures have been established and logic programmed to control the material feed. In addition,



PHOTO 1 Standard conveyor modules installed without guarding

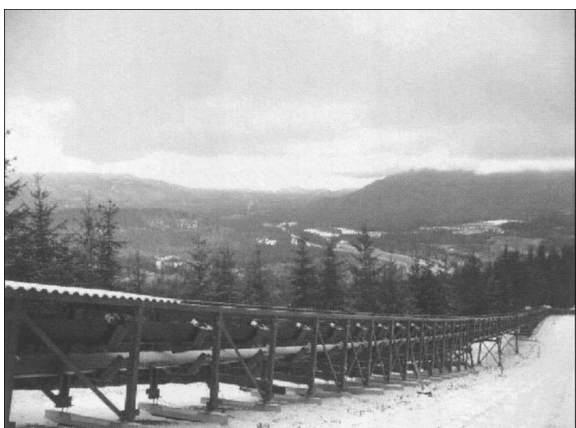


PHOTO 2 Transition conveyor modules approaching truss section

side guide rollers have been installed to restrict the belt side travel in certain areas. However, these rollers are not being utilized during normal running conditions.

DRIVE ARRANGEMENT

A total of 750 HP drive power is installed at the conveyor. Three 250 HP drives with Sumitomo reducers are located at the tail (upper) end. (See Figure 6.)

Each motor is controlled by a Siemens regenerative VFD, feeding power back into the electrical grid when the conveyor is loaded with more than ~500 stph (upper belt loaded only). Load sharing between all three drives is implemented with a torque-control loop.

Two of the drives are connected to the tail end pulley (Photo 7) and a third drive is mounted at the secondary drive pulley (Photo 8) located after the turn-over station.

The conveyor is normally stopped utilizing the VFDs on a 30 sec. linear ramp. In case of a power failure, VFD- or motor faults, a mechanical brake system from Svendborg at the tail pulley decelerates the conveyor. Two fail-safe calipers each mounted on two brake disks are powered by one common hydraulic power pack. The brake ramp is controlled by a PLC-independent brake controller (SOBO by Svendborg).

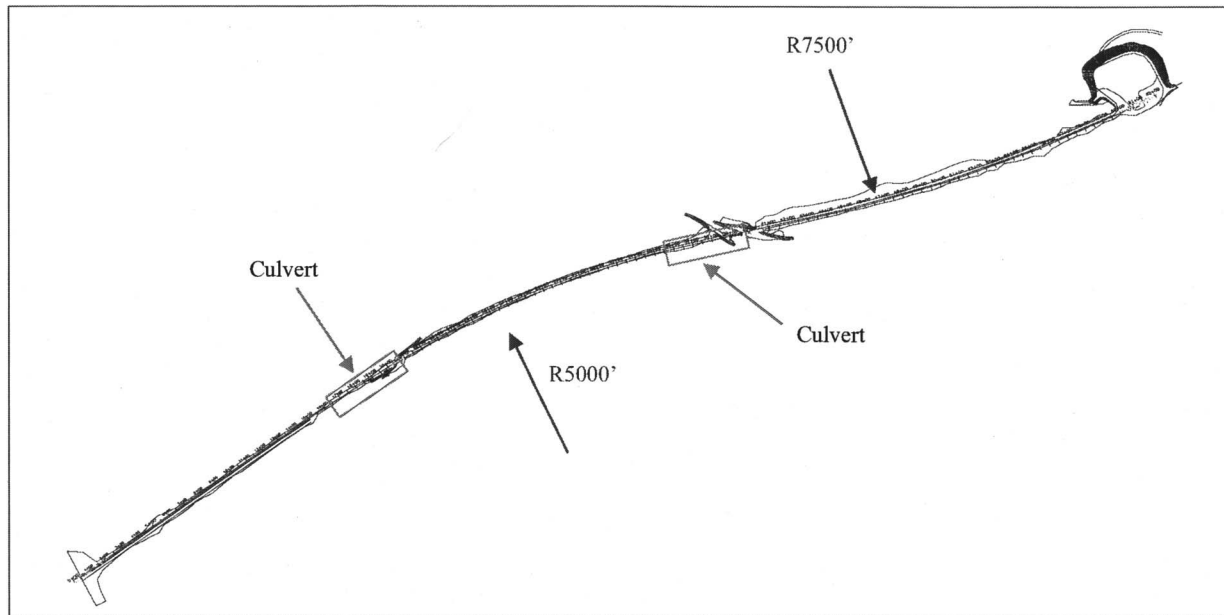


FIGURE 4 Overland conveyor—plan view



PHOTO 3 Upper culvert location

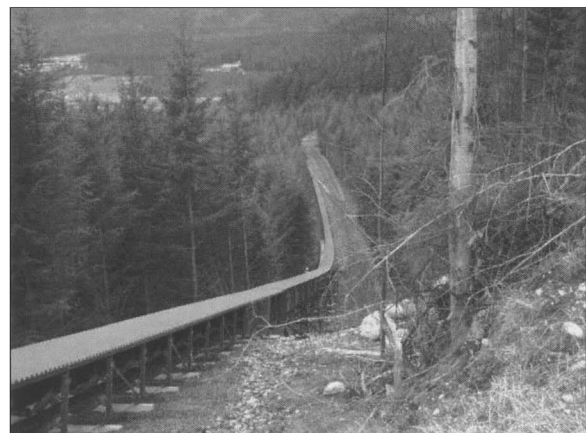


PHOTO 5 Conveyor routing, looking downhill



PHOTO 4 Aerial view of conveyor routing

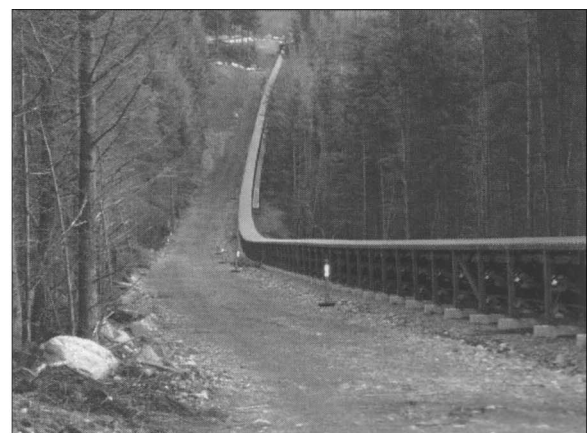


PHOTO 6 Conveyor routing, looking uphill at section with 22° ground inclination

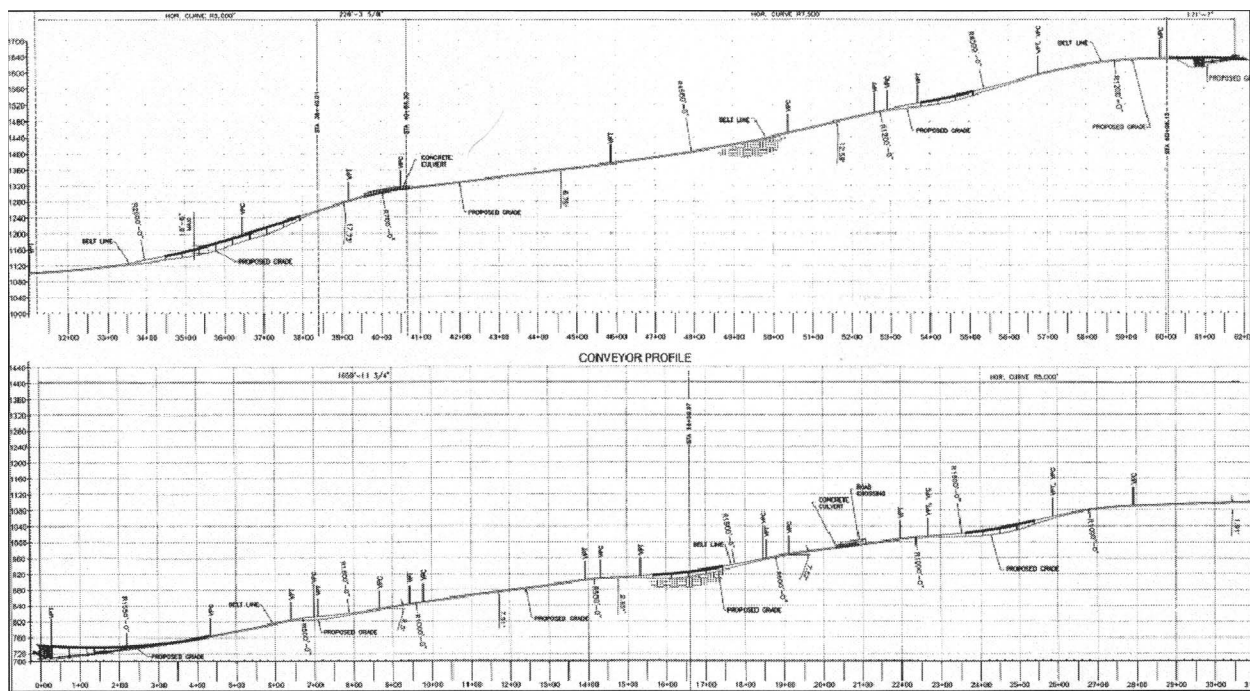


FIGURE 5 Overland conveyor—profile elevation

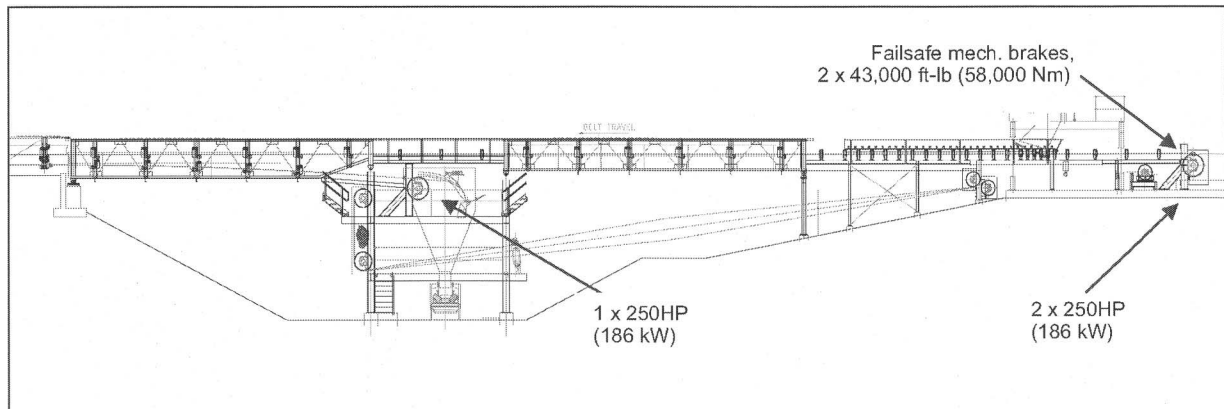


FIGURE 6 Drive arrangement



PHOTO 7 Primary drive with brakes at tall pulley



PHOTO 8 Belt turn-over and secondary drive tower

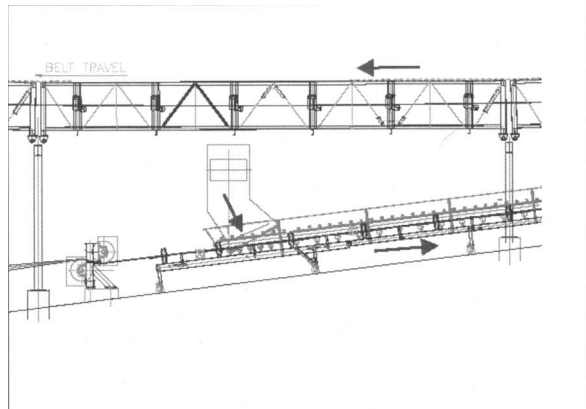


FIGURE 7 Loading of filter cake at bottom pit

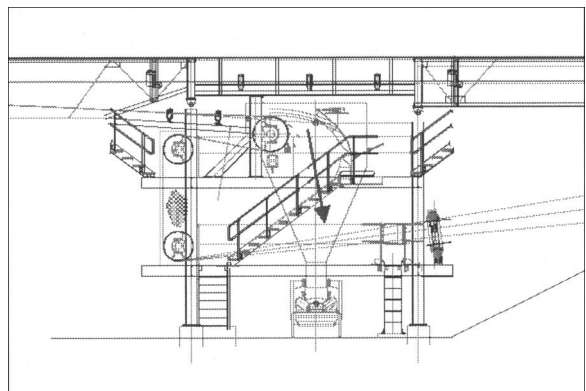


FIGURE 8 Discharge of filter cake at upper pit

TECHNICAL DETAILS

Uphill Conveying

The conveyor design allows for the future uphill carrying of a minimum of 280 stph of fines if material is not present on the upper belt (downhill conveyance) and 400 stph if material is loaded on the top side. To achieve this, provisions for a loading station (Figure 7) at the lower pit and a discharge "tripper" (Figure 8) near the upper pit have been included in the design.

Take-Up

A gravity type take-up is located on the return side at the head end and is complete with two bend pulleys and a take-up pulley with counterweight.

Conveyor Belt

The steel cord belt was manufactured for ThyssenKrupp Robins by Contitech AG. The belt specification is ST1800, 36" (914 mm) width, 6 mm top and 6 mm bottom cover with integrated belt rip detection loops (Photo 9). The belt rip detection sensors and associated control units are installed at both head and tail end.

Idlers and Spacing

Low profile idlers from Luff have been utilized. The troughing angle used is 45° for the upper strand and 35° for the lower strand. Idler spacing on both lower and upper belt is 7.5 feet. The idler banking varies between -15° and +15° with 1° increments.



PHOTO 9 Contitech 914 mm ST1800 6+6 RMAII



PHOTO 10 Belt Installation In November 2006

Pulleys

A total of 22 pulleys (incl. drive, tail, head, bent, take-up, snub and turnover pulleys) were supplied by Precision Pulley and Idler (PPI). The drive pulleys were provided with ceramic lagging.

Control

The control system consists of an Allen Bradley ControLogix PLC that interfaces to a Siemens PLC, installed inside the VFDs. The PLC monitors speed and safety devices of the conveyor. It also supervises the functioning of the VFDs and provides the parking command as well as an emergency brake signal to the mechanical brake controller (SOBO).

BELT INSTALLATION

The belt was installed by Contitech (Photos 10 and 11) with the belt reels placed on the bottom of the hill. The return strand was first pulled uphill before going around the tail pulley at the top. The partial lengths were strung utilizing a hydraulic winch, guide cables and snatch blocks. Due to the difficult terrain, the winch was fixed to a dozer. To prevent the belt from moving backwards during relocation of the winch and as a backstop during pulling, special retaining clamps were utilized.

The actual pull force was measured by a wireless strain gauge.



PHOTO 11 Belt installation utilizing dozer and excavator



PHOTO 12 Lower pit with overland conveyor head end, discharge chute, radial stacker, and load-out

TECHNICAL DATA—SUMMARY

Conveying Downhill		
Material	Sand and Gravel	
Max. Particle Size	8	in.
Density	100	pcf
Conveyor Capacity	1,000	st/hr
Conveying Uphill		
Material	Filter press fines	
Max. Particle Size	100	in.
Density	100	pcf
Conveyor Capacity	280	st/hr
General		
Ambient Max.	85	°F
Ambient Min.	10	°F
Conveyor Length	6,191.3	ft
Lift (vertical)	895.9	ft
Belt Width	36	in.
Carrying side trough	45	deg
Return side trough	35	deg
Belt Speed (theoretical)	1,000.0	ft/min
Power Requirement	643.0	HP
Installed Power	750	HP
Number of Drives	3	
Individual Drive Size	250	HP
Take-Up Type	Gravity	
Belt Rating	ST 1800	
Idler Spacing, Carrying	7.50	ft
Idler Spacing, Return Side	7.50	ft

.....

Thirty-Year-Old Transfer Point Challenge

Robert McEwen*

Conveyor equipment beyond its prime chronically suffers from a lack of understanding in today's plant environment regularly delivers more material than original designers ever expected. A case in point is a belt conveyor in a major hard rock mine/milling operation asking to bring the unit up to current standards while eliminating spillage and reducing airborne dust. The challenge was to keep the system going by revamping the system while keeping the same footprint and allowing for higher production rate. Thirty years of daily maintenance and dust collection costs have virtually disappeared by the end of this challenging upgrade.

INTRODUCTION

Aging mineral processing operations are able to extend life of equipment by retrofitting new technologies not available at the time of original construction. Thirty years have past, as well as a culture that no longer accepts high labour content.

This new standard for aging equipment, in most cases, can be retrofitted to meet new throughput demands without replacing the complete conveyor system.

MATERIAL HANDLING ISSUES

Retrofitting updated components saves the expense of replacing the conveyor footprint—stringers, supports, pulleys, idlers, incline, etc. Re-engineering of the conveyor is necessary to ensure speed increases; carrying capacity; support frame will take the load increases that is a normal requirement to justify the expenditure.

Traditionally, it was customary to erect a given mineral processing plants then try to fit conveyors in a given space; causing issues with many existing conveyor systems, i.e., limited transition distances, restricted skirtbox sizing, segregated materials, half-troughed belts, conveyor slopes to steep for material changes, lack of belt support, etc.

Conveyor Equipment Manufacturers Association (CEMA) revised recommendations for better belt support over the years since inception. Older conveyor systems have not kept up-to-date with these changes. A considerable number of conveyor systems were designed to

handle cotton fabric reinforced conveyor belts that are now using polyester nylon without considering belt compositions. Conveyor belt do have a considerable influence on the operation of conveyor system.

BACKGROUND COMMENTS

New system designs have solved many of these problems. Unfortunately, most clients cannot afford to replace their bulk material systems due to budget and market restraints. Tools used today did not exist during the time of construction. The conveyor industry has evolved to the point that many of the issues identified herein are solved an incorporated into new systems.

CONVEYOR ISSUES

The following issues are often evident on close examination:

- 1. Short transition distance**
 - Belt damage to carcass
 - Belt fabrication changes over time
- 2. Lack of belt support at transferpoint**
 - Distance between support idlers too far
 - Lack of belt support in transition distance
- 3. Loading in transition zone**
 - Turbulence due to lack of belt support
 - Off-centre loading
 - Material flow in opposing direction to belt
 - Centering plate causing backup of material
- 4. Rock box chute design**

* Drummond Equipment, Inc., Mississauga, Ontario, Canada.

- Material backup in chute
- 5. Excessive carry-back
 - Lack of material removal at head end
- 6. Dust collection pickup point
 - Pickup point in turbulent zone
- 7. Skirtbox length
 - Too short to reduce air velocity

CONVEYOR CHALLENGE

A major mining organization requested a conveyor audit to establish a benchmark for change on their thirty-year old system of bulk material handling equipment. An onsite audit revealed high maintenance areas that needed attention if there was any hope of maintaining the aged conveyor system while reducing maintenance staff, with a long term service, through attrition at the same time increasing production throughput.

One transfer point became a target for further investigation and upgrade. The key transfer point in question was located in the middle of the plant with limited windows of opportunity or space to make the changes. Dated drawings did not show the many attempts throughout the years of operation to improve material flow while reducing operational costs and overtaxed dust collection system.

Once the problems were identified by plant records, cleanup cost, production losses and potential for personal injuries, the transfer point became an obvious choice for upgrading to twenty-first century technology.

The following goals were established to improve the transfer while maintaining the existing footprint:

- Ensure efficient transfer of material.
- Eliminate fugitive material by 80% (spillage, carryback and dust).
- Design to handle 300-1,670 tph copper ore containing 0-6% moisture content.
- Allow for tramp material (steel, plastic, wood, etc.).
- Must be maintenance free for a period of twelve months from date of commissioning.
- Utilize standard components wherever possible.
- Maintain existing conveyor configuration, i.e., length, transition distance, incline, belt width, speed).
- Eliminate dust collection pickup point, if possible.

CONVEYOR SPECIFICATIONS

- Nickel/copper ore (-2")
- Bulk density of 100 #/cf
- Belt width 48"
- Capacity 1,670 tph
- Belt Speed 403 fpm
- Conveyor incline 18 degrees
- Maximum intermittent ore of -8"

SEQUENCE OF EVENTS

Total time from award of contract to commissioning was approximately twelve weeks:

- Collection of data
- Preparation design drawings
- Computer modelling
- Fabrication drawings
- Installation
- Commissioning
- Training
- As-Built drawings

- Component adjustments
- Monitoring

RE-ENGINEERING ELEMENTS

- Material Flow
- Skirtbox sizing
- Belt support
- Alignment
- Sealing
- Wearliners
- Drive motors

RESULTS

Initially, the transfer worked well and met expectations of the owner. After performing well for a two-week break-in period, an unacceptable wear pattern appeared on the liners. It was found that the liners were set improperly set for the tonnage.

New liners were supplied with high chrome magnetic casings were placed in high wear areas (see photo). Liners are now working well after proper adjustment after 8 months working life. The main advantage is the daily cleanup routine is eliminated and throughput tonnage increased. Skirtbox will be extended to permanently eliminate the dust collection pickup point altogether.

METHODOLOGY OF DESIGN

One tool that is available now that did not exist thirty years ago is computer modelling. It is now used to remodel existing transfer points showing the value of showing the material path as well as eliminating bottlenecks in the transfer point.

Discrete Element Modelling (DEM) has helped on difficult transfer points and a good check of calculations to prevent overloading the transfer point. Software allows virtual prototype transfer points for client presentations and optimizing design concepts. The tool improves reliability of theoretical designs prior to cutting steel.

The purpose of the study is to establish a benchmark for change with resorting to trial and error and provide a method of transferring the computer model directly to the shop floor. The resulting design would give the assurance that the traditional bottlenecks would be avoided. AutoCAD design drawings were provided based on existing drawings and field measurements. A curved lower deflector and upper were generated that showed the changes would be a vast improvement over the existing thirty year old and progressive field modifications. Material momentum was the important factor to a successful design.

Virtual design modeling is a visual tool to check theories of why and how the transfer point in question constantly spills material with minor changes of speed, flow and material size.

This method of analysis saves time and money for the designer, fabricator and client. Without this tool, it would be difficult to predict success or failure on aging conveyors.

WEARLINER MATERIAL SELECTION

Extremely hard, deep shaft, mine-ore requires a superior wearliner plate to prolong the working life of the transfer point to be successful in reducing maintenance costs in labour and reduced downtime.

A chrome alloy overlay was a wearliner of choice due to the impact loads and concentration of fines. The overlay

is designed to minimise the surface roughness inherent with traditional overlays. Client chose to use this as a test case for future transfer designs. There are a number of wearliner material choices on the market but should be investigated beforehand to ensure success. An accurate sieve analysis of the plant material is critical to any investigation of suitability.

CONVEYOR COMPONENTS

Belt was supported by impact cradles and retrofit bars on existing 20 degree carrying idlers to give superior support and low friction sliding to maintain existing power requirements. The skirtbox required wearliners and continuous apron seal to ensure sealing throughout the transfer. Dust collection system was not necessary due in part to alternating dust curtains through the transfer zone.

Upper and lower belt trackers installed before and after the tail pulley to ensure material would be contained and settle down before leaving the transfer zone.

SUMMARY

This project, to date, was successful in reducing plant labour content, health/safety issues, increased throughput and reduced demand on the dust collection system, for the client. Further investigation will be required for the remainder of the conveyor to address excess carryback, uniform idler usage and spacing.

Maintenance personnel indicated the project was a success and eliminated cleanup labour costs and saved shutdown time. A second transfer is being installed within the same circuit using the same methodology.

.....

Large-Scale Stacking System at the Freeport-McMoRan Safford Mine

Michael Schmalzel,* Andrew Osterloh,† and Grant Gruber‡

INTRODUCTION

Freeport-McMoRan Copper & Gold, Inc. (FMI) will soon begin copper production from the Dos Pobres and San Juan deposits near Safford, Arizona. Ore reserves total 615 M tons grading 0.36% copper, predominantly as chrysocolla. Copper extraction will be by leaching with sulfuric acid. Fluor Canada Ltd. provided EPCM services to design an ore handling and conventional SX/EW facility capable of producing a nominal 240 million pounds per year of cathode copper. The ore handling facility will process 114,000 tons per day of ore through three-stage, open-circuit crushing followed by agglomeration and product placement on the permanent leach pad. Stacking of ore on the leach pad will utilize Terra Nova Technologies' "Super Portable" mobile stacking system. The stacking system fleet consists of 13 self-propelled, crawler-mounted mobile conveyor units, each with 72-inch-wide belting and a capacity of 6,800 tons per hour, including ten 250-foot-long portable conveyors, a horizontal feed conveyor, a 285-foot-long horizontal conveyor and a 220-foot-long radial stacker.

PROJECT BACKGROUND

Project History

The Safford Leach Project is located in the Safford mining district in Graham County, Arizona, approximately eight miles northeast of the town of Safford and 170 miles east of Phoenix. The 3,360-acre property is located in the Gila River Valley, immediately south of the Gila Mountains, at elevations between approximately 3,000 and 5,400 feet above sea level. The Safford Leach Project is comprised of the Dos Pobres and San Juan deposits, two of five known copper ore deposits in the Safford mining district.

Time Frame. Phelps Dodge, now Freeport-McMoRan, acquired interest in the property in 1957 with the optioning of the Dos Pobres deposit. In the 1960s, exploration delineated sufficient sulfide mineralization to

warrant an underground operation, which was developed until 1982, when declining copper prices resulted in unfavorable economics. In 1990, district exploration for near-surface leachable copper mineralization generated renewed interest in the Dos Pobres deposit. Detailed mineralogical and metallurgical work indicated that a zone of leachable copper oxide ore existed above the sulfide portion of the deposit. The San Juan deposit was acquired in 1993 and project evaluation was initiated.

Geology and Deposit. The Safford mining district is located at the southern edge of the physiographic Transition Zone Province, between the Colorado Plateau and the Basin and Range Province. The district covers an area four by 15 miles, oriented northwest to southeast approximately parallel to the southwestern flank of the Gila mountain range. The Dos Pobres and San Juan ore deposits are located in the northwestern portion of the Safford mining district.

Host rocks for the Dos Pobres and San Juan oxide deposits are metavolcanics and metavolcaniclastics that are primarily andesitic in composition. Oxide mineralization at Dos Pobres is characterized by the presence of copper-bearing iron oxides, chrysocolla, tenorite, shattuckite, azurite, chalcocite, malachite, and native copper. Oxide mineralization at San Juan is characterized by the presence of chrysocolla, brochantite, malachite, cuprite, and minor chalcocite.

Project Fundamentals

The project includes development of mining, ore handling, leaching, hydrometallurgical, and support facilities for extraction and recovery of copper from the Dos Pobres and San Juan ore bodies (see Figure 1).

Ore reserves total 615 million tons grading 0.36% copper. Mine production rates will peak at approximately 287,000 tons per day during the 14 years of leach ore production. Leach ore will be processed at a constant rate of 114,000 dry short tons per day (dstpd). SX/EW facilities are capable of producing a nominal 240 million

* Freeport McMoRan, Safford, Arizona.

† Fluor Canada Ltd., Vancouver, British Columbia, Canada.

‡ Terra Nova Technologies, Inc., San Diego California.

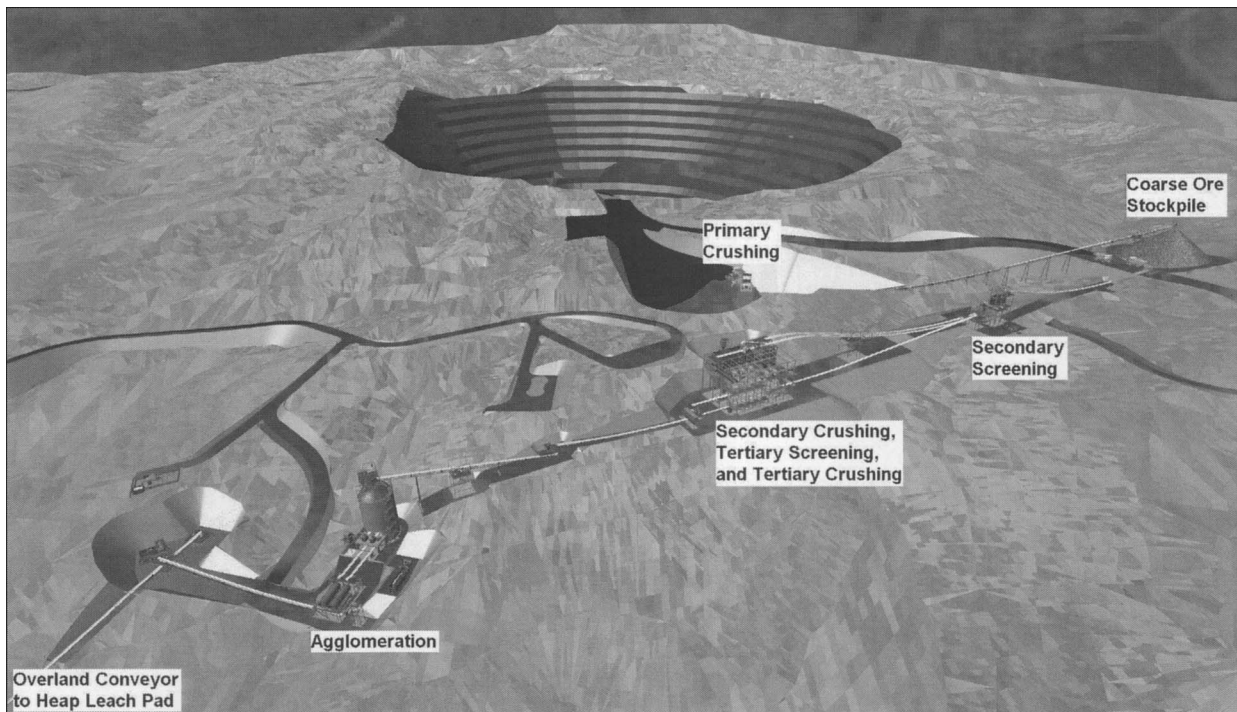


FIGURE 1 Safford site layout

pounds per year of cathode copper. Proven and probable reserves will provide for 14 years of operation followed by an additional four years of residual leaching.

The conventional open pit mine operation will involve drilling, blasting, loading by shovel, and truck haulage of the mined rock and ore from two separate pits. Production will be focused on the Dos Pobres pit for the first three years of mine operations before transitioning to the San Juan pit.

The ore handling process utilizes three-stage crushing, agglomeration, conveying, and stacking to prepare the ore for leaching.

The leach pad is being developed in three phases with an ultimate footprint of $4,080 \times 7,520$ feet and an ultimate height of 600 feet. The stockpile is developed in "retreat" stacking mode, with 30-foot-high stacked lifts. The stacking system consists of a series of portable conveyors and a radial stacker, fed from an overland tripper and operating across the width of the pad. The stacked ore is irrigated for 90 days and the leached copper reports as copper sulfate in solution in the presence of sulfuric acid.

The hydrometallurgical area includes solution extraction (SX) and electrowinning (EW) processes. During the SX operation, approximately 90% of the copper is extracted from the PLS into an organic phase. The copper in organic is stripped by a lean electrolyte solution; the resulting rich electrolyte is then heated and pumped into EW cells. Plating of copper occurs on stainless steel cathode blanks, which are harvested after six days and stripped yielding a copper grade of 99.999%.

PROJECT EXECUTION

Fluor Canada Ltd. (Fluor) was selected as the prime EPCM contractor for the Safford Leach Project. Key values utilized during all stages of the project include safety, environmental compliance, community relations, schedule, and budget. Fluor, acting as agents for Freeport-McMoRan Copper & Gold, Inc., was responsible for the general execution of engineering and procurement, as well as construction supervision and the management of consultants and contractors.

Plant Design and Process Overview

The ore handling facilities are designed to process 114,000 dstpd of copper-bearing ore, originating initially from the Dos Pobres open pit and later from the San Juan pit, throughout the 14-year mine life of the project. The process requires three strategic zones of operation to crush/screen, agglomerate, and stack the ore on the dedicated leach pad (see Figure 2).

Primary Crushing and Coarse Ore Stockpiling. In efforts to reduce capital and operating costs, the scale of the primary crushing facilities was minimized to take advantage of the predicted fine ROM ore gradation. Studies were conducted to evaluate gyratory crushers, mineral sizers, and jaw crushers with the goal of optimizing the size and type of the primary crusher. The jaw crusher was the preferred selection, based primarily on the fine ROM gradation, but also on the ability of the downstream secondary crushers to accept a feed size of 16 inches.

Twin stationary scalping grizzlies receive the ROM ore directly from the haul trucks. A rock breaker will reduce the size of any material larger than the expected ROM size. The grizzly design is based upon ore flow characteristic test

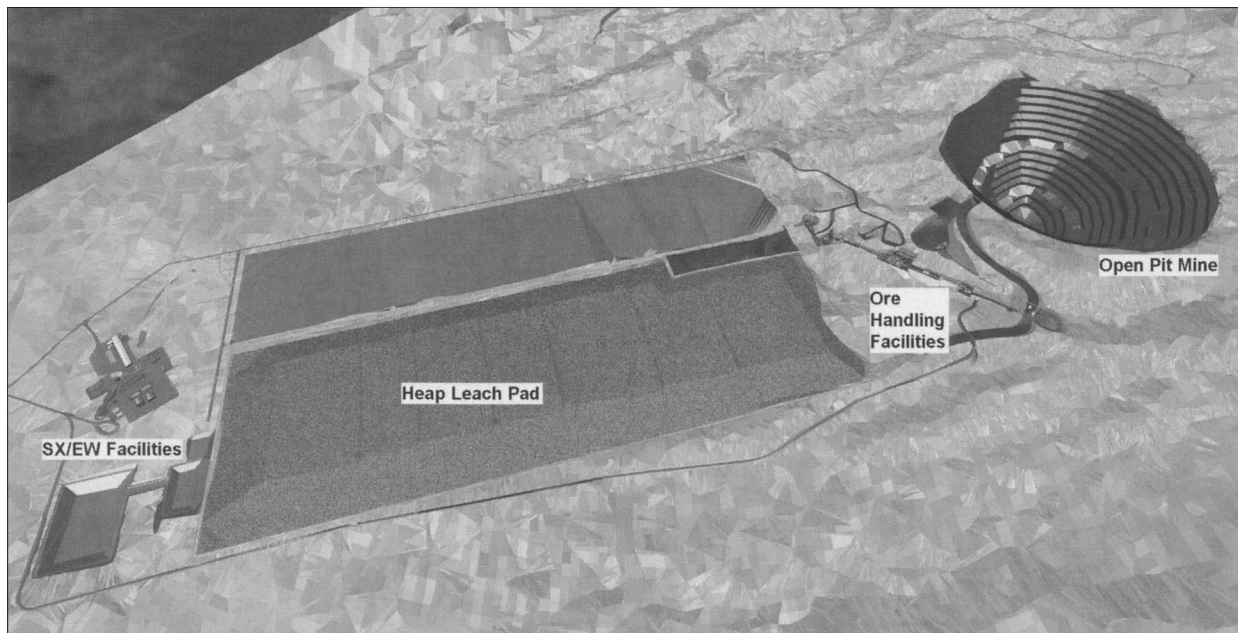


FIGURE 2 Safford ore handling flowsheet

work and includes multiple slope angles and tapered openings. The oversize ore from each of the fixed grizzlies is discharged directly to a central open surge bin which is reclaimed by a vibrating grizzly feeder, which is also used to control the feed rate to the jaw crusher. The 48 × 60 inch single-toggle jaw crusher is set at a nominal close side setting (CSS) of nine inches.

Undersize from the stationary grizzlies will be contained in separate surge bins each equipped with an apron feeder. The ore discharged by these two variable-speed apron feeders, together with the undersize from the vibrating grizzly feeder and the jaw crusher product, report to the coarse ore stockpile feed conveyor.

The uncovered coarse ore stockpile will have a “live” capacity of 30,000 tons and a total capacity of 140,000 tons. In the event that the delivery of ore to the primary crushing plant is interrupted, this live capacity will provide sufficient ore for five hours of continuous operation of the entire process downstream of the stockpile without bulldozing the stockpile.

Secondary and Tertiary Crushing. Numerous crushing circuit designs were prepared to establish the preferred process and equipment requirements. Physical test work was conducted on ore samples from the Dos Pobres and San Juan ore bodies and simulations were conducted based on the ROM gradation. Two secondary and four tertiary crushers will be installed to take advantage of the fine ROM gradation.

The coarse ore stockpile is reclaimed by three apron feeders, any two of which can supply the necessary design capacity. The apron feeder discharge reports to a common conveyor feeding the secondary screening plant surge bin.

The secondary screening plant surge bin feeds two parallel secondary screening circuits. Each circuit consists of a reclaim belt feeder which delivers ore to a double-deck vibrating “banana” screen (12 × 27 feet).

Oversize and middlings report to a belt conveyor feeding the secondary crushing plant. The undersize reports to the tertiary crushing plant via a belt conveyor.

The secondary crushing plant feed reports to a surge bin which distributes ore to two parallel and “open” secondary crushing circuits. Each circuit consists of a reclaim belt feeder delivering ore to a Metso MP1000 standard cone crusher with a CSS of 1.5 inches. This configuration, where secondary crushing occurs separate from secondary screening, allows direct and immediate control of the secondary crusher feed rate, so that full power draw can be achieved. The secondary crusher product is transported via two conveyors to the tertiary crushing plant feed conveyor, where it commingles with the secondary screen undersize and advances to the tertiary crushing plant feed bin.

A traveling tripper distributes the tertiary crushing plant feed to a common surge bin. This bin feeds four parallel and “open” tertiary crushing circuits. Each circuit consists of a reclaim belt feeder which delivers ore to a single-deck vibrating banana screen (12 × 27 feet). The screen oversize reports directly to a Metso MP1000 short-head cone crusher with a CSS of 0.5 inches. The tertiary crusher product reports to the fine ore conveyor. Screen undersize bypasses the tertiary crushers via a collection and a short transfer conveyor, and combines with the tertiary crusher product. The fine ore conveyor feeds a transfer point which includes an automatic sampling plant prior to discharge into the fine ore silo.

Agglomeration and Heap Leach Stacking. The fine ore silo distributes ore to two parallel agglomeration circuits. Each circuit consists of a reclaim belt feeder which discharges to an agglomeration drum feed conveyor. The agglomeration drums (15 × 45 feet) tumble the ore with a nominal 26 lb/ton sulfuric acid and sufficient water to increase the moisture content to 6.5% from a nominal content of 2.5%. The agglomeration

drum discharge reports to a common belt conveyor which transports the agglomerated product to the overland conveyor.

The overland conveyor transports ore down a corridor on the western edge of the heap leach pad. The heap leach pad is developed in three phases to minimize the initial purchase of stacking equipment and to delay the cost of installing the entire liner system.

Phase I of the heap leach will cover the eastern side of the leach pad ($2,500 \times 5,730$ feet), with an adjoining area for ROM material ($2,100 \times 1,790$ feet). Phase II will cover the western side of the leach pad ($1,580 \times 5,730$ feet), and will require the agglomeration discharge conveyor to be extended farther to the west, to feed a relocated overland conveyor. Also included in Phase II is an adjoining area for ROM material ($1,980 \times 1,790$ feet). Lastly, Phase III will build upon Phases I and II in complete lifts and will require the purchase of additional stacking equipment.

Stacking System Design Considerations

Achieving the design copper recovery target depends upon continued leaching of the ore below the lift being stacked. This secondary leaching must not be jeopardized by reduced permeability as a result of excessive compaction. Test work by an independent geotechnical consultant limited the stacking system equipment ground bearing pressure to a maximum of 20 psi. To minimize compaction, the stacking system would need to be crawler mounted to maintain minimal ground bearing pressures during both operation and relocation.

In efforts to minimize capital costs, the ore handling facilities were designed to maximize asset efficiency. Extensive investigation to determine the maximum possible asset efficiency was conducted, including benchmarking of existing FMI operations, Fluor experience, and dynamic simulations by an independent consultant. It was determined that the primary crusher would be designed considering a 74.5% asset efficiency while the remaining ore handling facilities, including the stacking system, would be designed considering a 76.5% asset efficiency. In order to maintain the high asset efficiency, it was necessary for the stacking system design to consider the following:

- A robust, easily-maintainable design,
- A control system capable of controlling both the stacking system and the agglomeration circuit,
- Independently and highly mobile equipment to reduce relocation times, and
- High degree of standardization for mechanical, electrical, and instrumentation components.

In order to minimize the size of the operations crew and support equipment fleet, the stacking system equipment must be capable of relocating and operating on all encountered terrains. For maximum versatility, it was necessary for the stacking system equipment to be self-leveling, to have head- and tail-end luffing capabilities (where applicable), and to be capable of relocating on slopes of up to ten degrees. It was also necessary for equipment to be capable of operating in both straight-line and askew configurations.

Stacking System Vendor Selection Process

During the initial feasibility study, several vendors were asked to provide budget quotations for a stacking system.

Vendors responded with a variety of systems; the subsequent detailed analysis by Fluor and FMI indicated the grasshopper-type stacking system was optimal.

At the commencement of detailed engineering, vendors were asked to re-bid based on a set of more rigid operational constraints and process requirements. Vendors were encouraged to submit unique stacking alternatives that were specifically tailored to the size and complexity of the Safford project. The quotations submitted based on the refined specification were generally of two types: grasshopper-type systems with a radial spreader/stacker and mobile-bridge-type systems with discharge booms.

Detailed evaluation again indicated that the grasshopper-type system was optimal for the Safford Leach Project. The grasshopper system provided the high degree of flexibility and mobility required to maintain the asset efficiency while maintaining a low ground-bearing pressure. The stacking system contract was eventually awarded to Terra Nova Technologies, Inc. (TNT).

HEAP LEACH STACKING SYSTEM

The Super Portable stacking system in operation at Safford is designed to stack 6,800 dstph and is comprised of a transfer conveyor, a 7,400-foot-long, 60-inch-wide regenerative overland conveyor with mobile tripper, and a fleet of mobile, self-propelled conveyors:

- (10) 250-foot-long, 72-inch-wide Super Portable Conveyors (six "Ramp" and four "Standard"),
- (1) 110-foot-long, 72-inch-wide Horizontal Feed Conveyor,
- (1) 285-foot-long, 72-inch-wide Horizontal Conveyor with continuous receiving hopper, and
- (1) 190-foot-long, 72-inch-wide Radial Stacker with a 30-feet-long telescoping "stinger" conveyor.

Operating Description

Agglomerated ore from the agglomeration drums is conveyed to the Overland Conveyor. The mobile, rubber-tired Overland Tripper travels along the length of the Overland Conveyor and "trips" material off the conveyor and onto the first in a string of Super Portable Conveyors. Material moves along the string of Super Portable Conveyors to the Horizontal Feed Conveyor, which transfers material into a 250-feet-long continuous receiving hopper on the Horizontal Conveyor. The Horizontal Conveyor then transfers material to the Radial Stacker, which discharges material in 30-foot lifts on the leach pad. The Horizontal Conveyor and Radial Stacker units are semi-permanently coupled together and function as one unit during normal operation (see Figure 3).

The stacking system operator commences stacking on the right side of the pad and builds a pile of material of uniform height by adjusting the Radial Stacker slewing speed. At this time, the Horizontal Conveyor is being fed at the tail end of the 250-feet-long continuous receiving hopper and the Radial Stacker's 30-feet-long telescoping stinger is fully extended. Once the Radial Stacker is slewed to the far-left position, the stinger is retracted by approximately 1.5 feet and the slewing travel motors are reversed. This procedure is repeated until the entire 30 feet stinger is fully retracted, which occurs after approximately 20 passes. Once this occurs, the entire Horizontal Conveyor/Radial Stacker unit retreats by 30 feet, a distance equivalent to the length of the stinger.

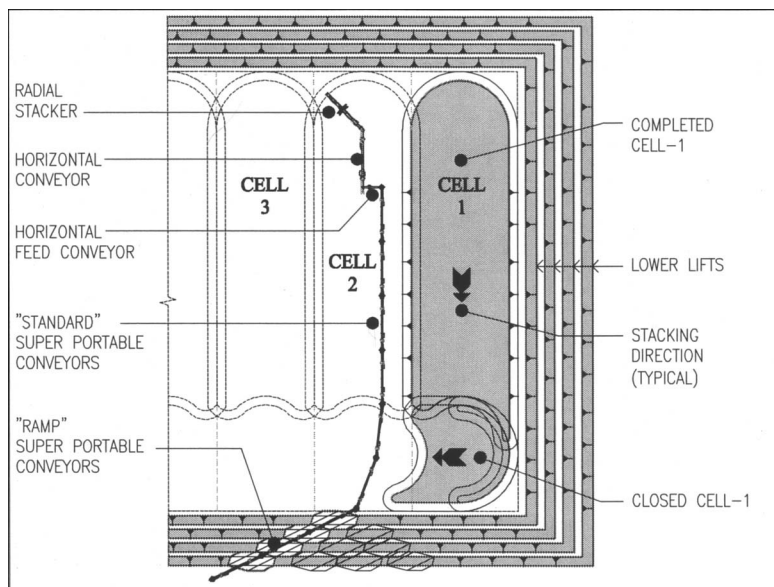


FIGURE 3 Stacking system equipment schematic

While retreating, the stinger is returned to the extended position. When this process, referred to as indexing, is complete, normal stacking operation resumes. Material flow continues uninterrupted during this procedure.

This indexing procedure is repeated until the Horizontal Conveyor is being fed at the head end of the continuous hopper. At this point, the system is shut down so the final Super Portable Conveyor can be removed from the operating line. Following the removal of the final Super Portable Conveyor, the Horizontal Feed Conveyor is repositioned to the head end of the "new" final Super Portable Conveyor. Once again, the Horizontal Feed Conveyor is feeding the tail end of the Horizontal Conveyor. Following final adjustments and connections, normal stacking operation is resumed. The indexing and Super Portable removal sequence continues until the stacking of the cell is complete.

In order to reduce downtime during cell-to-cell relocations, as each Super Portable Conveyor is removed from the operating line, it is repositioned to the next cell. When the stacking of a cell is complete, this leaves just the relocation of the Horizontal Feed Conveyor and Horizontal Conveyor/Radial Stacker unit to the next cell. Three cells are accessed from each ramp. The cell-to-cell relocation after the third cell is stacked requires additional downtime as the Overland Tripper is repositioned and the "Ramp" Super Portable Conveyors are moved to the next ramp.

The stacking sequence continues until the final cell of the lift is stacked. The entire stacking system then relocates to the first cell of the next lift using service ramps located at the ends of the leach pad.

Stacking System Equipment Description

Overland Conveyor. The Overland Tripper can be positioned at any location along the length of the 7,400-foot-long, 60-inch-wide downhill Overland Conveyor. This feature added significant complexity to the design of the control and belt loading features. Specifically, the ore

load—and hence the conveyor tension, power and inertia—varies significantly with the Overland Tripper position. To accommodate these large variations in operating parameters, the conveyor is equipped with an intelligent control system which operates dual 600 horsepower (HP) drives with variable frequency drive (VFD) controls and a dual-disk hydraulic braking system on the tail drive pulley.

TNT engaged an independent conveyor specialist to develop the control system and conduct a dynamic analysis of the conveyor under possible operating conditions. The control system monitors conveyor belt speed and power draw in order to determine the braking force and deceleration necessary to bring the conveyor to a controlled stop under the given operating condition. To prevent material spillage as a result of the significant difference in stopping times of the Overland Conveyor and the stacking system equipment, the control system is designed to stop the Overland Conveyor in the shortest time possible that does not impart undue stress and dynamic forces into the system.

Overland Tripper. The Overland Tripper, which straddles the Overland Conveyor, is 70 feet long and is designed to "trip" ore directly from the Overland Conveyor to the first Super Portable Conveyor. The Overland Tripper is rubber-tire mounted (see Figure 4) for relocation, but during operation is supported by hydraulic outriggers with leveling capabilities. On-board the Overland Tripper are power and control cable reels which connect to drop points along the length of the Overland Conveyor.

Super Portable Conveyor. The Super Portable Conveyors are 250 feet long and are propelled by two sets of Caterpillar 325 crawlers (see Figure 5). Each Super Portable Conveyor is essentially a mobile belt conveyor supported on a boxed steel truss which is propelled by crawlers. "Ramp" Super Portable Conveyors are equipped with dual 250-horsepower drives as they are required to transport material from the Overland



FIGURE 4 Overland tripper



FIGURE 5 Super Portable conveyor

Tripper up the pad slope to the top of the current lift. "Standard" Super Portable Conveyors are equipped with a single 250-horsepower drive as they need only to transport material along the top of the leach pad to the next conveyor in the operating line. In general, each unit includes:

- Head- and tail-end luffing,
- Self-leveling,
- Access and maintenance platforms and walkways,
- Electrical panels, including motor control center and operator panel,
- 13.8 kV/480V transformer, and
- 150-kW diesel generator for relocating.

Complete with steel structure, conveyor components, electrical equipment, and propulsion gear, each unit weighs approximately 120 tons.

Horizontal Feed Conveyor. The Horizontal Feed Conveyor is 110 feet long and is propelled by one set of Caterpillar 312 crawlers and one set of Caterpillar 320 crawlers (see Figure 6). The Horizontal Feed Conveyor is positioned perpendicular to both the final Super Portable and the Horizontal Conveyor. The Horizontal Feed Conveyor is equipped with head-end hydraulic luffing cylinders and a pivoting discharge bang plate to provide correct positioning over and trajectory into the Horizontal Conveyor receiving hopper. The Horizontal Feed Conveyor is designed to walk axially or sideways.

Horizontal Conveyor/Radial Stacker Unit. The Horizontal Conveyor and Radial Stacker are two separate machines, but are connected by a slewing bearing / pin arrangement and operate together as a single unit.



FIGURE 6 Horizontal feed conveyor

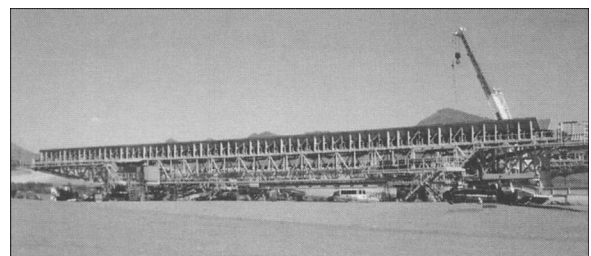


FIGURE 7 Horizontal conveyor

During normal stacking operation, the unit retreats in unison as cell stacking progresses. During relocation between cells and lifts, the two units can be relocated together or decoupled and relocated independently.

The Horizontal Conveyor is 285 feet long and is propelled by two sets of Caterpillar 330L crawlers (see Figure 7). The Horizontal Conveyor has a 250-feet-long continuous receiving hopper, which corresponds to the length of a Super Portable Conveyor.

The Radial Stacker is 190 feet long with a 30-feet-long stinger and is propelled by two sets of Caterpillar 330L crawlers (see Figure 8). The tail end of the Radial Stacker is supported by and slews around a "tongue" on the head end of the Horizontal Conveyor. The Radial Stacker has head-end luffing capabilities and a 30 feet long telescoping discharge stinger. These features enable the stacking of ore in lift heights between 25 and 35 feet and in cell widths of up to 440 feet. The Radial Stacker also contains the operator control cabin from which, through the use of a radio control system, all stacking system functions are closely monitored and remotely controlled.

The Radial Stacker's 30-feet-long discharge stinger uses a continuous conveyor belt which allows the machine to stack ore uninterrupted while retreating. The two sets of crawlers under the front undercarriage have two functions, travel and slewing. For traveling, the crawlers are positioned parallel to each other. For slewing, the crawlers are positioned slightly askew, such that the two sets of tracks are aligned tangentially along the slewing arc line. In order to switch the crawlers between travel and slewing mode, the entire front end of the stacker is jacked off the ground with hydraulic cylinders and the crawlers are rotated to the desired position.



FIGURE 8 Radial stacker

with hydraulic cylinders. This prevents the imparting of undue stress into the stacker undercarriage.

Electrical System. The stacking system utilizes the site's main 13.8 kV power supply, which is fed to the equipment by drop points at 500-foot spacings along the length of the Overland Conveyor. Power is distributed to the stacking system through the Overland Tripper by way of a cable reel capable of storing 600 feet of 13.8 kV power cable.

Given the overall length of the stacking system (up to 10,000 feet when the Overland Tripper is at the head end of the Overland Conveyor and all the stacking equipment

is being utilized), distributing power at 13.8 kV was necessary to minimize voltage drops and cable size. Each piece of stacking equipment is interconnected with a 13.8 kV power cable and a control interlock cable. This leaves the stacking equipment effectively "daisy-chained" on the pad, like a series of extension cords. Each piece of stacking equipment is equipped with an on-board 13.8 kV / 480 V transformer. All motors on-board each piece of stacking equipment operate at 480 V.

SUMMARY

New plant designs reflect the industry's state of the art. Not an exception, the Freeport-McMoRan Safford Mine incorporates new concepts in the ore handling system, including the use of a jaw crusher in a large-scale mining operation, a secondary crushing plant configuration with the screening section separate from the crushing system, and the use of large-scale grasshopper-style stacking equipment. The stacking system particularly illustrates the evolving technology: while maintaining capital expenditures low, the coveted features of small-scale stacking systems are retained in the system, including the versatility afforded by grasshopper-type systems to stack ore optimally and the minimal surface compaction generally created by these systems, yet the Safford system transports ore at a much higher rate and provides improved reliability and maintainability. As always, we look to the next generation of plant designs to provide further insights.

INDEX

Index Terms

A

Aggregate, and environmentally low-profile conveyor	83
Aumund France	77

B

Belt feeders	
design case histories	61
design criteria	56
design of interface with bins and hoppers	53
and material loads	58
problems (flow, mechanical design, operations)	56
sizing and design variables	57
special applications	61
Bin flow	54
Bulk material flow characteristics	55

C

Cadman aggregate mine, downhill overland conveyor (case study)	83
Capital costs	4
Cement plant, and 17-km trans-border (India-Bangladesh)	
conveyor for transport of limestone (case study)	77
Cementos Moins Spain	77
Coal	
13.1-km overland conveyor for transport from preparation plant to terminal	71
Coal clearance systems (longwall mining)	43
and availability	45
modeling multiple factors in sizing of production rates	43
and restarting	46

<u>Index Terms</u>	<u>Links</u>
Conveyor belts	
environmentally low-profile downhill overland conveyor	
for aggregate in state forest	83
in large-scale stacking system for copper ore processing	93
transfer point retrofit (case study)	89
13.1-km overland conveyor for coal	71
17-km trans-border (India-Bangladesh) conveyor for limestone	77
Conveyor Equipment Manufacturers Association	89
Copper, and large-scale stacking system	93
D	
Design	
and construction of 17-km trans-border conveyor for limestone	77
distributed drives	13
environmentally low-profile downhill overland conveyor	
for aggregate in state forest	83
and idler roll function and selection	35
indentation rolling resistance and rubber belt backing	
loss	25
of interface between belt feeders and hoppers	53
numerical optimization method to compare life cycle	
costs of different conveyor configurations	3
of 13.1-km overland conveyor for coal	71
Distributed drives	13 22
layout alterations	21
sequenced starting	17
start-up profile	15
F	
Flexure resistance	5
Fluor Canada Ltd.	93 94
Freeport-McMoRan Copper & Gold, Inc., large-scale	
stacking system (case study)	93

Index Terms

Links

H

Heidelberg Cement	83
-------------------	----

I

Idler rolls	
bearing life	37
design considerations	36
role of	35
rotating resistance	6 36
seals	38
selecting	39
Indentation rolling resistance	6 32
and backing material characterization	27
calculation example	28
design curves	29
models	25
and strain amplitude	29

K

Kaltim Prima Coal 13.1-km overland conveyor (case study)	71
--	----

L

Lafarge France	77
Lafarge Surma Cement Limited, long overland trans-border	
conveyor (case study)	77
Larsen & Toubro, Ltd.	77
Limestone 17-km trans-border conveyor for	77

M

Modeling	
discrete element modeling of sag energy losses in	
conveyor belt system	65
discrete-event simulation models to quantify stockyard	
throughput capacity	47

Index Terms

Links

Modeling (*Cont.*)

factors in sizing of coal clearance systems for longwall mining	43
indentation rolling resistance	25
life cycle cost models	4
motion resistance models	5
numerical analysis in belt feeder design	53

N

Nickel/copper ore, and transfer point retrofit	89
--	----

O

Operating costs	4
-----------------	---

R

Retrofitting	89
Rubber belt backing materials, and indentation resistance	25

S

Sag energy loss	65
Simulation. <i>See</i> Modeling	
Stacking system for copper ore processing	93
Stockyard throughput capacity modeling	47
case studies	49
and equipment capacity	48
rule-of-thumb approach	47
simulation modeling	48
spreadsheet or hand calculation	47

T

ThyssenKrupp Robins Inc.	83
Transfer points, retrofitting	89